**The Thesis committee for Mehmet Ozen Gurbuz**
**Certifies that this is the approved version of the following thesis:**

# Tectonic and Sea Level Controls on the Back – Stepping Early Miocene Carbonate Platforms: Adana Basin, Turkey

**APPROVED BY**
**SUPERVISING COMMITTEE:**

**Supervisor:**

Xavier Janson

William Fisher

Elizabeth Catlos

# Tectonic and Sea Level Controls on the Back – Stepping Early Miocene Carbonate Platforms: Adana Basin, Turkey

**by**

**Mehmet Ozen Gurbuz, B.S.**

**Thesis**

Presented to the Faculty of the Graduate School of

The University of Texas at Austin

in Partial Fulfillment

of the Requirements

for the Degree of

**Master of Science in Geological Sciences**

**The University of Texas at Austin**

**December 2015**

# Dedication

To my family for their infinite support.

To my dog, Efe.

# Acknowledgements

First, I would like to thank my advisor, Dr. Xavier Janson for the support throughout graduate school and the process of completing this thesis. I am also grateful to learn from my committee member Dr. Bill Fisher in the classes and in the fields. I also thank to Dr. Elizabeth Catlos for being my committee member.

Turkish Petroleum Corporation financially contributes to cover my living expenses, and tuition during my study in the graduate school. I would also like to thank Turkish Petroleum Corporation and Reservoir Characterization Research Laboratory for funding my research.

I am grateful for Dr. Kemal Gurbuz for determining the thesis topic and field area and Hasan Rosyadi for the field assistance.

Foremost, I would like to thank my family members for their financial support and infinite love during my study in the University of Texas at Austin.

November 25, 2015

# Abstract

## Tectonic and Sea Level Controls on the Back – Stepping Early Miocene Carbonate Platforms: Adana Basin, Turkey

by

Mehmet Ozen Gurbuz, M.S.Geo.Sci.

The University of Texas at Austin, 2015

SUPERVISOR: Xavier Janson

The Karaisali complex exposes Miocene carbonate platforms that developed on a tectonically controlled, rugged antecedent topography during an ice-house system. The factors affecting platform initiation, architecture, facies distribution, and eventually drowning of those Miocene platforms remain poorly understood because of the stratigraphic and structural complexities of the Adana Basin. In this work, sedimentological and structural analysis supplemented by dating using strontium isotope lead to a better understanding of platform developing in a strongly subsiding basin.

Using twenty one measured sections, ultra-high resolution photopans, petrographic, and strontium isotope analysis; an interpreted depositional model and detailed cross section were built. The architecture of the platforms can be divided into two transgressive and two highstand systems tracts separated by a maximum flooding surface. This work shows that the small attached carbonate platforms of the Karaisali

Formation colonized a steep-rugged basement topography in a rapidly subsiding basin without any significant syn-sedimentary movement.

The combination of rapid subsidence with a subsidence rate of more than 400 m/MA and eustacy drove the carbonate platform to successively nucleate, aggrade with minor progradation, and eventually drown on basement highs. The relative sea level rise resulted in back-stepping of the carbonate platforms towards landwards and development of Early Burdigalian to Late Serravalian reefal carbonates on the paleo-highs of the antecedent topography further in northernwest.

# Table of Contents

List of Tables ..... x

List of Figures ..... xi

Chapter 1 - Introduction ..... 1

1.1 Study Area ..... 1

1.2 Previous Works of the Adana Basın ..... 3

1.3 Aim of the Study ..... 5

1.4 Data and Methods ..... 6

Chapter 2 – Geologic Overview ..... 9

2.1 Stratigraphy ..... 9

2.1.1 Substratum ..... 9

2.1.2 Cenozoic Deposits ..... 12

2.1.2.1 Oligocene – Early Miocene Deposits ..... 13

2.1.2.2 Early to Middle Miocene Deposits ..... 18

2.1.2.3 Middle Miocene to Pleistocene Deposits ..... 26

2.2 Structure ..... 29

2.2.1 Regional Structures of the Adana Basin ..... 29

2.2.2 Tectonostratigraphy of the Adana Basin ..... 33

Chapter 3 – Lithofacies and Sedimentary Environment Analysis ..... 40

3.1 Introduction ..... 40

3.2 Faunal Content ..... 40

3.3 Facies Descriptions (See Table 1) ..... 45

3.3.1 Facies A, Subfacies A1, and Subfacies A2: Coralgal Framestone/Boundstone Platey Coral Framestone ..... 45

3.3.2 Facies B, Subfacies B1, and Subfacies B2: Coralgal Mud Dominated Packstone/Wackestone and Coralgal Floatstone ..... 54

3.3.3 Facies C, Subfacies C1, and Subfacies C2: Coralgal Grain Dominated Packstone and Coralgal Rudstone.....57
3.3.4 Facies D, Subfacies D1, and Subfacies D2: Large Benthic Foraminiferal Floatstone and Packstone.....60
3.3.5 Facies E: Small Benthic Foraminiferal Packstone.....64
3.3.6 Facies F: Planktonic Foraminiferal Coralgal Packstone.....66
3.3.7 Facies G: Planktonic Foraminiferal Large Benthic Foraminiferal Coralgal Packstone.....69
3.3.8 Facies H: Argillaceous Coralgal Wackestone.....73
3.3.9 Facies I: Shale/Marl/Siltstone.....73
3.3.10 Facies J: Debris Flow/Slumps/Rock Fall.....76
3.3.11 Facies K: Bivalve Floatstone.....76
3.12 Comparison of the Facies Model with Previous Studies.....78

Chapter 4 – Stratigraphic Architecture and Platforms Evolution Model.....81
4.1 Stratigraphic architecture.....81
4.1.1 Vertical Facies Succession.....81
4.4.1.1 East Platform.....86
4.1.1.2 Middle Platform.....97
4.1.1.3 West Platform.....101
4.1.1.4 Lower Fore – Reef and Transitional Environment.....111
4.1.2 Depositional Model.....114

Chapter 5 – Discussion.....125
5.1 Driving Mechanisms for Drowning.....125
5.2 Were the East and West Platforms Coeval?.....126

Chapter 6 – Conclusion.....133

Appendix A.....135

References.....148

VITA.....160

# List of Tables

Table 1: Facies Characteristics.....46

# List of Figures

Figure 1: (A) Location map of the Adana Basin and main tectonic setting of Turkey, WAEP, Western Anatolian Extensional Province; EACP, Eastern Anatolian Compressional Province; NAF, North Anatolian Fault; EAF, East Anatolian Fault; DSF, Dead Sea Fault; Hellenic T., Hellenic Trench; Cyprus T., Cyprus Trench (Radeff, 2014). (B) Tectonic Setting of the Adana Basin (Radeff, 2014). (C) Tertiary basins and main tectonic elements in southern Turkey, EF, Ecemis Fault; DSF, Dead Sea Fault Zone; EAF, East Anatolian Fault Zone; KB, Karsantı Basin; MB, Manavgat Basin (modified from Safak et al., 2005).....2

Figure 2: Geological map of the study area (E-East Platform, M-Middle Platform, W-West Platform) (faults shown by solid black lines are compiled from General Directorate of Mineral Research and Exploration N33 and N34 geological map and geological maps of Lagap (1985) and Ekmekyapar (2006))....8

Figure 3: Miocene stratigraphy of the onshore basins in southern Turkey (Robertson, 1998). .....10

Figure 4: Generalized basement and Miocene stratigraphy of the Adana Basin (Gul, 2007).....11

Figure 5: (A) Photopan of folded and faulted Permian Carboniferous argillaceous limestone, marl, and shale, photo showing a plunging anticline. (B) Devonian folded carbonates including black limestone. (C) Oblique slip fault cutting Permian Carboniferous carbonates.....12

Figure 6: Geological map of the Adana Basin (after Yetis and Demirkol, 1986; Unlugenc, 1993; Yetis et al., 1995; Faranda et al., 2013).....14

Figure 7: Generalized stratigraphy of the Adana Basin (after Ilgar et al., 2013).15

Figure 8: (A) Poorly developed channel geometry in the Gildirli Formation – sandy to muddy matrix and moderately sorted. (B) (Close up view) Reverse grading indicating debris or grain flow – polymict pebble sandstone – relatively rounded clasts – distal to the source. (C) Coarser relatively subangular conglomerates – proximal to the source, poorly sorted, reddish color indicating terrestrial environment, erosive cycle top (red line).....17

Figure 9: (A) lowermost part of the Kaplankaya Formation - poorly sorted pebble - cobble sandstone and conglomerate with calcareous matrix. The subangular clasts consist of dolomite, limestone, quartz, and locally chert. (B) Upper section of the lowermost part of the Kaplankaya Formation – the clasts are relatively moderately sorted and smaller. (C), (D) The uppermost Section of the Kaplankaya Formation – argillaceous mollusk floatstone - the basement clasts are not available anymore – carbonate content was relatively enhanced.....20

Figure 10: (A) Normal fault and resulted joint sets (upper left in the photo). (B) Orthogonal joint sets. (C) Bivalve floatstone. .....21

Figure 11: The Kopekli shale and silty marl alternating with Globigerina large benthic foraminiferal floatstone and Globigerina coralgal packstone.25

Figure 12: Messinian Evaporites in the Adana Basin. (A) Evaporites at the top of the Handere Formation (B) Enterolithic Gypsum (C) Crystalline Gypsum with a Chevron Growth Structure (D) Crystalline Gypsum with a Grassy Growth Structure (E) Nodular Gypsum (F) Gypsarenite with Wave-ripple Cross Lamination (The coin is 2 cm) (Ilgar et al., 2013).28

Figure 13: (A) Detailed bathymetry of the Adana-Cilicia Basin (Aksu et al., 2014). (B) Structural map and topographic map of southern Turkey showing the main structural elements and locations of the Neocene basins (half arrows indicate transform/strike slip faults) (Walsh – Kennedy et al., 2014). .....30

Figure 14: (A) Major structural elements of the Adana – Cilicia Basin (yellow areas show the onland Pliocene – Quaternary deposits) (Aksu et al., 2014). (B) (close – up view of A) Structural map of the Onshore Adana Basin (Burton – Ferguson et al., 2005) (filled rectangles and triangles are the ticks on the hanging walls of normal and thrust/reverse faults, respectively). .....36

Figure 15: (A) Seismic map of the basement – Miocene unconformity and NE – SW cross – line showing the location of the model (contours showing the depths below sea level in seconds of 2 – way travel time), (B) Model of Miocene tectono - stratigraphic development in the Adana Basin (post – Miocene extensional regimes are not considered in the model) (Ilgar et al., 2013). .....39

Figure 16: Distribution of the faunal elements of the Karaisali Formation (modified from Hallock and Glen, 1986). .....41

Figure 17: Platey coral framestone. .....51
Figure 18: Thin section photomicrographs of coralgal framestone. (A) Porites head corals (black) and thin branching Porites corals (red) (M: Mollusk, HC: Head Coral, BC: Branching Coral, CCRA: Crustose Coralline Red Algae). (B) Branching Porites Framestone. (C) Branching Porites Corals (micritization, LMC microspar and spar). .....52
Figure 19: Thin section photomicrographs of coralgal framestone and boundstone (A) Brain coral encrusted by crustose coralline red algae (CCRA) and Planorbulinid foraminifera (P) (Mud – filled burrows (B), microspar calcite cement (MC)). (B) Dead oil (DO) or organic matter in interparticle porosity. (C) Argillaceous coralgal framestone (M: Mollusk, BRY: Bryozoan, G: Globigerina sp.). (D) Multi – layered encrustations (L: Lithothamnion red algae, A: Acervulinid foraminifera, ART: Articulated red algae, S: Serpulid worm tubes, C: Conceptacles of Lithothamnion sp.). .....53
Figure 20: Outcrop photo showing coral algal floatstone - argillaceous lower section thickening upward. .....55

Figure 21: (A) and (B) Outcrop photo showing coral algal floatstone – rhodoliths. (C) and (D) close up view of (B). (E) and (F) Thin section photomicrographs of coralgal floatstone - reworked coralgal fragments (CRL: coral, MC: microspar calcite cement, A: Acervulinid foraminifera, OM: organic matter, P: Planorbulina, L: Lithophyllum red algae, LB: large benthic foraminifera, PC: Pecten sp.,M: mollusk, R: rhodolith, G: Gastropod, LD: Lepidocyclina sp.) ((E) slightly argillaceous). .....56

Figure 22: Outcrop photo showing relatively thin bedded coral algal grain dominated packstone. .....58

Figure 23: Thin section photomicrographs. (A) Coralgal rudstone. (B) and (C) Coralgal grain dominated packstone. (CRL: coral, MC: microspar calcite cement, A: Acervulinid foraminifera, MG: Miogypsina, P: Planorbulina, LP: Lithophyllum red algae, L: Lithothamnion red algae, CCRA: Crustose coralline red algae) ((A) slightly argillaceous). .....59

Figure 24: (A) Outcrop photo of large benthic foraminiferal packstone. (B) Close up view of (A). .....62

Figure 25: Thin section photomicrographs of large benthic foraminiferal packstone (O: Operculina sp., A: Amphistegina sp, L: Lepidocyclina sp.).....63

Figure 26: Thin section photomicrographs of small benthic foraminiferal packstone (S: Soritidae, M: Miliolid, SP: Spiroloculina sp., B: Borelis melo melo, P1: Peneroplis farsensis or Cibicides, T: Triloculina sp., P: Peneroplid, ME: Micritic envelope). .....65

Figure 27: (A) Outcrop photo of planktonic foraminiferal coralgal packstone. (B) Close up view of (A).....67
Figure 28: Thin section photomicrographs of planktonic foraminiferal coralgal packstone (G: Globigerinidae).....68
Figure 29: (A) Outcrop photo of planktonic and large benthic foraminiferal coralgal floatstone (Facies G), argillaceous coralgal wackestone (Facies H), marl/shale/siltstone (Facies I), and underlying bivalve floatstone of the Kaplankaya Formation. (B) Outcrop photo of planktonic and large benthic foraminiferal coralgal packstone.....70
Figure 30: Thin section photomicrographs of planktonic and large benthic foraminiferal coralgal packstone (G: Globigerinidae, O: Operculina sp., SC: Sponge Spicule, C: Clay).....72
Figure 31: Outcrop photo of argillaceous coralgal wackestone (Facies H), marl/shale/siltstone (Facies I). .....74
Figure 32: Thin section photomicrographs of argillaceous coralgal wackestone (G: Globigerinidae, M: Mollusk, C: Clay, R: Red Algae). .....75
Figure 33: Outcrop photo of rock fall and olistoliths (indicated by red lines) (Facies J).....76
Figure 34: Outcrop photos of bivalve floatstone (B) enriched in echinoderms (Facies K).....77
Figure 35: Facies distribution of the study area. .....80
Figure 36: Legend of the lithofacies.....83
Figure 37: Legend of the allochems, lithology, textural components, and structure for the measured sections.....84

Figure 38: Platform and measured section locations (dash lines represent the platform locations and the solid lines show the locations of the measured sections; E: East Platform, M: Middle Platform, W: West Platform, T: Transitional zone). .....85
Figure 39: Measured section E-1.....89
Figure 40: Interpreted ground – based photomosaic of north face of the East Platform (dash red line is the E-1 logging path, solid red line represents the drowning unconformity, and sample numbers are labeled).....90
Figure 41: Measured section E-3.....91
Figure 42: Interpreted ground – based photomosaic of south face of the East Platform (dash red line is the E-2-1, E-2-2, and E-2-3 logging paths, solid red line represents the drowning unconformity and thinner solid red line is the angular unconformity between dolomite basement and Miocene deposits). .....93
Figure 43: Interpreted ground – based photomosaic of east face of the East Platform (dash red line is the E-4-1, E-4-2, and E-4-3 logging paths, solid red line represents the drowning unconformity). .....95
Figure 44: Drowning Signals (A) formation of rhodoliths and leaching (B) early marine cementation (C) planktonic depth zone. .....96
Figure 45: Interpreted ground – based photomosaic of west face of the Middle Platform (dash yellow and black lines are the M-1 and M-2 logging paths, respesctively, yellow units are the rotational slides, and solid red line represents the drowning unconformity). .....99
Figure 46: Measured section M-1.....100

Figure 47: Interpreted ground – based photomosaic of south face of the West Platform (red dash lines are the W-1-1 and W-1-2 logging paths).103
Figure 48: Measured section W-1-1. .....105
Figure 49: Measured section W-1-2. .....107
Figure 50: Interpreted ground – based photomosaic of south face of the West Platform (red lines are the W-1 and W-2 logging paths, yellow dash line shows the path of the rock sampling, red line represents the angular unconformity, blue dash line is the maximum flooding surface). ..108
Figure 51: Interpreted ground – based photomosaic of the strike section of the West Platform (red dash lines are the W-3-1 and W-3-2 logging paths, red line represents the angular unconformity). .....110
Figure 52: Measured sections T-1. .....112
Figure 53: Measured sections T-2. .....113
Figure 54: 87Sr/86Sr versus age (Age error = +/- 0.43 m/MA. The numbers in the chart indicate the sample IDs).....115

Figure 55: Cross section showing the facies distribution from the lower fore – reef of the East Platform to the reef core of the West Platform has been demonstrated using E-2, E-2-1, E-2-2, E-2-3, T-1, T-2, T-3, T-4, W-2-1, W-2-2, W-1-1, and W-1-2 measured sections and facies changes were walked out and recorded in the field. (Solid red line: angular unconformity overlying the substratum and underlying the Karaisali or Kaplankaya Formations, solid yellow line: drowning unconformity, dash yellow line: its correlative conformity, dash blue line: maximum flooding surface, yellow boxes: locations of the samples for the strontium isotope analysis and the results of the 87Sr/86Sr data). .117

Figure 56: Digital elevation model of the study area (yellow solid line: location of the east to west profile illustrated in 68B, red dash line: location of the cross section represented in Figure 65, WP: Western Platform, T: Transitional Zone, and EP: Eastern Platform). .....118

Figure 57: Generalized Depositional Model. .....123

Figure 58: Early to middle Miocene age, stages, biozonation, sequences, isotopic curves and sea-level reconstruction modified after Janson et al. (2010) and Piller et al. (2007). Geochronology, geomagnetic polarity chrons, biozonations of planktonic foraminifers and calcareous nannoplankton modified after Lourens et al. (2004). Sequence stratigraphy and sea-level curve (after Hardenbol et al. (1998) and oxygen isotope stratigraphy (dashed curve after Abreu & Haddad (1998) partly recalibrated and correlated to regional chronostratigraphy of the Central ParaTethys from Piller et al. (2007). The solid oxygen isotope curves come from Miller et al. (1998). The sea-level reconstructions come from the New Jersey continental margin (solid line from Kominz et al. (2008) and dashed line from Miller et al. (2005)). Sea-level curves for the Mut basin from Bassant et al. (2005) and from this study. The climate column contrast an oxygen isotope derived relative temperature curve from Zachos et al. (2001) with two mean annual temperature curve for Germany (Mosbrugger et al. 2005) and Turkey (Akgun et al. 2007). .....132
Figure 59: Measured section E-2-1. .....135
Figure 60: Measured section E-2-2. .....136
Figure 61: Measured section E-2-3. .....137
Figure 62: Measured section E-4-1. .....138
Figure 63: Measured section E-4-2. .....139
Figure 64: Measured section E-4-3. .....140
Figure 65: Measured section M-2.....141
Figure 66: Measured sections W-2-1 and W-2-2. .....142

Figure 67: Measured sections W-3-1. .....143
Figure 68: Measured sections W-3-2. .....145
Figure 69: Measured sections T-3. .....146
Figure 70: Measured sections T-4. .....147

# Chapter 1 - Introduction

Reefal carbonates extensively developed at various times of Miocene with diverse characteristics in the Mediterranean region (Esteban, 1996). Lower to Middle Miocene reefal carbonates are distributed worldwide. They developed underglobal open - oceanic and humid tropical conditions. In contrast, Late Miocene reefs have a more restricted distribution because of the global cooling trend during the late Miocene and developed in semi-arid and subtropical environments (Franseen et al., 1996a; Esteban, 1996). The Miocene carbonates are well exposed around the Mediterranean and have been widely studied the western, central, and eastern Mediterranean, such as southern Turkey, Italy (Vecsei and Sanders, 1999), Spain (Franseen and Mankiewicz, 1991; Pomar, 1991; Pomar et al., 2004).

## 1.1 Study Area

The Adana, Iskenderun, Mut, Karsanti, Manavgat, Cilicia, and Iskenderun depocenters are the Neocene basins developed in a structurally complex area in southern Turkey, on the eastern coast of the Mediterranean Sea (Figure 1) (Pralle, 1994; Safak et al., 2005; Gul, 2007).

Miocene carbonates in the Adana Basin are the focus of this study because they share common trends within the other Mediterranean Miocene basins but their unique regional tectonic controls related the basin subsidence linked to the collision of Eurasian and Arabian plates.

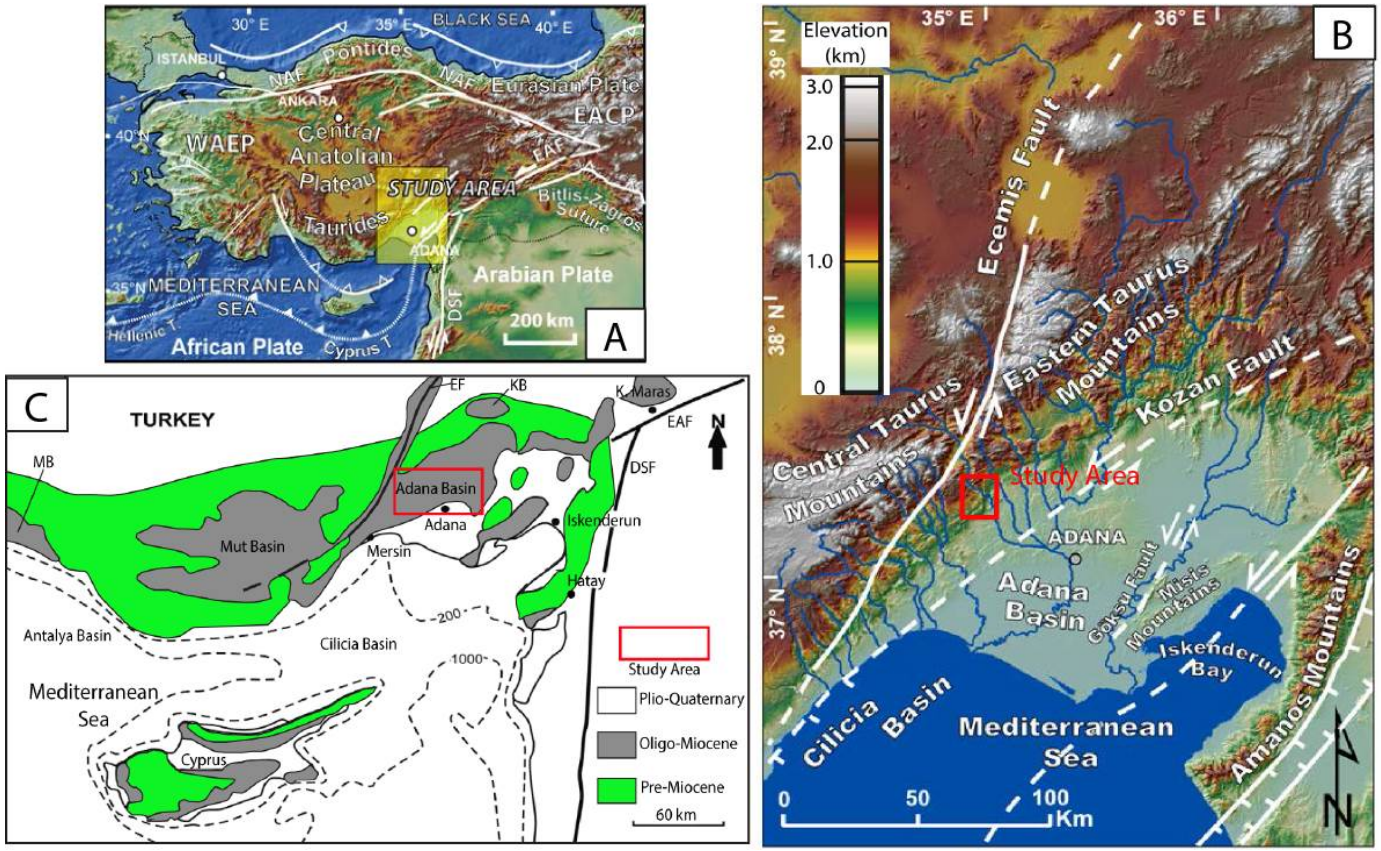


Figure 1: (A) Location map of the Adana Basin and main tectonic setting of Turkey, WAEP, Western Anatolian Extensional Province; EACP, Eastern Anatolian Compressional Province; NAF, North Anatolian Fault; EAF, East Anatolian Fault; DSF, Dead Sea Fault; Hellenic T., Hellenic Trench; Cyprus T., Cyprus Trench (Radeff, 2014). (B) Tectonic Setting of the Adana Basin (Radeff, 2014). (C) Tertiary basins and main tectonic elements in southern Turkey, EF, Ecemis Fault; DSF, Dead Sea Fault Zone; EAF, East Anatolian Fault Zone; KB, Karsantı Basin; MB, Manavgat Basin (modified from Safak et al., 2005).

The Adana Basin is an intra-mountain basin currently located in a fore-arc setting (Aksu et al., 2005). It is located in the southwest of the triple junction point of the Dead Sea Transform Fault, the Misis–Kyrenian Zone, and the East Anatolian Fault Zone in the southeastern of Turkey in the east of the Mediterranean Sea (Figure 1). The basin is bounded by Central Anatolian Plateau-Taurides Mountains, the left–lateral strike slip Ecemis Fault Zone to the west, by Misis–Andirin fault system in east, and by the Mediterranean Sea in south. It is one of the largest Neocene troughs presently situated in north of the Florence Rise and Cyprus Arc which are the convergent boundary between the African and Aegean–Anatolian plates (Aksu et al, 2005). The basin connects with the Cilicia Basin which is its deeper water offshore extension in southwest. Seyhan, Ceyhan, Goksu, and Tarsus Rivers form a major deltaic complex that provides the major siliciclastic input from Central Anatolian Plateau-Taurides Mountains into the current and potentially Neogene basin and the Mediterranean Sea (Aksu et al, 1992). The modern bathymetry is dominantly controlled by the Misis–Kyrenia Fault Zone, Cyprus Arc, and sediment input of the main rivers (Aksu, 2005). The modern continental shelf is less than 5 km and the water depth increases towards the south gradually up to 1000 km.

### 1.2 Previous Works of the Adana Basin

There are ongoing debates about the tectonic history and sequence stratigraphic framework of the basin because of its structural and stratigraphic complexity (Williams et al., 1995; Burton, 2002; Ilgar et al., 2013; Cosentino et al., 2010; Cipollari et al., 2013; Aksu et al., 2014). Recent studies have been focused on the Adana Basin since it is one of the unique basins that have recorded the tectonic development of the eastern Mediterranean.

Blumenthal (1947 and 1952) made the first geologic map of Adana and Nigde regions, described the basement rocks, and Miocene conglomerates of the Adana Basin. Ternek (1957) identified the formations that are potentially source, reservoir, and seal rocks; moreover, the potential traps were defined. The first stratigraphic study showing a chronostratigraphic chart was made by Schmidt (1961). The structure and regional stratigraphy of the Adana, Mut, and Antalya Basins were studied by Ozer et al. (1974). Oztumer et al. (1974) studied the biostratigraphy of these basins and dated the basinal deep water shales as Langian-Serravalian age. The geological map of the north part of the Adana Basin was proposed by Ilker (1975). The reefal carbonates of the Karaisali Formation were subdivided into six subfacies and the factors that control reef development were described by Gorur (1979). Nazik and Toker (1986) made a planktonic foraminifera analysis and assigned the Langhian to Serravallian age for the basinal shales. Yalcin and Gorur (1984) and Yetis (1988) further described the Neocene succession of the Adana Basin. The tectono – stratigraphic evolution of the Adana Basin has been studied more recently by Pralle (1994), Williams et al. (1995), Burton (2002), Aksu et al. (2005 and 2014), Burton-Ferguson et al. (2005), Toker et al. (2007), Schildgen et al. (2012), Walsh-Kennedy et al. (2014), and Radeff (2014).

Many studies have been conducted on the turbiditic sands of the Langhian - Serravalian deep–water fan (Cingoz Formation) and its feeder submarine canyon–fill deposits (Schmidt, 1961; Nazik and Toker, 1986; Yetis, 1988; Nazik and Gurbuz, 1992; Gurbuz and Kelling, 1993; Yetis et al., 1995; Satur, 1999; Cronin et al., 2010; and Satur et al., 2000 and 2004). Sedimentology of late Miocene to early Pliocene units in the Adana Basin was studied by Cosentino et al. (2010 and 2012), Faranda et al. (2013), Cipollari et al. (2013), and Ilgar et al. (2013). Gorur (1994) proposed a model showing

how the reefal platforms developed on a normal-faulted substratum blocked with a syn–sedimentary movement.

### 1.3 AIM OF THE STUDY

The Karaisali Formation is an early to middle Miocene reefal carbonates that developed in the Adana Basin in south-central Turkey. Small carbonate platforms developed on the paleo topographical highs that controlled the reef initiation, geometry, and distribution of the facies.

The objective of this research is to unravel the interaction between antecedent topography, structural framework, and relative sea-level fluctuations in creating the architecture of Miocene platforms. More specifically, we are testing the hypothesis that those Miocene platforms developed in a rapidly subsiding basin without significant syn-sedimentary movement associated with the substratum topography in contrast to the model developed by Gorur (1994) and widely used by subsequent studies.

The exceptional outcrops in the study area provide a unique analogue for carbonate platforms that developed on tectonically controlled rugged antecedent topography in an ice-house system.

The specific research goals were:

1) To propose a depositional model for the reef complexes.
2) To make a detailed cross section between two parallel reef platforms to correlate facies from shelf to inter-reef to basin.
3) To demonstrate the global and regional controls over the initiation, growth, and drowning of the carbonate platforms.

## 1.4 DATA AND METHODS

This research is based on the field study performed in Kiralan-Karaisali village in Adana (Figure 1 and Figure 2). The field work consisted on a detailed geologic mapping of the study area and the collection of 21 measured sedimentological sections. Measured sections included observation about lithology, strike and dip of the beds and faults, lineaments of the fractures and joints, fabric, bioclast type, grain size, and sedimentary structures were recorded.

Ground-based GigaPan Photomosaic and photopans were shot to record ultra-high resolution photo panorama of the various outcrops from different perspectives. These were merged using GigaPan Stitch software. The ultra-high resolution images were used for tracing and correlating beds, and locating observations about bed orientation, extent of slumps, and debris flow.

An east-west cross-section was made using the measured sections, a publically available digital elevation model, the field GPS data, elevation data from the 1/25,000 scale topographic maps, and the high resolution GIGAPAN photomosaic.

A total of 752 rock samples were collected and their locations were imported into Google Earth using the GPS coordinates. The samples were cut through 2 cm x 4 cm and 59 thin sections were made and impregnated with blue epoxy. These thin sections were studied for recording the grain size, allochems, porosity, and fractures. In addition, these samples were carefully examined for unlatered bivalve clast and twenty samples were chosen for strontium isotope analysis. While choosing the samples, three criteria were ranked for the samples, namely as, the size of the mollusk, diagenesis, and location of the samples. On the selected samples, the bivalve clasts were microdrilled and the collected powder was shipped to the Neptune Isotope Laboratory of the University of Miami for the strontium isotope analysis. The value of $^{87}Sr/^{86}Sr$ was calibrated using SRM987 standard

and the standard deviation on the mean of the SRM987 was determined. After calibration, the measured values were normalized to an accepted $^{87}Sr/\ ^{86}$ Sr value of 0.710248 for the SRM 987.

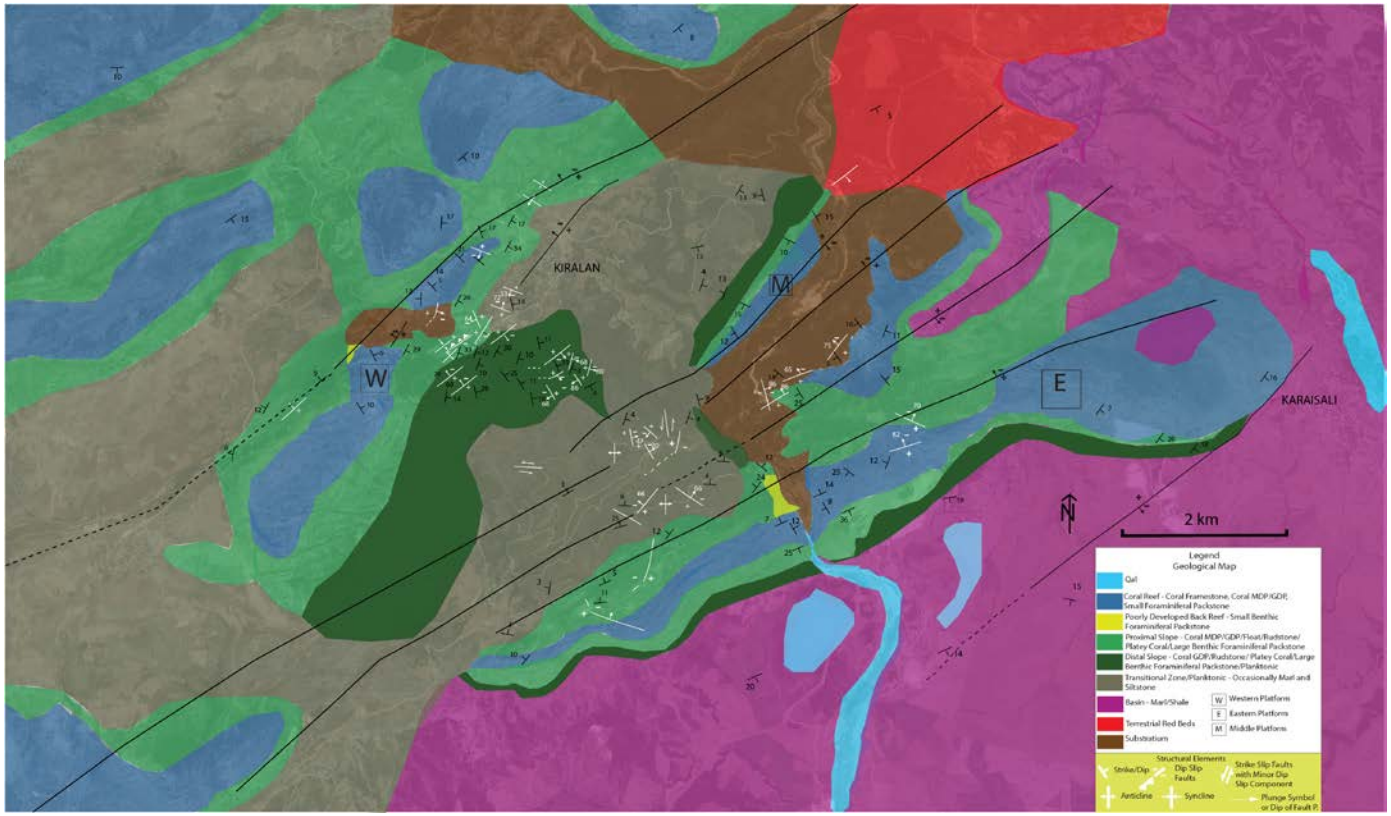


Figure 2: Geological map of the study area (E-East Platform, M-Middle Platform, W-West Platform) (faults shown by solid black lines are compiled from General Directorate of Mineral Research and Exploration N33 and N34 geological map and geological maps of Lagap (1985) and Ekmekyapar (2006)).

# Chapter 2 – Geologic Overview

## 2.1 STRATIGRAPHY

The Adana Basin is one of the largest Cenozoic depocenters in southern Turkey. The Miocene stratigraphic correlation of the various basins in southern Turkey is shown in Figure 3. The basin is bounded by the Ecemis and Kozan Fault Zone to the north and Misis Structural High to the south east. The basin consists of 6000 - 8000 m thick Miocene to recent sediments in its thickest part. The general stratigraphy of the Adana basin is described below.

### 2.1.1 Substratum

Pre-Neocene rocks are relatively complex in both stratigraphically and structurally in the Adana Basin. Mesozoic platform carbonates and Palaeozoic rocks of the Tauride Belt were tectonically overlain by the late Cretaceous Ophiolitic Melange which constitutes a significant component of the eastern Mediterranean region (Sengor and Yilmaz, 1981; Dilek and Moores, 1990) (Figure 4). Continued subduction of the Neotethyan ocean floor, following the emplacement of ophiolites resulted in the terminal closure, amalgamation of the continental fragments, and termination of marine deposition by the late Eocene (Sengör and Yilmaz, 1981, Clark and Robertson 2002). The Paleozoic rocks include Permian Carboniferous heavily folded limestone and dolomite of the Tauride Belt (Yetis and Demirkol, 1986) and Devonian coralline limestone and sandstone (Ilgar et al., 2013). In the research area, the Permian Carboniferous shelf shallow marine argillaceous limestone, marl, shale, and dolomitized limestone were exposed. Devonian coralline limestone, blackish green shale, and sandstone were observed in the north of the study area (Figure 5) (Lagap, 1985; and Unlugenc, 1986). Both of the formations were folded and the contact between them was faulted.

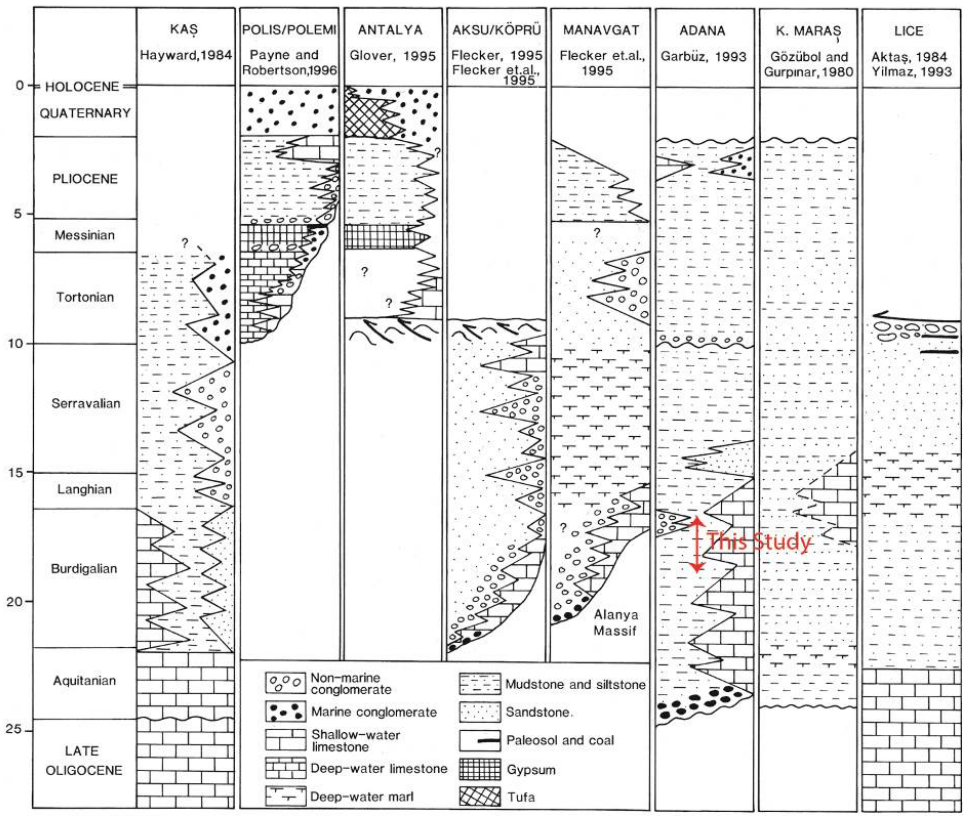


Figure 3: Miocene stratigraphy of the onshore basins in southern Turkey (Robertson, 1998).

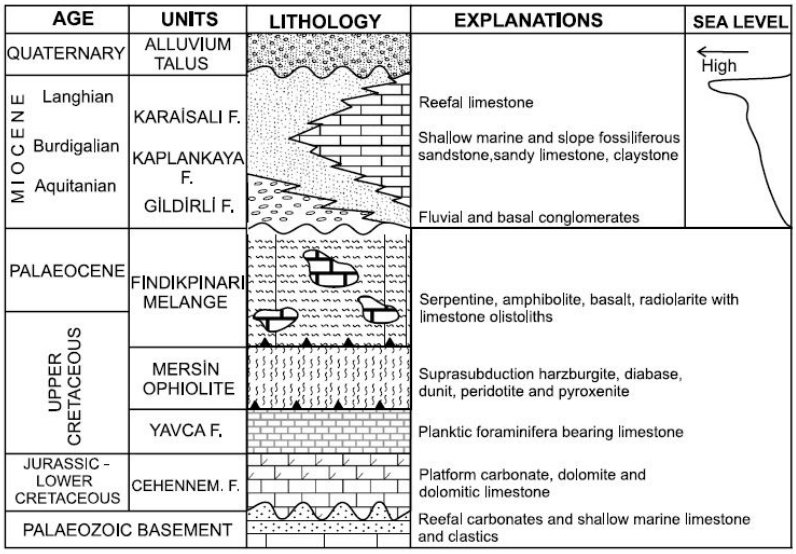


Figure 4: Generalized basement and Miocene stratigraphy of the Adana Basin (Gul, 2007).

Mesozoic rocks consist of the Triassic sandstone and conglomerate, Jurassic-Cretaceous limestone and dolomite, Upper Cretaceous clayey–sandy planktonic foraminifera-bearing limestone and calciturbidite, Upper Cretaceous Mersin Ophiolite, and Upper Cretaceous–Paleocene Fındıkpınarı Mélange (Demirtaslı et al., 1984). The Upper Cretaceous shelf limestone and calciturbidite were mostly dolomitized, brecciated, intensely fractured, and locally included chert nodules. The regressive sediments, transgressive basal conglomerate, or the reefal carbonates have an unconformable contact with the pre-Neogene substratum in the study area.

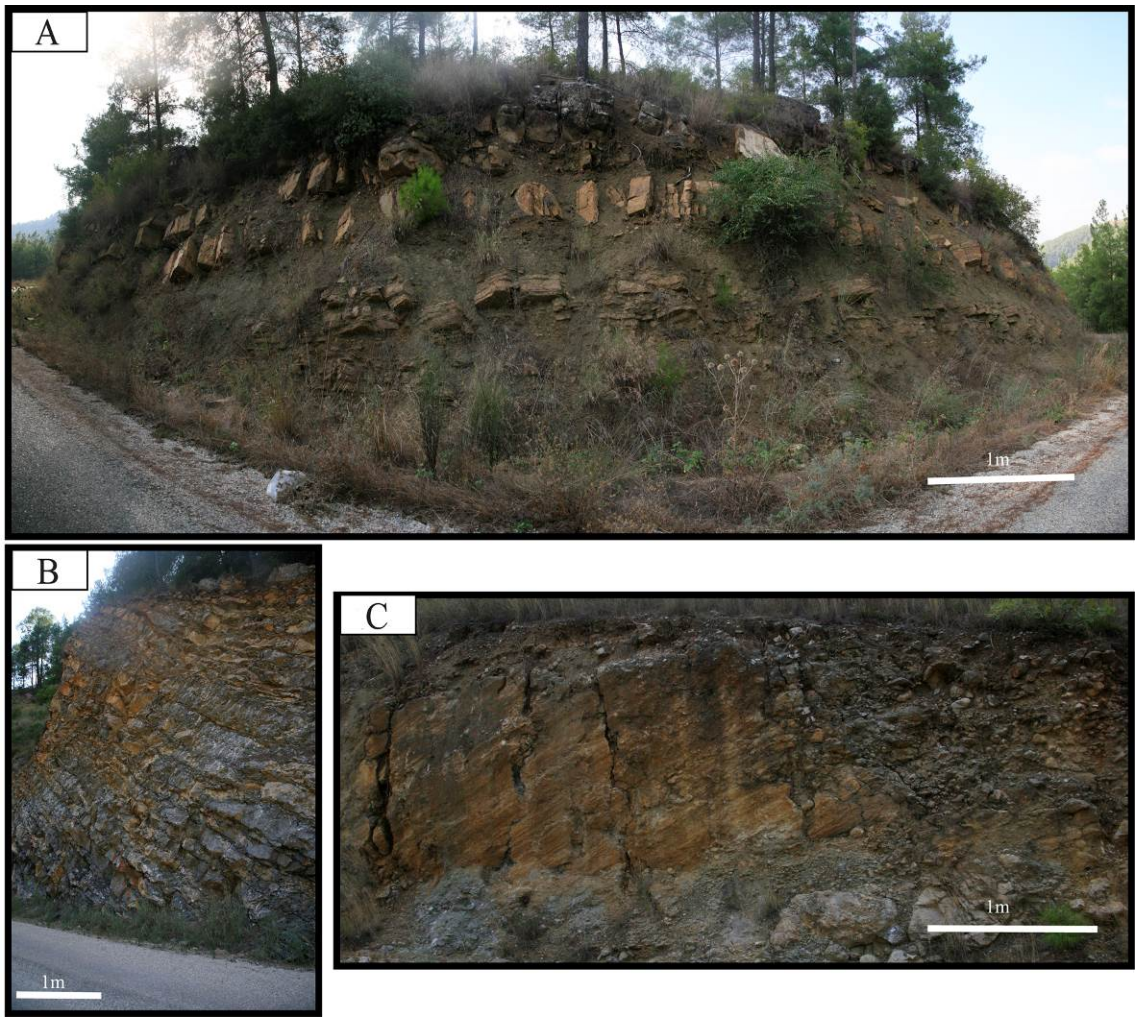


Figure 5: (A) Photopan of folded and faulted Permian Carboniferous argillaceous limestone, marl, and shale, photo showing a plunging anticline. (B) Devonian folded carbonates including black limestone. (C) Oblique slip fault cutting Permian Carboniferous carbonates.

### 2.1.2 Cenozoic Deposits

Within the Cenozoic interval, four megasequences were defined by Unlugenc et al. (1990) and Gurbuz (1999). Megasequence 1 includes the lacustrine sediments of the Karsantı Formation and the fluvial conglomerates and sandstones of the Gildirli Formation. Megasequence 2 represents the initial transgressive basal conglomerate of the

Kaplankaya Formation and the carbonates of the Karaisalı Formation. Megasequence 3 is the submarine fan channel conglomerates and lobe deposits of the Cingoz and deep marine shale of the Guvenc Formations. Megasequence 4 consists of shallow marine reef, deltaic conglomerate, sandstone, and fluvial deposits of the Kuzgun and shallow marine oolitic limestone and gypsum-anhydrite of the Handere Formations. Figure 6 and Figure 7 show the geological map and generalized stratigraphy of the Adana Basin, respectively.

#### *2.1.2.1 Oligocene – Early Miocene Deposits*

The Oligocene Karsanti and the early Miocene Gildirli Formations are the first Cenozoic deposits in the Adana Basin. The deposition of these regressive units occurred in major half graben controlled by the large scale extensional deep rooted basement faults which offset the ophiolitic thrust sheet in the north of the Adana Basin (Gorur, 1992; and Williams et al., 1995).

The Karsanti Formation consists of alluvial fan deposits of dominantly derived ophiolitic material (Williams et al., 1995) and lacustrine sediments of the intramontane basin deposits (Schmidt, 1961; Gurbuz and Kelling, 1993; Unlugenc et al, 1991, 1993; Yetis et al., 1995; Gurbuz and Unlugenc, 2001).

The Gildirli Formation has an erosional contact with the underlying pre-Tertiary basement rock. The formation was first defined by Schmidt (1961) as lower Miocene sediments which filled canyons and bays under continental and tidal influence that predated the Miocene sedimentation. The Gildirli Formation was described by Gorur (1992) as alluvial fan deposits. The lenticular geometry, cross bedding, and imbrication in the conglomerates are consistent with deposition in fluvial channels while the red mudstones with calcrete horizons represent flood plain deposits (Allen 1965 and 1974). After the Kaplankaya Formation was distinguished, the Gildirli Formation has been

reinterpreted as a prograding alluvial fan, fluvial, and fan delta system, feeding into a submarine canyon head (Satur 1999, Satur et al. 2000 and 2005).

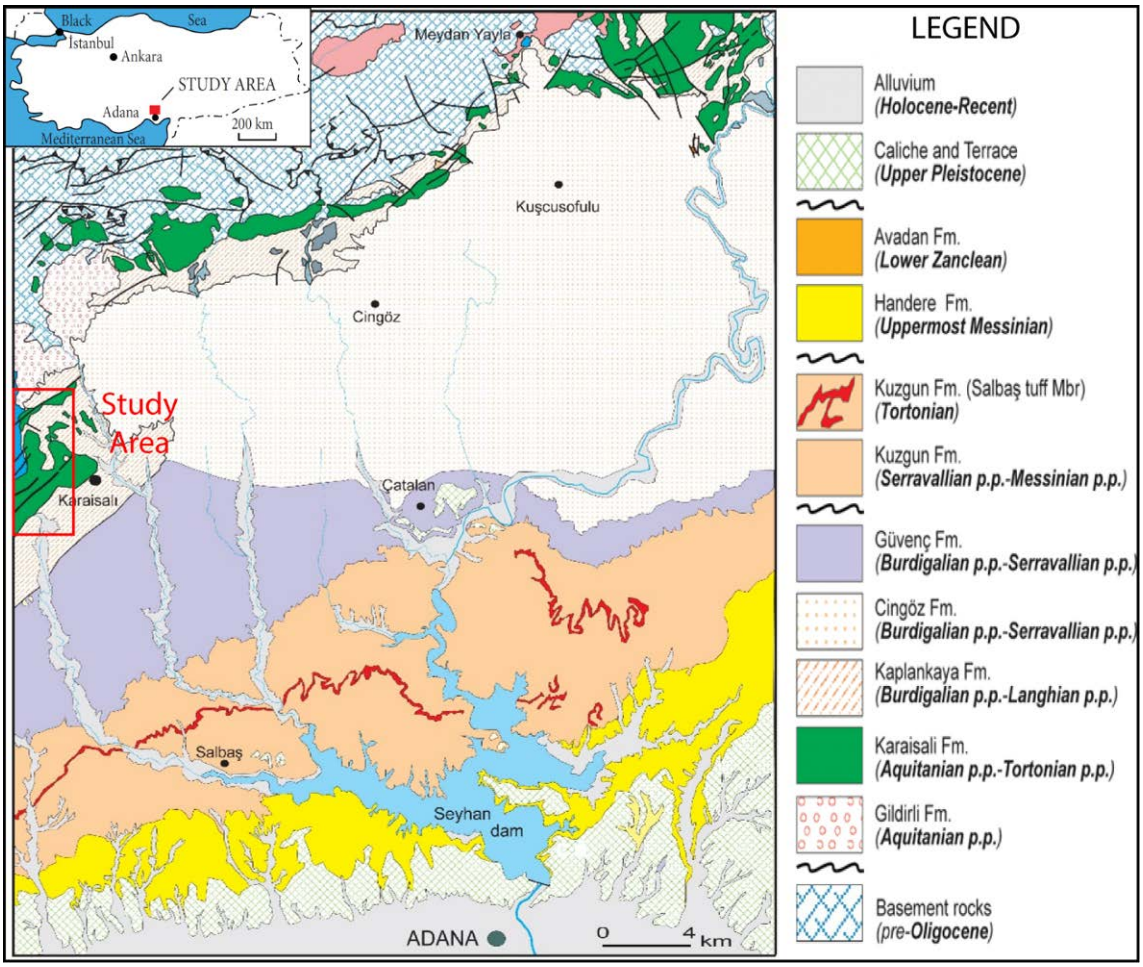


Figure 6: Geological map of the Adana Basin (after Yetis and Demirkol, 1986; Unlugenc, 1993; Yetis et al., 1995; Faranda et al., 2013).

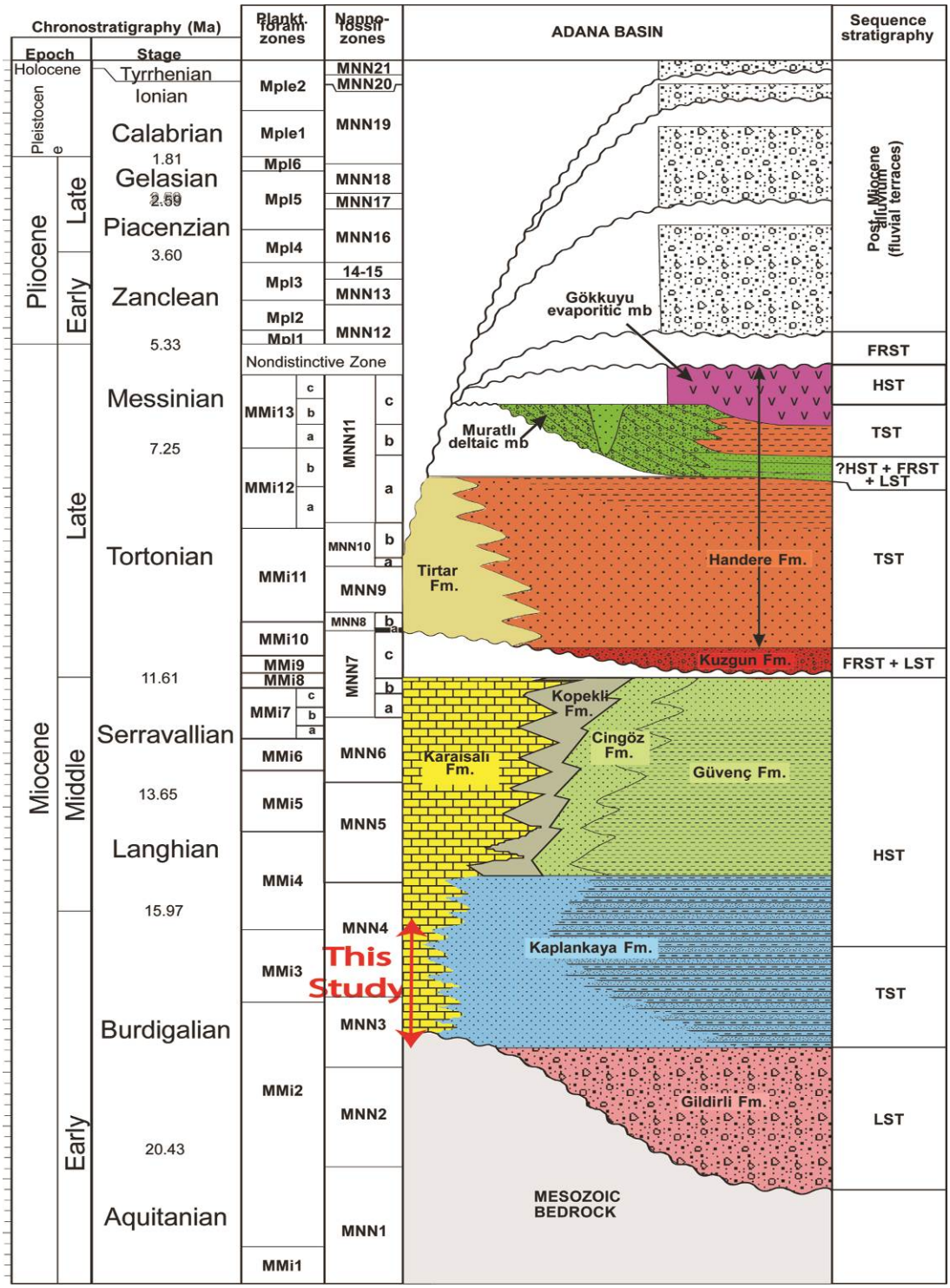


Figure 7: Generalized stratigraphy of the Adana Basin (after Ilgar et al., 2013).

The Gildirli Formation consists of fining upward cycles with thicknesses of 2-20 m. The Gildirli Formation consists of fining upward cycles with thicknesses of 2-20 m. The typical cycle starts with polymict red conglomerates, pebbly sandstone, alternations of sandstone and siltstone, and cycle tops are represented by reddish brown parallel laminated mudstone (Yetis et al., 1995). Poorly sorted massive to thick bedded polymict conglomerates include limestone, chert, igneous, and ophiolitic clasts. Sandstones are also in polymict character with argillaceous matrix poorly sorted and regular bedded (Gorur, 1985; Yetis et al., 1995; and Derman and Gurbuz, 2007). The formation shows varying thickness up to 300 m in the troughs and few meters in paleotopographic highs (Yalcin and Gorur, 1984). It laterally and vertically interfingers the transgressive basal conglomerates of the Kaplankaya Formation and exposed in the north of the study area as polymict reddish brown to reddish yellow colored conglomerates and sandstones alternating with siltstones and mudstones (Figure 8). In other regions of the study area, the substratum was overlain unconformably by the reefal carbonates or the transgressive conglomerates.

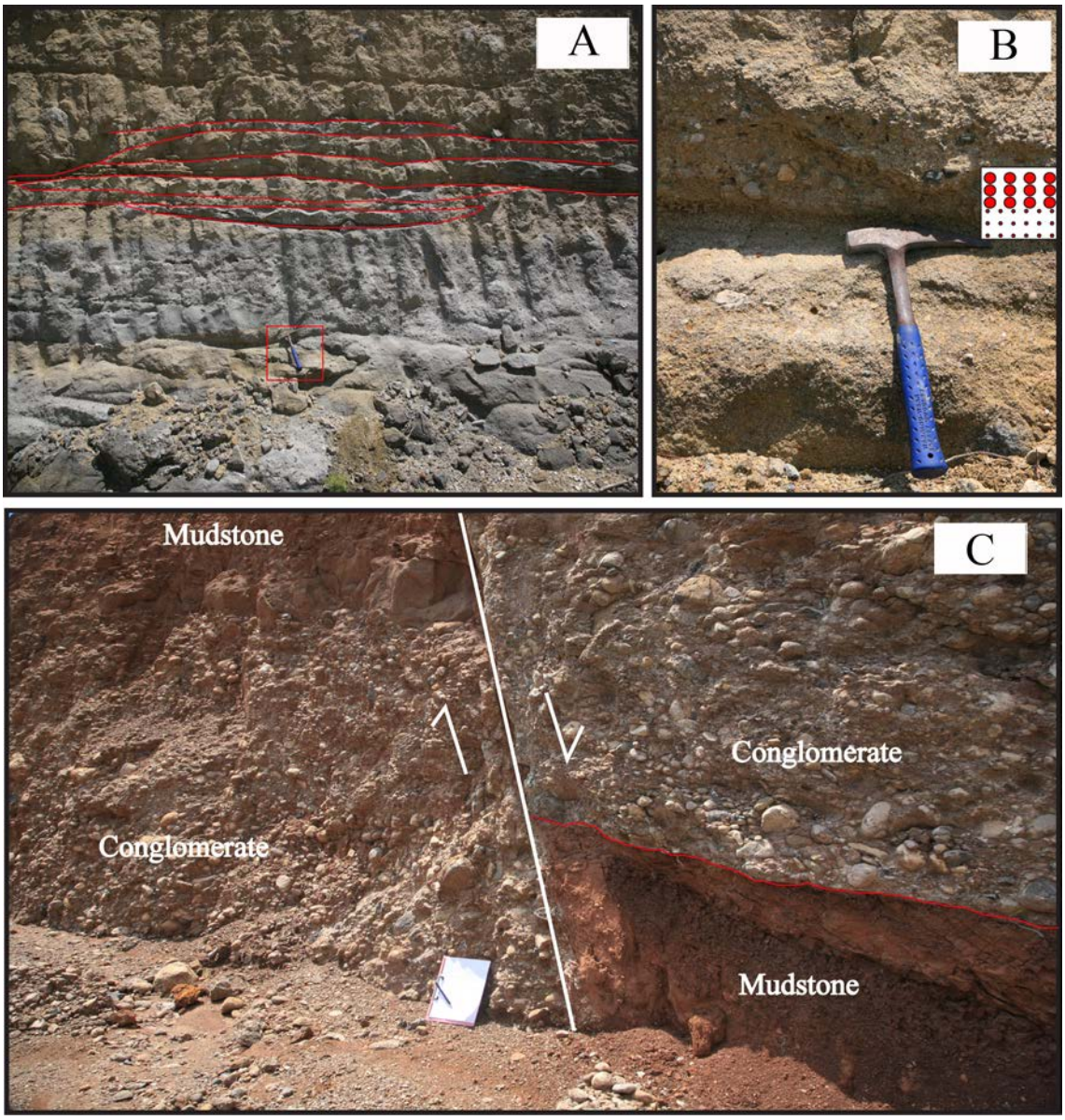


Figure 8: (A) Poorly developed channel geometry in the Gildirli Formation – sandy to muddy matrix and moderately sorted. (B) (Close up view) Reverse grading indicating debris or grain flow – polymict pebble sandstone – relatively rounded clasts – distal to the source. (C) Coarser relatively subangular conglomerates – proximal to the source, poorly sorted, reddish color indicating terrestrial environment, erosive cycle top (red line).

#### *2.1.2.2 Early to Middle Miocene Deposits*

The eustatic sea level rise during the Miocene transgression (Schmidt, 1961; Yetis 1988; and Yetis et al., 1995) resulted in a shallow marine environment in the Adana Basin. The late Aquitanian to early Langhian Kaplankaya Formation consists of basal conglomerates, fossiliferous sandstones, siltstones, mudstone, and marls. The lower parts of the formation contain coarse sandstone to siltstone with skeletal and non-skeletal clasts of Cretaceous carbonate mudstones (Gorur, 1985 and Yetis et al, 1995). The thickness of the formation is 5 to 100 m and mainly controlled by the paleotopography. It conformably overlay the Gildirli Formation or unconformably rest on the pre-neogene substratum rocks with angular unconformity. The Kaplankaya transgressive deposits pass both laterally and vertically into Karaisali reefal carbonates and basinal shales of the Guvenc Formation (Schmidt, 1961; Gorur, 1979; Yetis et al., 1995; and Nazik, 2004). According to Yetis et al. (1995), Unlugenc (1993), and Cronin et al. (2010), the Kaplankaya Formation was deposited during Burdigalian to early Langhian based on the studies of the foraminiferal and ostracod assemblages. The field observations showed that the Kaplankaya Formation is widespread in the study area and its characteristics were mainly depended on paleotopography. In the depressions, the lower part of the formation consists of poorly sorted siltstone-sandstone, pebble-cobble sandstone, and conglomerate with calcareous matrix. The clasts consist of dolomite, limestone, quartz, and locally chert. In the upper parts, the limestone content increases and it shows relatively well sorted clasts; whereas, the size and amount of non-carbonate clasts decrease. Cream colored argillaceous mudstone and argillaceous bivalve floatstone are the dominant subfacies in the upper sections showing typical transgressive cycles with an increase in the amount of Red Algae, Echinoid, Mollusks, and *Globigerina sp.* (Figure 9 and Figure 10). Those facies overlay the dolomitic Mesozoic basement either with an angular unconformity or nonconformity

representing the sequence boundary. The formation passes laterally and vertically to the younger Karaisali Formation. On the paleotopographic highs, the deposition of the Kaplankaya Formation is rare and if present it is relatively thin. Both on the paleo-highs and the upper parts of the paleo slope, these transgressive deposits are rich in skeletal clasts, and the size of dolomite and other basement clasts are smaller and more angular than the ones that accumulate in the depressions. The maximum size of the pre-Neogene clasts are 4-6 cm, but dominantly 1-2 cm. On the paleo-highs, the Kaplankaya Formation consists of basal transgressive conglomerates that grade vertically into mudstone and argillaceous floatstone underlying the Karaisali Formation. On the substratum paleoslope, Kaplankaya Formation is onlapping the deformed Cenozoic Formations.

The Burdigalian–late Serravalian (early Tortonian) Karaisali Formation is the main topic of this study and its lithostratigraphy will be explained in details in Chapter 3. The Karaisali limestones are commonly light gray, creamy white and yellowish gray massive, thick to medium bedded bioclastic carbonate unit locally rich in clays. The development of the small attached carbonate platforms was mainly controlled by the antecedent topography, water depth, subduction rates, and water temperature. The carbonate platforms preferentially developed on paleotopographic highs and gradually backstepped towards the northern margin of the Adana Basin under the combined effects of eustasy and regional subsidence. The Karaisali carbonates show an onlapping relationship with the pre-Neogene rocks on the paleoslopes.

In the past, the Karaisali Formation was interpreted as a platform carbonate succession with abundant reefal elements (Gorur, 1979). The evidences for this interpretation are based on the control of the paleotopography on the distribution of the reef complexes and sea-level control on the vertical stacking patterns. These packages can

be interpreted as depositional sequences depended on the bedding patterns and the geometry of the clinoforms (Derman and Gurbuz, 2007).

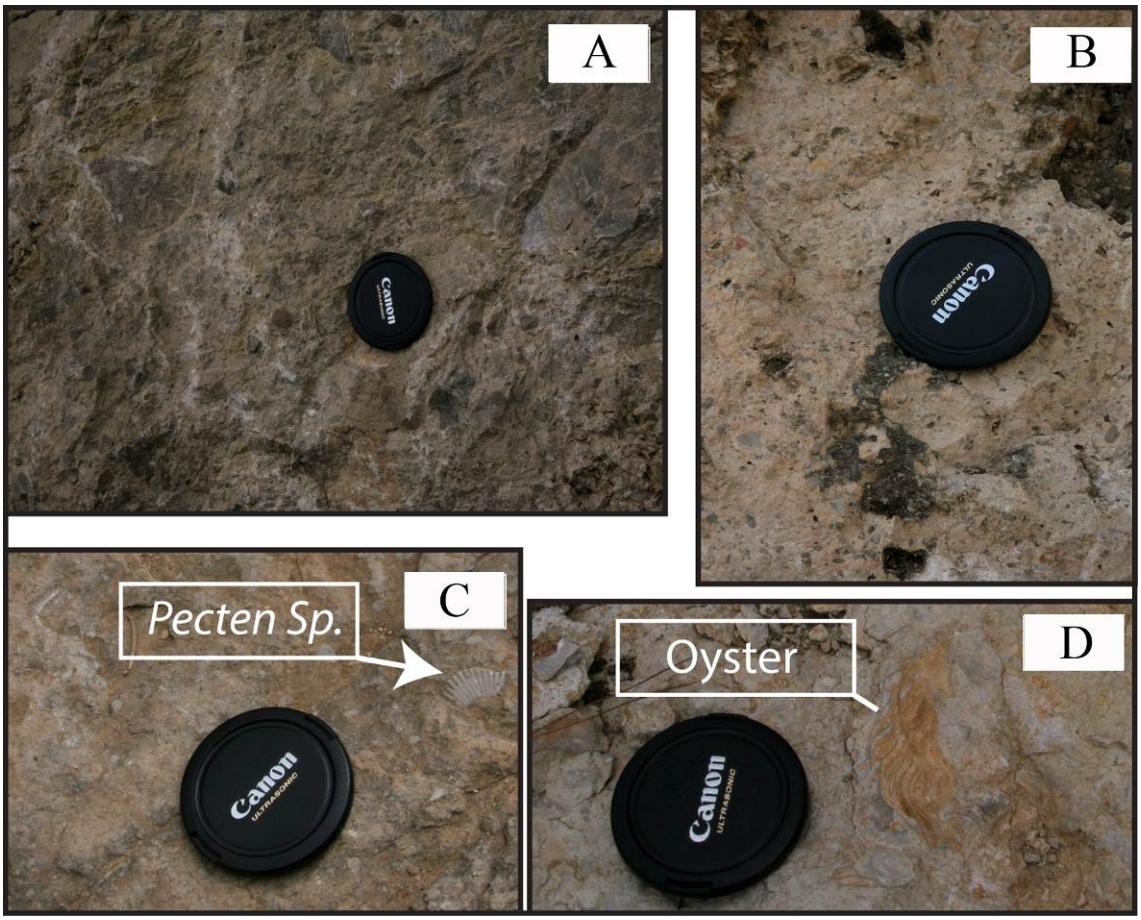


Figure 9: (A) lowermost part of the Kaplankaya Formation - poorly sorted pebble - cobble sandstone and conglomerate with calcareous matrix. The subangular clasts consist of dolomite, limestone, quartz, and locally chert. (B) Upper section of the lowermost part of the Kaplankaya Formation – the clasts are relatively moderately sorted and smaller. (C), (D) The uppermost Section of the Kaplankaya Formation – argillaceous mollusk floatstone - the basement clasts are not available anymore – carbonate content was relatively enhanced.


Figure 10: (A) Normal fault and resulted joint sets (upper left in the photo). (B) Orthogonal joint sets. (C) Bivalve floatstone.

Gorur (1979) subdivided the Karaisali formation into six subfacies;

1) Coralgal Packstone and Boundstone
2) Small Benthic Foraminiferal – Algal Packstone
3) Coralgal Wackestone – Packstone
4) Large Benthic Foraminiferal – Algal Packstone
5) Globigerinid Argillaceous Wackestone
6) Globigerinid Algal Packstone

This classification and identification of the subfacies of the Karaisali Formation have been almost one of the unique studies in the reef carbonates based on petrographic purposes. Furthermore, as far as the author knows, there have been no published studies presenting the measured sections in a detailed manner for these carbonates. Current study is based on the aforementioned classification stated by Gorur (1979), although subfacies have been modified to the certain level.

The Cingoz Formation was named, defined, and divided into three units by Schmidt (1961), namely as the Ayva, Topalli, and Kopekli Member. The third member - the Kopekli shale was included into the deep marine shale – the Guvenc Formation by Yetis et al. (1995). However, the field observations show that the Kopekli and Guvenc Formations have different characteristics and fauna content. The Kopekli shale is more proximal to the Karaisali carbonates, and it is rich in carbonate content and allochems; whereas the Guvenc Formation is located in deep marine basin, more distal to carbonate rocks, and rich in clay contents. Therefore, these two formations should be separated based on the depositional environments and petrographic properties.

The late Burdigalian–early Serravalian Cingoz Formation, which developed on the northwest margin of the Adana Basin, is thick deep water turbitidic sands with two

interfingering members: the Ayva and Topalli Members (Gorur, 1979; Gorur, 1985; Yetis and Demirkol, 1986; Unlugenc and Demirkol, 1988; Yetis, 1988; Unlugenc et al., 1991; Nazik and Gurbuz, 1992; Gurbuz and Kelling, 1993; Unlugenc, 1993; and Yetis et al., 1995). The thickness of the formation changes from 1000 meters in the west to 3200 metres in the east (Gurbuz and Kelling, 1993; and Yetis et. al, 1995).

The Cingoz Formation includes poorly sorted, channelized conglomerates, or sandstones which wedge out and interfinger interbeds of sandstone or shale (Derman and Gurbuz, 2007). The lowermost part of the formation – Ayva Member which is 200 m thick proximal turbidities (Gorur, 1985) represented by channelized conglomerates or sandstones which clasts are polymict–Paleozoic recrystallized limestone, Upper Cretaceous carbonate mudstone, or an igneous origin. The upper Cretaceous clasts are prevalent and derived from a local point in the fault controlled northern margin. The beds are moderately developed planar bedded or medium to large scale planar cross-stratified and slump deposits were locally developed (Yalcin and Gorur, 1984). These proximal turbidities laterally and vertically grade into the distal turbidities – Topalli Member – with a thickness of more than 50 meter (Gorur, 1994). The Topalli Member of the Cingoz Formation consists of moderately to well sorted, highly variable grain size, and variable centimeter scale bedded sandstones with erosive bases, scour and fill, flute, and groove casts. These sandstones interbedded with silty, calcareous, and fissile shale (Yalcin and Gorur, 1984). This shale is locally carbonaceous and includes quartz, calcites, feldspars, and smectite, illite, and kaolinite clay minerals (Gorur, 1994). According to the paleocurrrent analysis of Gorur (1985), turbidities were transported from the northern fault -controlled margin of the Adana Basin. The scarceness of reef debris in the turbidities

reveals that the reef was not developing while the turbidity currents were flowing (Gorur, 1994).

Gurbuz and Kelling (1993) specified two submarine fan systems developed in the middle Miocene in the north of Adana Basin. Both fans consist of channelized inner fan and middle fan with thickening upward cycles and siltstones and shales of the lower fan. The Cingoz Formation represents retrogradational fans that are partly contemporaneous and overlay the Kaplankaya, Karaisali, and Guvenc Formations (Yetis et al., 1995).

The Kopekli Formation that had been defined as lower slope deposits was included in the Guvenc Formation (Yetis, 1988; and Yetis et al, 1995). In this study, these formations are not united. The Kopekli Formation, which is the lowermost fore-reef deposit, consists of silty marl, shale, and siltstone that are rich in reworked skeletal grains and in situ planktonic foraminifera. The Kopekli and Karaisali Formations are time-stratigraphic units - the Karaisali Formation was developed in paleohighs, whereas the Kopekli Formation deposited in depressions (Figure 11).

The Burdigalian to lower Tortonian Guvenc Formation which was first defined by Schmidt (1961) is the deep basinal equivalent of the reef complexes. The formation is olive green colored, rich in planktonic foraminifera, consisting of shale, marl, and siltstone. It was interpreted as a distal fan deposit because of the alternation of marls and thin sandstones, sedimentary characteristics, and gradation into the Cingoz Formation (Yetis, 1988; and Yetis et al., 1995). The lowermost to middle section of the formation shows a decrease in thickness of the beds related to an increase in the water depth. The middle to uppermost section displays abundant pyritization–poorly oxygenated environmental conditions. These basinal shales were overlain by storm–dominated shelf deposits (Gurbuz and Kelling, 1993). The other evidences of the shallowing upward trend

of the basin are the increased number of sandy detritus, benthic foraminifera, and the nannofossils at the uppermost section of the Guvenc Formation (Yetis et al., 1995).

The thickness of the Oligocene - early Miocene regressive deposits and early to middle Miocene transgressive deposits is 2.9 km (Yalcin and Gorur, 1984) or 4.6 km (Schmidt, 1961).

Figure 11: The Kopekli shale and silty marl alternating with Globigerina large benthic foraminiferal floatstone and Globigerina coralgal packstone.

#### *2.1.2.3 Middle Miocene to Pleistocene Deposits*

The late Serravalian to early Tortonian Kuzgun Formation was the first record of the emergence of the basin in the middle Miocene. The regression is shown up as the unconformity between the underlying basinal shales of the Guvenc Formation and overlying shallow marine to terrestrial deposits of the Kuzgun Formation (Yetis, 1988; Unlugenc, 1993; Yetis et al., 1995).

The Kuzgun Formation has been subdivided into 3 members; namely as, the Kuzgun, Salbas Tuffite, and Memisli Members (Yetis and Demirkol, 1986). The Kuzgun Member includes sandstones and sandy to pebbly conglomerates with minor amounts of siltstones and shales. The deposits consist of fining–upward cycles that are conglomerates at the erosive bases and siltstones at the top (Burton, 2002). Yalcin and Gorur (1984) interpreted the Kuzgun Member as the prograding alluvial, deltaic, beach, bar, lagoonal, and shallow-water deposits. The skeletal grains showed that this member was deposited in late Serravalian to early Tortonian (Yetis, 1988).

The Salbas Tuffite Member includes volcaniclastic sandstones, siltstones, and shales in the lower part and Tortonian Tuffite Member in the upper part (Yetis, 1988).

The Tortonian – Messinian Memisli Member consists of fining–upward cycles – cross stratified conglomerates at the bottom and organic rich bioturbated siltstones at the top (Yetis et al., 1995; and Burton, 2002).

According to Ilgar et al. (2013), the deposition of the Kuzgun Formation was ended by a regional flooding associated with an early Tortonian sea level rise (Figure 7).

The Tortonian Tirtar Formation is a reefal carbonate deposit and the time transgressive Handere Formation was deposited in the basin interior and comprises shoreface sandstones passing upward into finer-grained sandstones, siltstones, as well as mudstones of an offshore-transition environment, and the offshore mudstones. These

offshore mudstones represent flooding of the basin in the late Tortonian (Ilgar et al., 2013).

The latest Tortonian – Messinian sediments recorded the sharp regression with the deposition of the uppermost Handere Formation which consists of shallow marine sandstones, siltstones, and conglomeratic deposits of sharp-based deltas associated with incised fluvial valley fills. These conglomerates and offshore clastic deposits were overlain by the Messinian gypsum evaporites (Figure 12) without showing any evidence of the Zanclean regional marine transgression (Ilgar et al., 2013). The Kuzgun Formation was conformably overlain by a cyclical succession of anhydrites and black shales corresponding to the Mediterranean Salinity Crisis (MSC) (Cosentino et al., 2010). A first intra-Messinian unconformity – Messinian Erosional Surface ($MES_1$) separates underlying primary lower evaporites and overlying resedimented lower evaporites (Cosentino et al., 2013). The second unconformity ($MES_2$) cuts the lower evaporites, resedimented lower evaporites, and pre-evaporitic marls. Coarse grained fluvial deposits rest unconformable on these evaporitic units (Cosentino et al., 2010; Cipollari et al., 2013; and Faranda et al. 2013). Zanclean regional flooding resulted in the deposition of the marine gray clays of the Avadan Formation postdated the littoral marine lower Pleistocene deposits (Cipollari, et al., 2013), on the opposite view of Ilgar et al. (2013). The last unconformity (Middle Pleistocene) lay between the marine sediments and Upper Pleistocene continental deposits (the Kuransa Formation) of the Seyhan, Ceyhan, and Tarsus rivers (Cipollari et al., 2013).

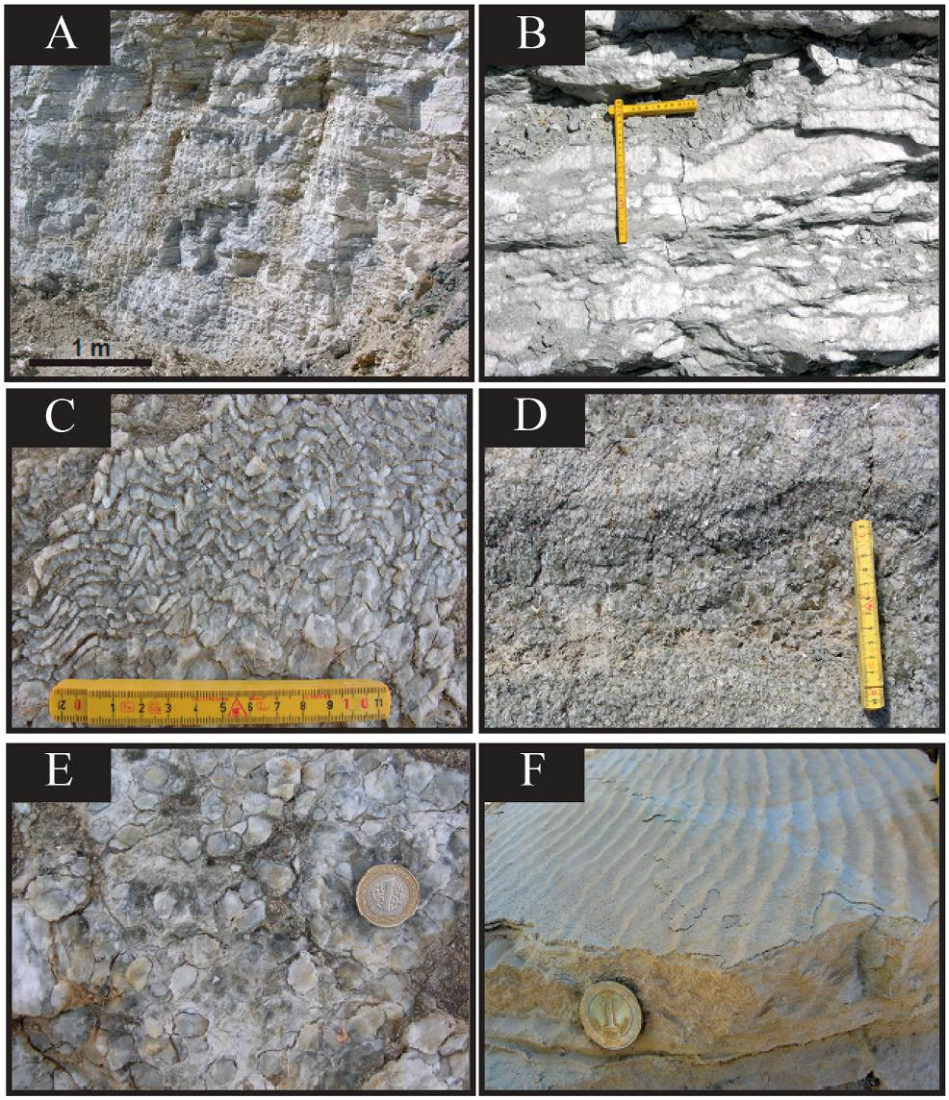


Figure 12: Messinian Evaporites in the Adana Basin. (A) Evaporites at the top of the Handere Formation (B) Enterolithic Gypsum (C) Crystalline Gypsum with a Chevron Growth Structure (D) Crystalline Gypsum with a Grassy Growth Structure (E) Nodular Gypsum (F) Gypsarenite with Wave-ripple Cross Lamination (The coin is 2 cm) (Ilgar et al., 2013).

## 2.2 STRUCTURE

The main focus of this study is the stratigraphic architecture of the early Miocene carbonates of the Karaisali Formation. However, this study higlights the regional structural controls on the development of the carbonate platforms, therefore an overview of the structural history of the basin is warrented.

The Adana Basin is a large elongate trough bounded by Ecemis Fault Zone to the West, the Kozan Fault Zone and Taurides to the north; and Misis Structural High to the southeast (Figure 13). The basin is located in the west of the triple junction point of the East Anatolian Fault Zone, the Dead Sea Transform Fault, and the Kyrenian-Misis Thrust Zone. The Dead Sea Transform Zone (DST) and East Anatolian Fault Zone (EAT) are intraplate north-south and northeast trending sinistral strike slip faults, respectively (Bozkurt, 2001). The basin was affected by the collision of the Arabian and Eurasian plates, Hellenic-Cyprian subduction in the southwest and westward movement of the Anatolian microplate with the North and East Anatolian Transform Faults, (NAT) and (EAT), respectively (Sengor et al, 1985; and Bozkurt, 2001).

### 2.2.1 Regional Structures of the Adana Basin

The primary structural objects are discussed separately to better understand the tectonic framework of the basin.

Northeast–southwest trending major fault zones (Kozan, Amanos-Larnaka, and Misis-Kyrenia Faults) are the splays of the East Anatolian Transform Fault and have been active since mid-Tertiary. These fault zones are controlling the structural framework of the Neocene basins (Sengor et al., 1985 and Aksu et al., 2014).

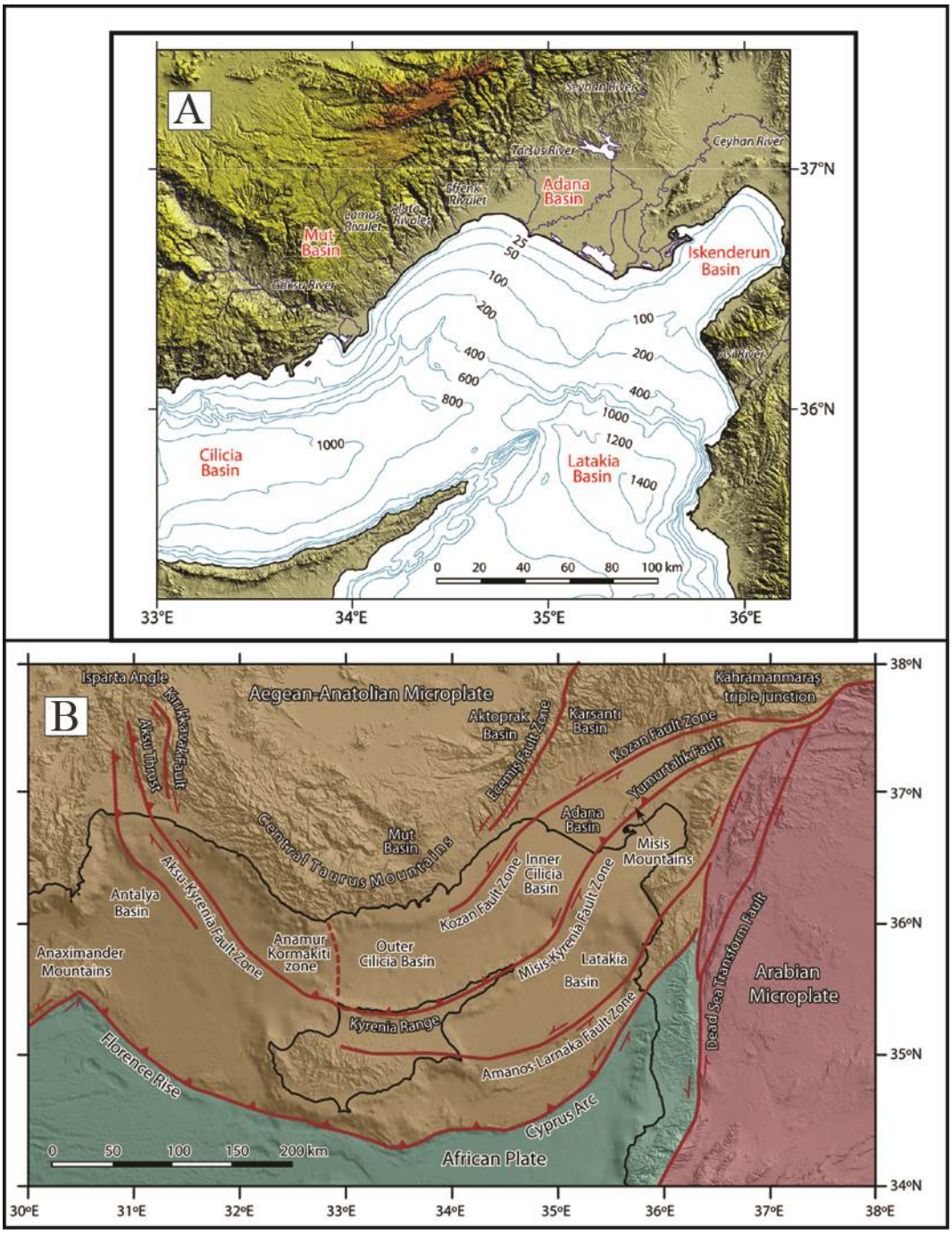


Figure 13: (A) Detailed bathymetry of the Adana-Cilicia Basin (Aksu et al., 2014). (B) Structural map and topographic map of southern Turkey showing the main structural elements and locations of the Neocene basins (half arrows indicate transform/strike slip faults) (Walsh – Kennedy et al., 2014).

Kozan Fault Zone

The Kozan Fault Zone, which is one of the splays of the East Anatolian Fault extending from the triple junction point, bounds the Adana Basin in north and west (Figure 13) (Duman and Emre, 2013; and Burton-Ferguson et al., 2005). The fault zone is characterized by the several ENE-WSW and NNE-SSW trending, high–angle extensional faults in the Adana-Cilicia Basin. Northeast trending with southeast dipping normal dip-slip faults cut down through Tortonian and lower Miocene deposits with steep dip, however the main phase of faulting occurred in upper Pliocene to Quaternary (Aksu et al., 2014).

In the north of the Adana Basin, Pliocene to Quaternary age northeast striking and southeast dipping, northwest striking and northeast dipping normal fault sets of the Kozan Fault Zone cut down through the Tortonian and lower Miocene deposits (Aksu et al., 2014).

Regionaly, the offset of the sinistral strike slip Kozan Fault Zone is 20 to 35 km corresponding to 0.43-0.75 cm/yr sinistral slip (Aksu et al., 2014).

Ecemis Fault Zone

The Ecemis Fault Zone (EFZ) is a tectonically active transtensional tectonic unit which is bounding and subdividing the Adana Basin in the north (Figure 13). EFZ is separating the rapidly subsiding Adana Basin from the more slowly subsiding Mut Basin to the west (Ozel and Pekcetinoz, 2007). This active fault is extending in the offshore in southwest of the Adana Basin (Doyuran et al., 1989).

The activity of the Ecemis Fault Zone started in earlier or mid–late Miocene (Jaffey and Robertson, 2001). It was mainly a sinistral strike–slip fault in the mid–late

Miocene time; however, it was dominated by extension during the Pliocene–Quaternary time (Jaffey and Robertson, 2001).

The sinistral offset of the fault has been about 65 km since late Eocene (Bozkurt, 2001 and Jaffey and Robertson, 2001).

Misis Structural High

The Misis Structural High is located in south and southeast of the Adana Basin (Figure 13). Misis – Andirin complex has been explained as an accretionary prism resulted from the collision of the Eurasian and African Plates during mid-Eocene to early Miocene (Aksu et al, 2005). In Langhian – Serravalian, post – suture shortening and southward thrusting were the main structural regime (Robertson et al., 2004). Thrusting, folding, and transpression were occasionally active as late as Tortonian, whereas sinistral strike slip faults dominated during Pliocene to Quaternary (Robertson et al., 2004). The Misis Structural High is separating the Adana from the Iskenderun Basins.

Taurus Mountains

The Adana Basin is bounded by the Taurus Mountains in north and northern west (Figure 13). This structural high is northeast – southwest elongated eastern segment of the Alpine fold and thrust belt. The Miocene basin fill of the Adana Basin was initiated by the load - induced flexure responding to thrusting in the Taurus Mountains to north (Williams et., 1995). The Taurus Mountains and the SE margin of the Central Anatolian Plateau have been uplifting relative to the Adana Basin by the Ecemis and Kozan Fault Zones starting in the late Tortonian (Cipollari et al., 2013).

Cyprus Arc

The Cyprus Arc is located in south of the Adana–Cilicia Basin is the convergent boundary between the African and Arabian Plates and Aegean–Anatolian Microplates

(Figure 13) (Bridge et al., 2005). The Cyprus Arc is a boundary separating two different regimes: transtensional structures dominated microplate in north and contractional microplate in south (Aksu et al., 2005). The uplift of the Cyprus and Kyrenia Range initiated in late Miocene with a decrease in rates in middle Pleistocene (Poole and Robertson, 1992; Kempler, 1998; and Harrison et al., 2004).

### 2.2.2 Tectonostratigraphy of the Adana Basin

There have been several studies about tectonic framework of the Adana Basin; however, the proposed models show different scenario for the basin development because of the structural and stratigraphic complexity of the basin.

Biju-Duval and Montadert (1977) and Vidal et al. (2000) described the basin as a marginal trough associated with the plate collision. Jackson and McKenzie (1984) interpreted the basin as a part of forearc - basin complex. Others have interpreted it as a pull apart basin related to the extension associated with the movement along the East Anatolian Transform Fault (Sengor et al., 1985; and Dewey et al, 1986). Kelling et al. (1987) and Gokcen et al. (1988) described the Adana Basin as a foreland basin dominated by transtensional regime. Kempler and Garfunkel (1994) interpreted that the basin was formed in an extensional regime. The Adana Basin was dominated by left-lateral transtension in the early Miocene, under transpression during the late Miocene, and under transtension from late Miocene to recent (Karig and Kozlu, 1990).

Pralle (1994) proposed a model for the development of the Adana Basin that involved thrusting of ophiolite and Taurides Mountains nappes during the Mesozoic to Paleocene followed by early to the middle Miocene extensional regime as foreland basin of the continuing thrusting, and ultimately followed by the Pliocene to recent uplift.

Williams et al. (1995) proposed a tectonostratigraphic model of the Adana Basin. Extensional faulting in the north of the basin created a half graben. The carbonate platforms of the Karaisali Formation developed on tectonic highs associated with the footwall crests of extensional faults. These early Miocene extensional faults developed due to the load-induced flexure resulting from the renewed thrusting in the Taurides to the north. The continuous thrusting to the north of the Adana Basin caused a major subsidence and a deep underfilled foreland basin. Pliocene to recent extensional faults were reactivated with relatively small offsets. The south and north of the basin were uplifted during Tortonian to Messinian and Pliocene, respectively.

Burton (2002) offered a highly contrasting model for the structural development of the Adana Basin which was developed as a foreland piggyback basin in the early to middle Miocene. This foreland basin was mainly controlled by the southward - propagating thrust sheets that were located in the north of the basin. The anticline crests of successive thrust sheets were the basement highs. The progressive descending of the thrust sheets towards south resulted in the development of the transgressive system tract reefal carbonates on these paleohighs. The successive reef deposits, which were drowned with the continued movement to the basin direction, were followed by highstand systems tract deeper marine deposits.

High resolution multi-channel onshore and offshore seismic data have recently enhances the understanding of the tectonic framework of the Adana Basin. Walsh - Kennedy et al. (2014) suggested that there had been an ancestral Miocene Basin consisting of the Adana, Cilicia, Mut, Latakia, Mesaoria, and Iskenderun Basins. This ancestral basin was then separated during late Miocene to Pliocene – Quaternary tectonic activities (Walsh – Kennedy et al., 2014). The Adana and Mut Basins were separated by the Ecemis

Fault Zone (Ozel et al., 2007). The Misis Structural High isolates the Adana and Iskendrun Basins.

Aksu et al. (2005, 2014), Bridge et al. (2005), and Walsh-Kennedy et al. (2014) interpreted the Adana Basin as an intramontane basin, currently located in a forearc setting. The Miocene transgressive sedimentation started on the lithotectonic units of the Pre-Miocene Tauride Mountains in a foredeep basin dominated by the compressional settings of the Tauride fold and thrust belt. Misis – Kyrenia Fault Zone that is corresponding to the culminations of the Tauride thrusting event divided the foredeep into two large piggy-back basins; namely as, the Adana-Cilicia and the Iskenderun – Latakia – Mesaoria Basins (Aksu et al., 2005). The thrusting stopped in the early Messinian followed by the NE-SW trending faults defining the boundary of the Adana and Cilicia Basins (Aksu et al., 2005) (Figure 14).

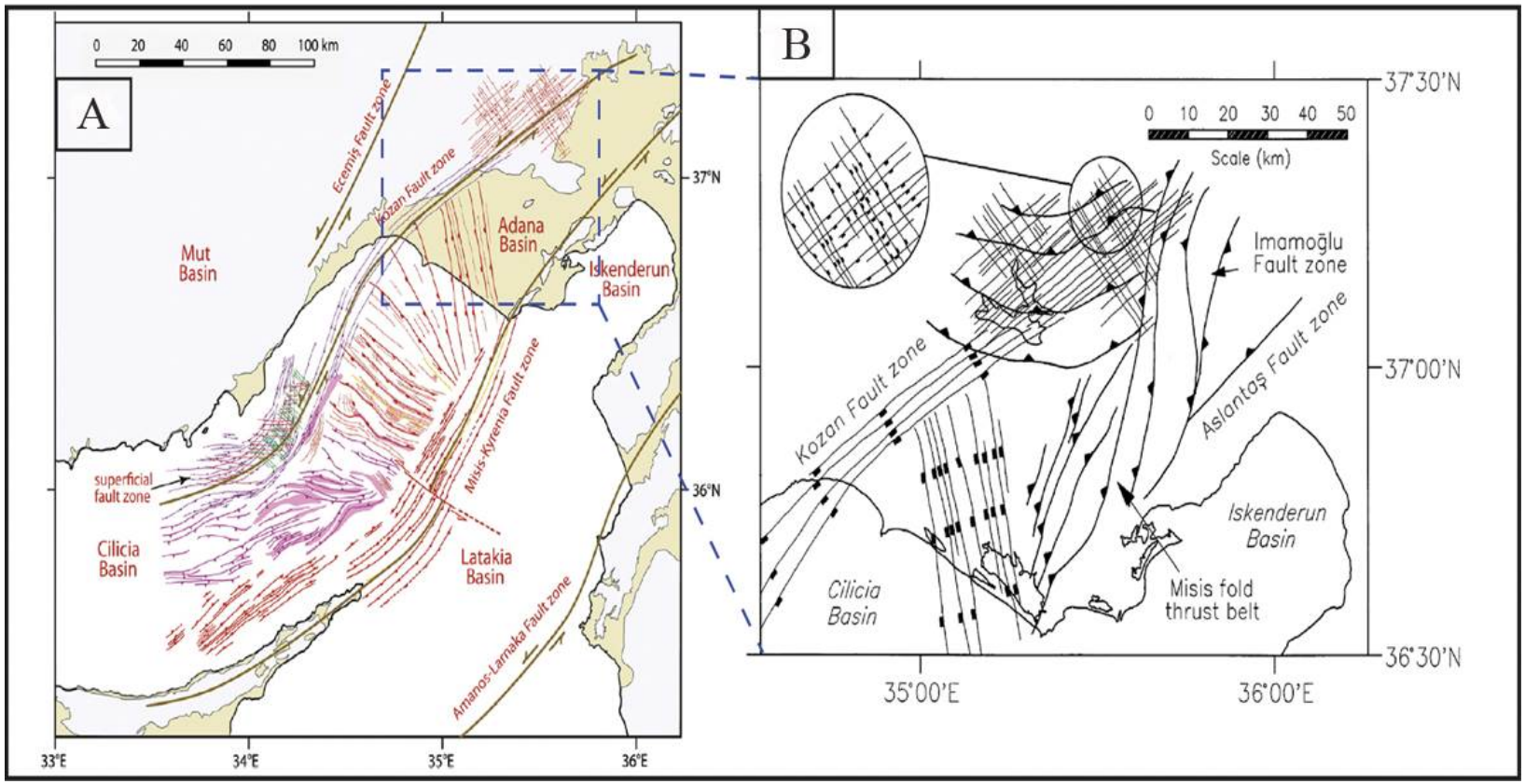


Figure 14: (A) Major structural elements of the Adana – Cilicia Basin (yellow areas show the onland Pliocene – Quaternary deposits) (Aksu et al., 2014). (B) (close – up view of A) Structural map of the Onshore Adana Basin (Burton – Ferguson et al., 2005) (filled rectangles and triangles are the ticks on the hanging walls of normal and thrust/reverse faults, respectively).

Ilgar et al., (2013) proposed a tectono-stratigraphic model concentrating on the late Miocene depositional events (Figure 15). The Adana Basin initiated as a wedge–shaped flake changed into the foreland by flexural subsidence controlled by the load of the SE - moving up faults, inflated, eroded, and followed by the Tauride front (Ilgar et al., 2013).

Thick Burdigalian – Serravalian deposits – the Kaplankaya, Karaisali, and Cingoz Formations are the results of the subsidence of the foreland basin and the middle Burdigalian marine transgression caused the drowning of a foreland shelf zone and succeeded by a late Budigalian to Serravalian normal regression (Ilgar et al., 2013).

The emergence of the basin related to a late Serravalian to early Tortonian eustatic sea–level fall is represented by the formation of the erosional unconformity, incision of the river valleys, and the deposition of the alluvial sediments of the Kuzgun Formation by the 2$^{nd}$ marine transgression in an early Tortonian sea-level rise. The reefal carbonates of the Tirtar Formation was developed as superimposing over the earlier reef complexes of the Karaisali Formation and contemporaneously the sandstones, siltstones, and mudstones of the Handere Formation of the off-shore transition environment and deep marine mudstones marking the maximum flooding surface in late Tortonian (Ilgar et al., 2013).

The piggyback basin developed within the Adana Basin by the latest Tortonian to early Messinian (about 7.8 to 6.4 Ma) orogenic thrusting and the resulting uplift originated the forced regressive sediments of the uppermost Handere Formation and the Misis Structural High emerged in the latest Tortonian to early Messinian (Ilgar et al., 2013). The foredeep was relatively subsided with the load of the thrust – sheets (post-thrusting isotatic subsidence) resulting in the deposition of the hypersaline marine transgressive sediments followed by the emergence of the basin and the development of the erosional

unconformity related to the late Messinian sea level fall of the Mediterranean Sea (Ilgar et al., 2013).

In conclusion, there had been a strong tectonic influence on the initiation, growth, and drowning of the carbonate platforms.

Burdigalian Karaisali reefal platforms preferentially developed in the paleotopographic highs in the study area. These tectonic highs were interpreted to be formed in response to either an extensional faulting (Williams et al., 1995) or a compressional regime (Burton, 2002; Aksu et al., 2005, 2014; Ilgar et al., 2013).

Continous thrusting of the Tauride Mountains towards SE resulted in the the uplift of the basin margin and subsidence in the Adana Basin (Williams et al., 1995, Burton, 2002; Aksu et al., 2005, 2014; Ilgar et al., 2013).

The growth strata was not observed in the platform margins in the study area, hence there were not syn-sedimentary normal faults during the development of the platforms in contrast to Gorur (1994). The ages of the small extensional faults observed in the thesis area are estimated to be Serravalian to Tortonian (personal communication with Turkish Petroluem Corporation).

The reefal platforms were drowned with the continued subsidence in the Adana Basin.

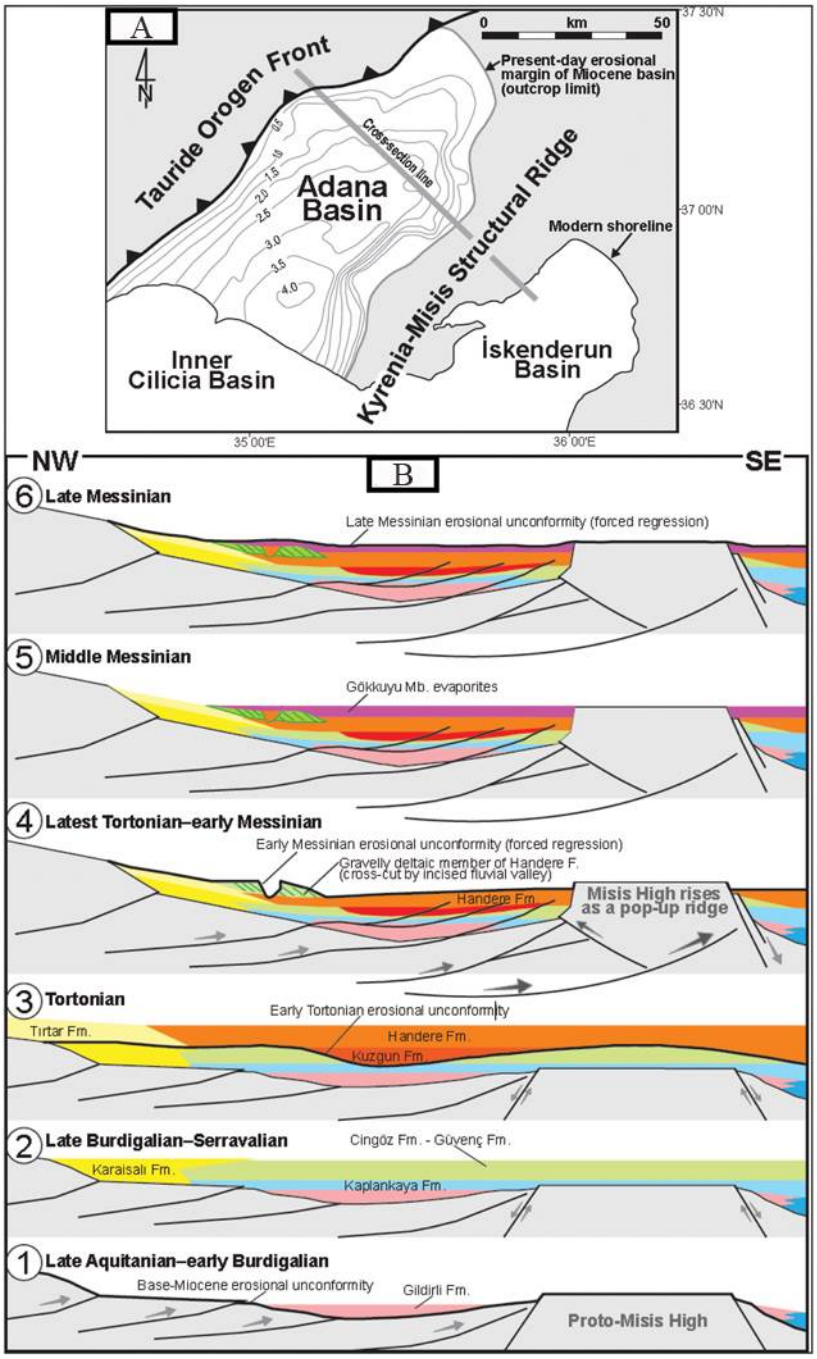


Figure 15: (A) Seismic map of the basement – Miocene unconformity and NE – SW cross – line showing the location of the model (contours showing the depths below sea level in seconds of 2 – way travel time), (B) Model of Miocene tectono - stratigraphic development in the Adana Basin (post – Miocene extensional regimes are not considered in the model) (Ilgar et al., 2013).

# Chapter 3 – Lithofacies and Sedimentary Environment Analysis

## 3.1 INTRODUCTION

The facies and subfacies in the carbonates of the Karaisali Formation were identified based on field observations. Gorur (1978 and 1994) previously defined six lithofacies in the Karaisali Formation.

In this study, ten facies and eight subfacies were identified based on the allochems, sedimentary structures, and sedimentary textures using the nomenclature of Dunham (1962) along with Embry and Klovan (1971) classifications.

## 3.2 FAUNAL CONTENT

The Karaisali Formation consists of diverse fauna that existed in the tropical and subtropical Miocene seas. In this section, the major skeletal grains and their distribution on the depositional profile will be discussed. The existence of certain allochems, their size variations, and other field observations are the key observation for interpretation of the identification of the depositional environment and the understanding of the paleoecology of the study area. Figure 16 shows the idealized distribution of the skeletal grains that was built based the model of Hallock and Glenn (1986) and modified based on the field observations.

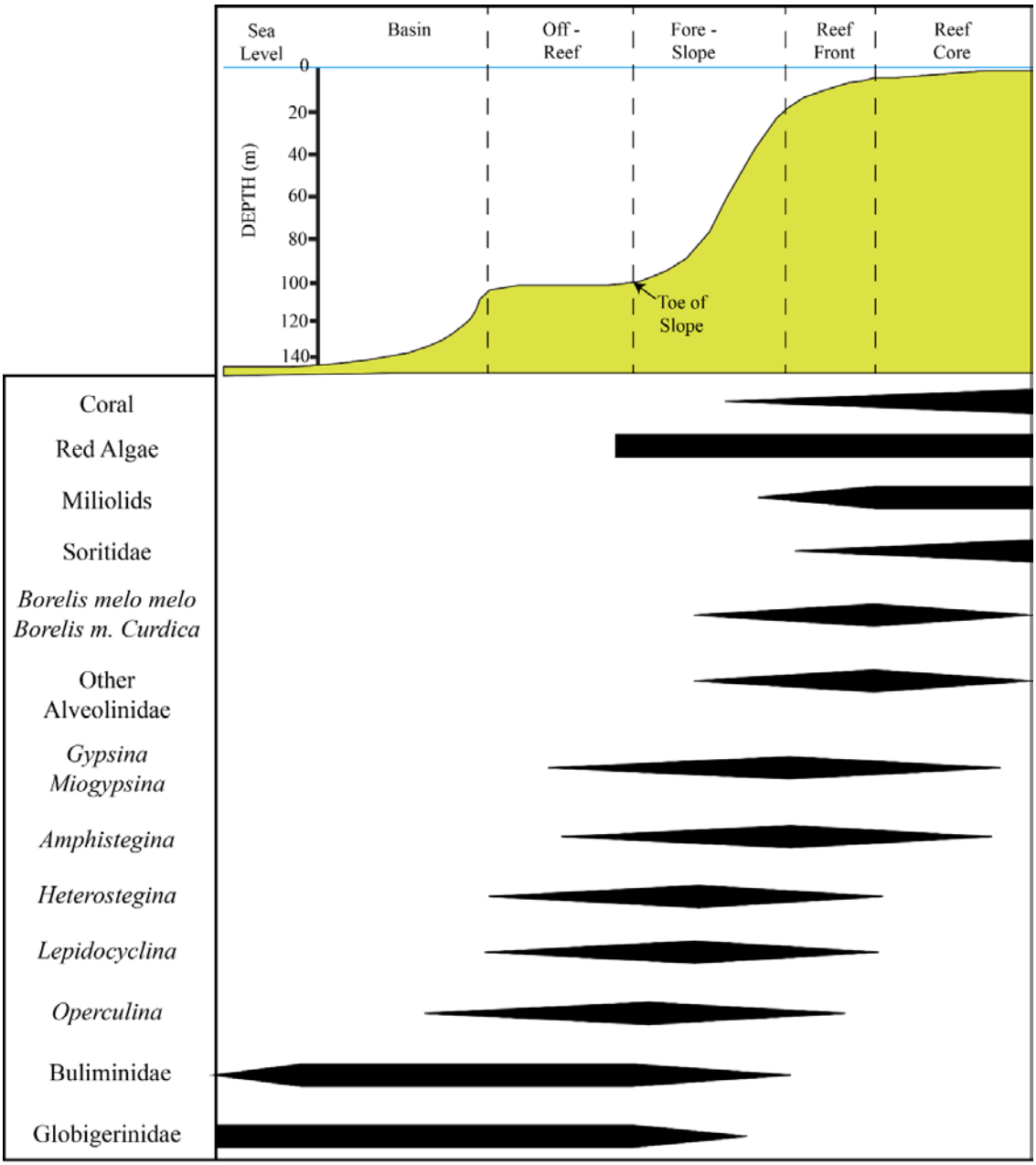


Figure 16: Distribution of the faunal elements of the Karaisali Formation (modified from Hallock and Glen, 1986).

**Coral**

Hermatypic coral reefs were the single type of corals observed in the study area where coral diversity was very low and dominated by *Porites*, whilst *Tarbellastraea and Favia* to a smaller extent. *Porites* and *Tarbellastraea* are the major coral types in Miocene times (Esteban, 1996). The preponderance of the *Porites* corals implies an impoverished environment for the coral growth (Bassant, 1999).

Domal, massive, and thin to medium branching *Porites* corals are the main reef builders and abundant in paleo highs that provided a clean shallow water environment suitable for the reef growth. On the other hand, in a muddy argillaceous setting, such as, in paleo - topographic slopes, *Porites* corals are only occasionally.

**Red Algae**

Coralline red algae are most common bioclast observed in the in the study area. It is found mutually in the platform interior, reef crest, slope and the basinal setting. Crustose coralline red algae observed in the study area consist of *Lithophyllum*, *Sporolithon*, and *Lithothamnion* species.

Encrusting forms are the main growth morphology in the reef crest and reef–fore as a result of the adaptation to high energy environment (Scholle and Ulmer- Scholle, 2003; Wilson and Vecsei, 2005; Flugel, 2009; Braga et al., 2010). Branching and articulated growth habits in the slope have indicated the evolution of the species in response to the environmental conditions such as low-light as well as low to moderate energy environments (Scholle and Ulmer- Scholle, 2003; Flugel, 2009). Rhodoliths are an excellent indicator of a hydrodynamic energy (Flugel, 2009). The frequency of overturning of the rhodoliths control the external shapes; branched and spherical rhodoliths are formed in shallow and quiet waters and in sheltered zones, whilst

ellipsoidal rhodoliths are commonly observed in higher energy environments (Flugel, 2009). And also, the internal growth patterns are controlled by the energy of deposition; the ellipsoidal, spheroidal, and laminar internal growth forms are abundant in higher water energy and the branching and columnar internal growth forms indicate low-energy environments (Piller and Rasser, 1996; Flugel, 2009).

Coralline red algae are photosynthetic-light dependent organisms; hence, the accumulation of algae in deep marine settings can be attributed to fragmentation and reworking of algal debris with the storm or turbidity currents and transportation to the toe of slope or deep water basin.

In conclusion, the coralline red algae is a very important organism for the reef complexes because its binding habit of the corals contribute significantly to the early cementation of the reef framework which makes them more resistant to the wave energy.

**Foraminifera**

It is the most helpful allochem for the paleoecological and paleodepositional interpretations (Bosence and Allison, 1995; Bassant, 1999; Beavington – Penney and Racey, 2004). Based on thin section analysis, foraminifera were divided into three main groups: small benthic foraminifera, large benthic foraminifera, and planktonic foraminifera.

Small benthic foraminifers represent the suborder Miliolina and the three main groups of Miliolids, Soritidae, and Alveolinidae that are common in protected environments and restricted settings (Janson, 2010; Bassant, 1999; Beavington – Penney and Racey, 2004); furthermore, Miliolids and rotaliids are typical allochems for the low-energy settings during highstand periods (Saller et al., 1992; Wilson and Vecsei, 2005).

The Miliolids are typical for the most distal, whilst Soritidae is common in the most proximal within the quiet shallow water settings (Bassant, 1999).

Large benthic foraminifers are good paleoecological indicators (Hallock, 1979; Hallock and Glenn, 1986; Beavington – Penney and Racey, 2004). Large benthic foraminifers show the suborder hyaline walled Rotaliina and includes three main families; Amphisteginidae, Nummulitidae, and Lepidocyclinidae. The Nummulitidae observed in the research area are *Heterostegina sp.* and *Operculina sp.* since the Assilina and Nummulites became extinct in the early Oligocene and in the late Middle Eocene, respectively.

*Heterostegina sp. and Operculina* sp., present in the study area, showed variations in regular test size, i.e. smaller sizes in the proximal slope and larger sizes in the distal settings. In favorable environmental settings, foraminifera are expected to mature relatively fast and hence, to have smaller test sizes (Hallock and Glenn, 1986). Therefore, proximal slope settings are favorable environmental settings for foraminifera with relatively higher nutrient supply, enhanced symbiotic relationship with red algae, high – light intensities, and other factors in the euphotic zone. On the other hand, unfavorable environmental conditions bring about larger foraminiferal tests and slowly growing rate, as in the oligotrophic zone (Bradshaw, 1957).

Buliminidae are the benthic foraminifers that were observed in deepest fore-slope along with basin settings and often found together with planktonic foraminifera that are mainly represented by Globigerinidae. Various encrusting foraminifers, developed in different settings, are dominantly associated with crustose coralline red algae in the reef core forming multilayered encrustations and a rigid reef framework. Encrusting foraminifera was also seen in the rhodoliths.

**Other Skeletal Grains**

Field observation along with the microscopic investigations indicated the presence of diverse fauna consisting of various allochems including mollusks, bryozoans, echinoderms, ostracods, brachiopods, and worm tubes. Of these allochems, bryozoans have large varieties – mainly encrusters and ramose forms. Mollusks – mainly pelecypods with lesser amounts of gastropods and scaphopods – were present in the region extending from the reef core to the lower slope.

## 3.3 FACIES DESCRIPTIONS (SEE TABLE 1)

Table 1 presents the facies characteristics of Karaisali Formation and Kopekli Formation.

### 3.3.1 Facies A, Subfacies $A_1$, and Subfacies $A_2$: Coralgal Framestone/Boundstone Platey Coral Framestone

The lithofacies is cream to creamy grey colored, mainly massive to locally thick bedded reefal limestone with diverse fauna. The fabrics of the reef core facies are boundstone, framestone, and bafflestone (Figure 17).

The diverse fauna includes in situ corals, encrusting, branching, and articulated coralline red algae, encrusting foraminifera and bryozoan, and minor amounts of small and large benthic foraminifera, echinoderms, and mollusks. Domal, massive, platey, and branched *Porites* corals form the main coral framework. Crustose coralline red algae, bryozoans, and encrusting foraminifera contribute significantly to the early cementation of the boundstone. Reworked coral, red algae fragments, and other allochems are filling the cavity spaces inside the coral framework. The matrix is composed of micrite and later diagenetic products - sparry calcite and microspar.

| Facies | Facies Name | Fabric | Sorting | Fauna | Sedimentary Structures Bedding Style | Other Features | Depositional Environment | Hydrodynamic Energy |
|---|---|---|---|---|---|---|---|---|
| A1 | Coralgal Framestone/ Boundstone | Framestone/ Boundstone | Poor | Corals, encrusting red algae, encrusting foraminifera, occasionally small benthic foraminifera, echinoderm, mollusk, bryozoan, and rare Ostracods | massive to thick Bedded bioturbated | In-situ framework, red algal encrustations, and occasionally argillaceous | Reef core (mostly) forereef | high |
| A2 | Platey Coral Framestone | Framestone | Poor to moderate | Corals, encrusting red algae, encrusting foraminifera, echinoderm, mollusk, bryozoan | platey - segmented | In-situ framework and occasionally argillaceous | Reef core to forereef | High to moderate |
| B1 | Coralgal MDP/ Wackestone | Mud Dominated Packstone/ Wackestone | Moderate to well | Coral, red algae, occasionally small benthic foraminifera, echinoderm, mollusk, and bryozoan | thick bedded | Reworked coralgal debris < 2mm and occasionally argillaceous | Reef core to uppermost slope (mostly) | low to moderate |
| B2 | Coralgal Floatstone | Floatstone | Poor to moderate | Coral, red algae, occasionally small benthic foraminifera, echinoderm, mollusk, and bryozoan, and rare Ostracods | thick bedded | Reworked coralgal debris > 2mm and occasionally argillaceous | Reef core to lower slope (mostly upper slope) | moderate to low |

Table 1: Facies Characteristics.

| Facies | Facies Name | Fabric | Sorting | Fauna | Sedimentary Structures Bedding Style | Other Features | Depositional Environment | Hydrodynamic Energy |
|---|---|---|---|---|---|---|---|---|
| C1 | Coralgal GDP | Grain Dominated Packstone | Poor to moderate | Coral, red algae, echinoderm, mollusk, bryozoan, and occasionally small and large benthic foraminifera | medium bedded | Reworked coralgal debris< 2 mm and occasionally argillaceous | Reef core to lower slope (mostly middle to lower slope) | High to moderate |
| C2 | Coralgal Rudstone | Rudstone | Poor | Coral, red algae, echinoderm, mollusk, bryozoan, and occasionally small and large benthic foraminifera | medium bedded | Reworked coralgal debris > 2mm | Reef core to lower slope | High to moderate |
| D1 | Large Benthic Foraminiferal Coralgal Floatstone | Floatstone | Poor | Large benthic foraminifera (Amphistegina sp., Heterostegina sp., Operculina sp., Lepidocyclina sp., and Miogypsina sp.), coral, red algae, echinoderm, mollusk, bryozoan, and occasionally small benthic foraminifera | medium to thick bedded | Reworked coralgal debris > 2mm and large benthic foraminifera either in situ or reworked | Reef core to slope (mostly upper to lower slope) | moderate |

Table 1: cont.

| Facies | Facies Name | Fabric | Sorting | Fauna | Sedimentary Structures Bedding Style | Other Features | Depositional Environment | Hydrodynamic Energy |
|---|---|---|---|---|---|---|---|---|
| D2 | Large Benthic Foraminiferal Coralgal Packstone | Packstone | Poor | Large benthic foraminifera (Amphistegina sp., Heterostegina sp., Operculina sp., Lepidocyclina sp., and Miogypsina sp.), coral, red algae, echinoderm, mollusk, bryozoan, and large benthic foraminifera | thin to medium bedded | Reworked coralgal debris < 2mm and large benthic foraminifera either in situ or allochthonous | Upper to lower slope | moderate |
| E | Small Benthic Foraminiferal Coralgal Packstone | Packstone | Moderate to well | Small benthic foraminifera (Borelis melo Fichtel and Moll, Borelis curdica Reichel, and other Alveolinids, locally Soritidae, Spiroloculina sp., Triloculina sp., and other Miliolids, Rotalia sp.), coral, red algae, mollusk, bryozoan, and benthic foraminifera | medium to thick bedded | Autochthonous small benthic foraminifera deposited in sheltered zones within the reef frameworks or allochthonous transported by wave turbulence or currents | Platform interior to forereef | Moderate to Low |
| F | Planktonic Foraminiferal Coralgal Packstone | Packstone | Moderate | Planktonic foraminifera (Globigerinidae), coral, red algae, echinoderm, mollusk, Serpulid tubes, Bulminid foraminifera, and occasionally small benthic foraminifera | thin to medium bedded locally ripple laminated | In-situ accumulation of planktonics and reworked reef debris | Openshelf (during drowning) to lower slope | low |

Table 1: cont.

| Facies | Facies Name | Fabric | Sorting | Fauna | Sedimentary Structures Bedding Style | Other Features | Depositional Environment | Hydrodynamic Energy |
|---|---|---|---|---|---|---|---|---|
| G | Planktonic Large Benthic Foraminiferal Coralgal Packstone | Packstone | Moderate | Planktonic foraminifera (Globigerinidae), Large benthic foraminifera (Amphistegina sp., Heterostegina sp., Operculina sp., Lepidocyclina sp., and Miogypsina sp.), coral, red algae, echinoderm, mollusk, bryozoan, Bulminid foraminifera, Serpulid, and worm tubes | thin to thick bedded locally ripple laminated | In-situ accumulation of planktonics, reworked reef debris, and in situ large benthic foraminifera or allochthonous transported by currents | Openshelf (during drowning) to lower slope | low |
| H | Argillaceous Coralgal Wackestone | Wackestone | Moderate to well | Planktonic foraminifera (Globigerinidae), coral, red algae, echinoderm, mollusk, Serpulid tubes, and Bulminid foraminifera | thin to medium bedded locally ripple laminated | In-situ accumulation of planktonics and reworked allochthonous debris | Lower slope to deep marine | low |
| I | Marine Shale/Marl/Siltstone | | | | thin to medium bedded | allochthonous | Lower slope to deep marine | low |
| J | Debris Flow/Slumps/ Rock Fall | | Poor | | | Debris/Gravity flow | Middle to lower slope | |
| K | Bivalve Floatstone | Floatstone | Moderate to well | Oysters and Pecten sp. with red algae fragments | medium bedded | Allochthonous Autochthonous | Forereef to Slope | low to moderate |

Table 1: cont.

Figure 18A shows the coralgal framestone composed of locally burrowed *Porites* head corals encrusted by crustose coralline red algae along with thin branching *Porites* corals and mollusks. Thin section images of the coralgal boundstone are illustrated in Figure 19A. The coral was encrusted by crustose coralline red algae (CCRA) and Planorbulinid foraminifera (P) and bioturbated by mollusks (B). Later, micrite filled the burrows. Presence of organic matter or dead oil (DO) in interparticle porosity is common in coralgal boundstone facies. Microspar (MC) and sparry calcite cement were the later diagenetic products. Figure 19D illustrates the multi – layered encrustations in the coral algal boundstone.

## Interpretation

As a response to the hydrodynamic energy, the corals have dominantly branching and platey morphology on the reef-front and massive to dome shape on the reef crest. The hydrodynamic energy in the reef core is medium to high, whilst it is low in the lower slope settings. The platey corals do not only exist in the lower slope environments, but they are also present in the reef crest since they are highly resistant to the wave energy (Bassant, 1999). The coralgal boundstone and framestone facies occasionally developed in an argillaceous matrix in the lower slope settings and planktonic foraminifera and thin branching *Porites* corals are the diagnostic allochems of these settings.

Figure 17: Platey coral framestone.

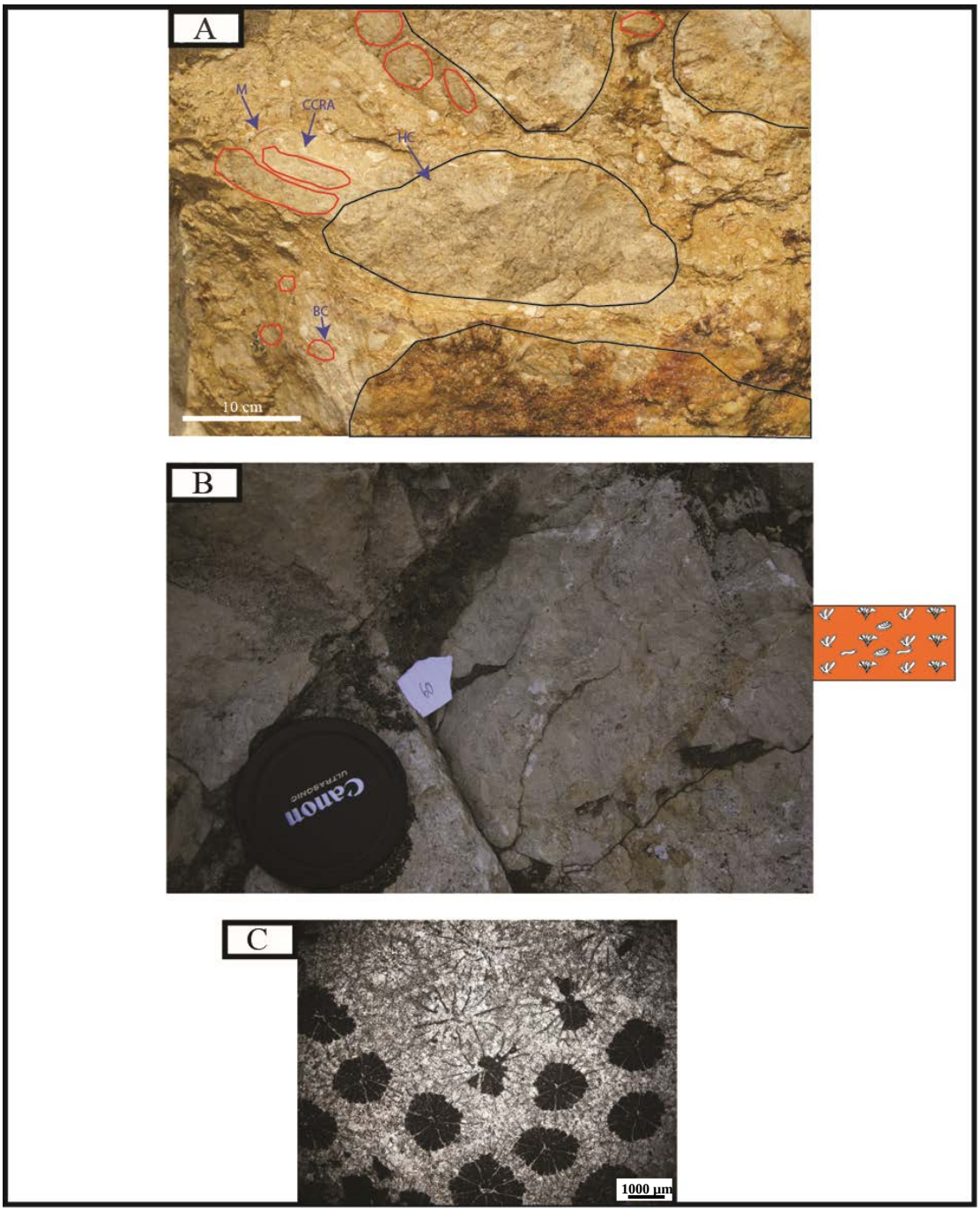


Figure 18: Thin section photomicrographs of coralgal framestone. (A) Porites head corals (black) and thin branching Porites corals (red) (M: Mollusk, HC: Head Coral, BC: Branching Coral, CCRA: Crustose Coralline Red Algae). (B) Branching Porites Framestone. (C) Branching Porites Corals (micritization, LMC microspar and spar).

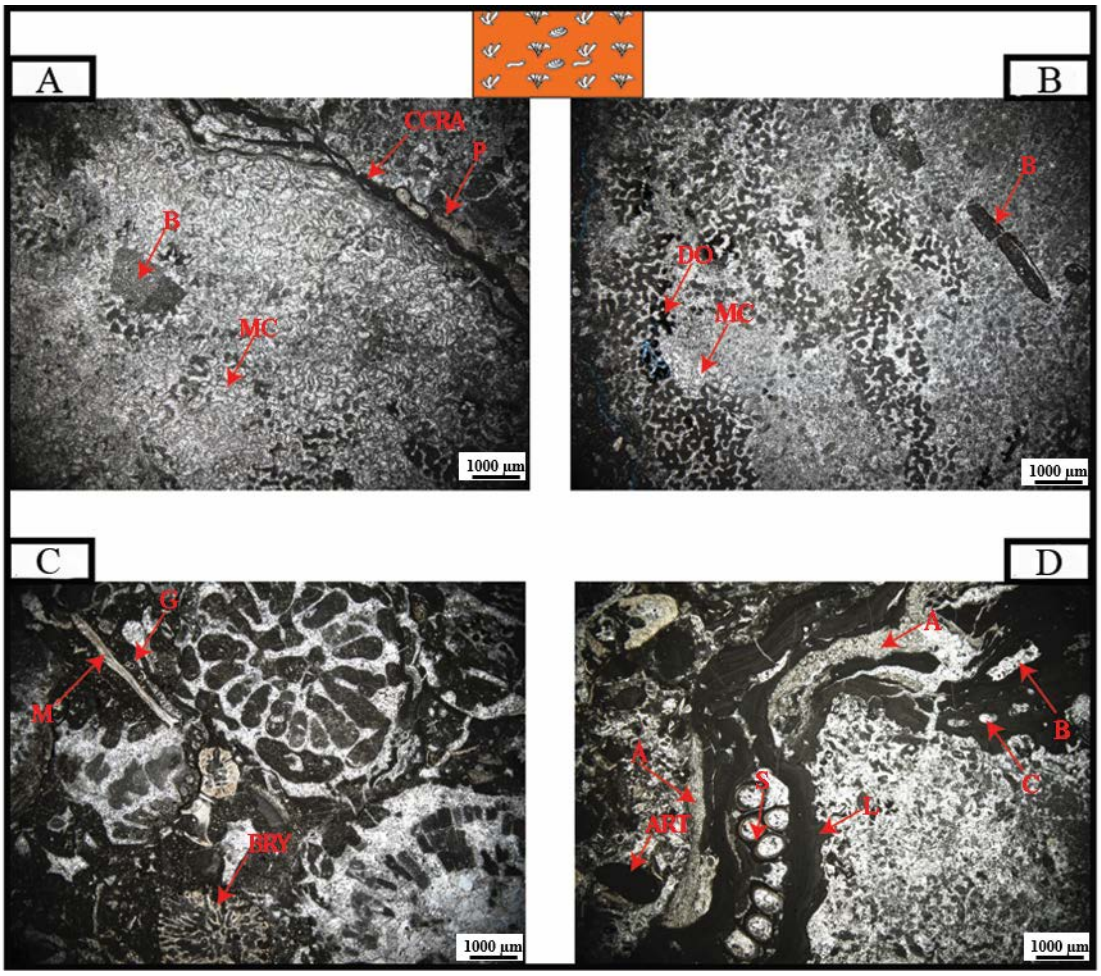


Figure 19: Thin section photomicrographs of coralgal framestone and boundstone (A) Brain coral encrusted by crustose coralline red algae (CCRA) and Planorbulinid foraminifera (P) (Mud – filled burrows (B), microspar calcite cement (MC)). (B) Dead oil (DO) or organic matter in interparticle porosity. (C) Argillaceous coralgal framestone (M: Mollusk, BRY: Bryozoan, G: *Globigerina sp.*). (D) Multi – layered encrustations (L: *Lithothamnion* red algae, A: Acervulinid foraminifera, ART: Articulated red algae, S: Serpulid worm tubes, C: Conceptacles of *Lithothamnion sp.*).

### 3.3.2 Facies B, Subfacies $B_1$, and Subfacies $B_2$: Coralgal Mud Dominated Packstone/Wackestone and Coralgal Floatstone

The facies is gray to creamy white colored, decimeter to meter well – bedded, and mud dominated limestone consisting of reworked reef debris; and in situ bryozoan, small and large benthic foraminifera, mollusk, echinoderm, rare ostracods, and brachiopods (Figure 20). The average grain size of the moderately to well sorted mud dominated packstone and wackestone is ~1 mm (grain sizes are ranging between a few microns and 2 mm). Grains of reworked red algae clasts are mostly subangular to occasionally subrounded. The grain size of the poorly to moderately sorted floatstone ranges from microns to 6 cm, with the average of 2 - 3 mm. The grain size and the mud content of the facies decrease from the upper slope towards the lower slope (Gorur, 1994).

**Interpretation**

The facies can be observed in the area ranging from reef core to upper fore–slope, but dominantly exists in the upper fore–slope and reef–front adjacent the reef framestone with the dip amounts up to $30^0$ – $40^0$. Furthermore, coralgal mud dominated packstone and floatstone were locally developed in the reef core (Gorur, 1994). The hydrodynamic energy is interpreted as low to moderate because of the high mud content and the environment of deposition, respectively.

The hydrodynamic energy is ranging from low to moderate because of its mud dominated fabric. Moderate energy is related to its depositional environment, i.e. close to the reef crest, depositional environment was affected by waves and storms. The coralgal floatstone locally includes rhodoids indicating the fact that hydrodynamic energy was periodically high and the rate of deposition was relatively slow for the multiple overturning of the red algae clasts and formation of the rhodoliths (Figure 21) (Bassant, 1999).


Figure 20: Outcrop photo showing coral algal floatstone - argillaceous lower section thickening upward.

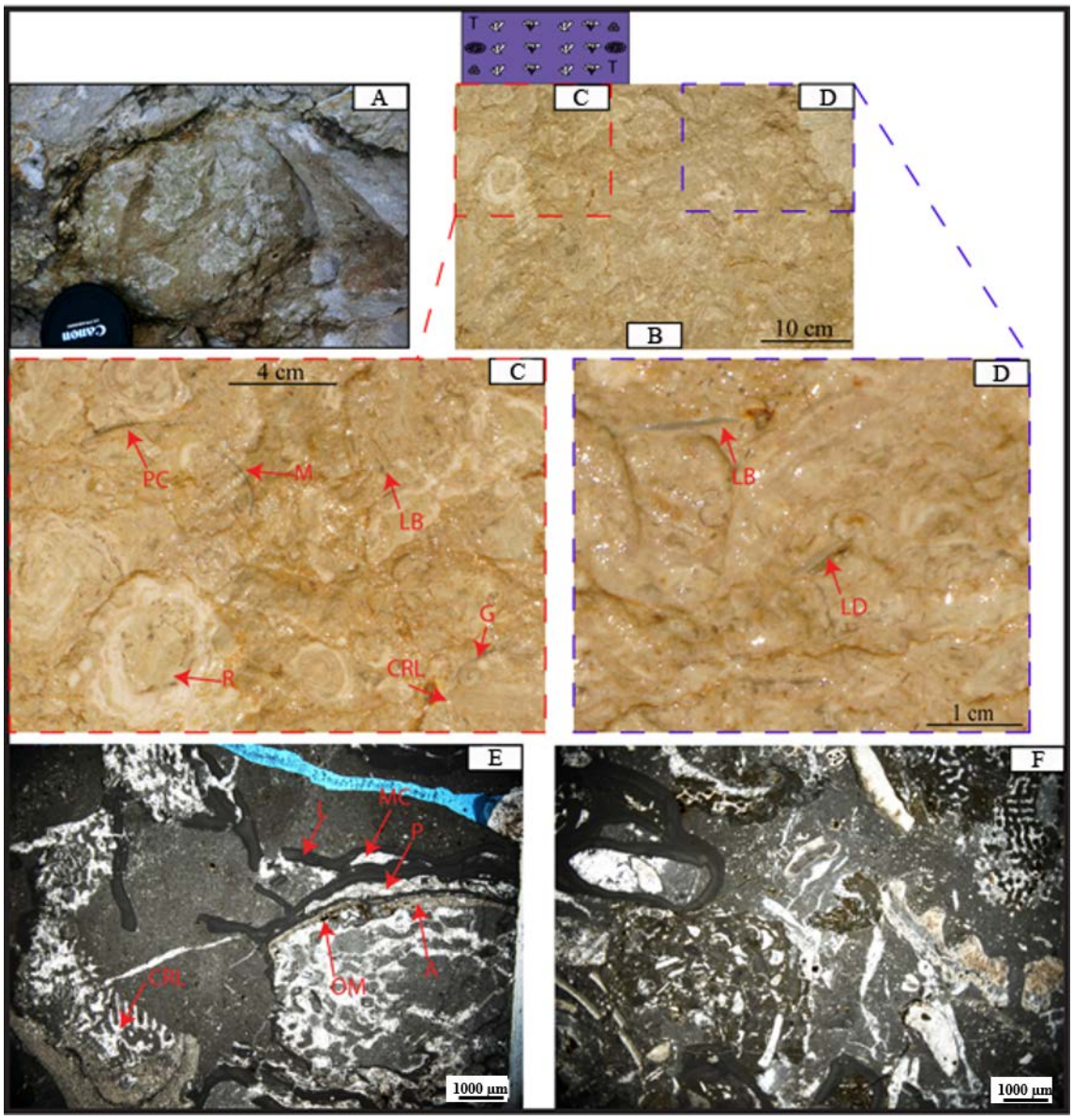


Figure 21: (A) and (B) Outcrop photo showing coral algal floatstone – rhodoliths. (C) and (D) close up view of (B). (E) and (F) Thin section photomicrographs of coralgal floatstone - reworked coralgal fragments (CRL: coral, MC: microspar calcite cement, A: Acervulinid foraminifera, OM: organic matter, P: *Planorbulina*, L: *Lithophyllum* red algae, LB: large benthic foraminifera, PC: *Pecten sp*.,M: mollusk, R: rhodolith, G: Gastropod, LD: *Lepidocyclina sp.*) ((E) slightly argillaceous).

### 3.3.3 Facies C, Subfacies $C_1$, and Subfacies $C_2$: Coralgal Grain Dominated Packstone and Coralgal Rudstone

The creamy white to gray colored facies is thin to medium well bedded and poorly sorted bioclastic limestone including dominantly reworked coral and red algae fragments with minor amounts of mollusks, bryozoans, echinoderms, small and large benthic foraminifers (Figure 22 and Figure 23). Subfacies $C_1$ – coralgal gdp is relatively well sorted and thinner bedded with respect to Subfacies $C_2$ – coralgal rudstone which is consisting of poorly sorted reef debris with angular and sharp edges. The average grain size of the moderately to well sorted mud dominated packstone and wackestone is ~1 mm (ranging from few microns to 2 mm) and the grains of reworked red algae clasts are mostly subangular to occasionally subrounded in shape. For Subfacies $C_2$, grain sizes changes from microns to 8 cm with the average of 2 – 3 mm, whilst in the case of Subfacies $C_1$, grain sizes vary from a few microns to 2 mm. Both of them are occasionally argillaceous and include rhodoliths. The beds of Facies C exhibit dips up to $30^0$; $0^0 – 10^0$ in the reef core and $5^0 – 30^0$ in the reef-front and fore-reef. From the upper to lower fore-reef, the amount of coral debris gradually decreases and that of coralline red algae increases in Facies C.


Figure 22: Outcrop photo showing relatively thin bedded coral algal grain dominated packstone.

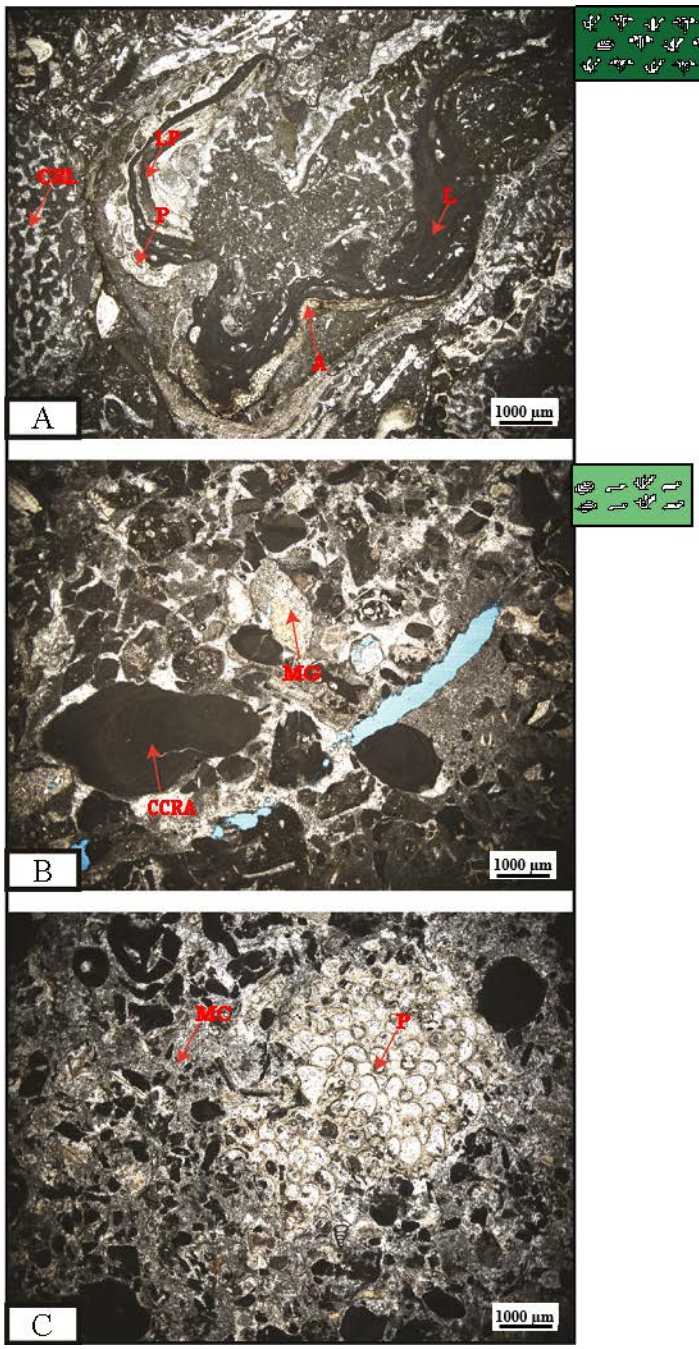


Figure 23: Thin section photomicrographs. (A) Coralgal rudstone. (B) and (C) Coralgal grain dominated packstone. (CRL: coral, MC: microspar calcite cement, A: Acervulinid foraminifera, MG: *Miogypsina*, P: *Planorbulina*, LP: *Lithophyllum* red algae, L: *Lithothamnion* red algae, CCRA: Crustose coralline red algae) ((A) slightly argillaceous).

**Interpretation**

Facies C has been interpreted to be deposited from the reef core to the lower fore-reef. Subfacies $C_1$ is the characteristic of the middle to lower fore-reef (Pomar et al., 1996; Esteban, 1996), whilst the coralgal rudstone was mainly deposited on the upper to middle fore-reef basinward side of Facies B, although there is no unique pattern. A common transition between Subfacies $C_1$ and Subfacies $C_2$ is that Subfacies $C_2$ grades into Facies B in landward direction and Subfacies $C_1$ in downdip direction. Both of the subfacies also occur in the reef core. The hydrodynamic energy for Facies C is interpreted as moderate based on the small amounts of mud in the matrix.

### 3.3.4 Facies D, Subfacies D1, and Subfacies D2: Large Benthic Foraminiferal Floatstone and Packstone

Facies D features gray to brownish gray colored, thin to thick bedded, and moderately sorted limestone consisting of dominantly in situ large benthic foraminifera and reworked reef debris; and less amounts of bryozoan, small benthic foraminifera, mollusk, echinoderm, and planktonic foraminifera.

Subfacies $D_1$ is more mud dominated and includes coarser reef debris; hence the rock exhibits floatstone fabric. The grain size varies from a few microns to 6 cm with an average of 2 - 3 mm. The fragments of coral and algae debris are angular to subrounded in shape. On the other hand, Subfacies $D_2$ is more grain supported and subrounded to subangular shaped reworked coralgal clasts are finer with a mean grain size of 1 mm. Facies D displays dip angles of $5^0$ to $25^0$ with the gradual decrease from upper fore-reef to the basin. Subfacies $D_1$ is medium to thick bedded, whilst Subfacies $D_2$ is thin to medium bedded (Figure 24).

There is an observable faunal change in Facies D from the upper to the lower fore-reef, i.e. Facies D includes relatively large amounts of *Amphistegina sp., coral fragments, Borelis Melo,* and Miliolids, whilst further downdip, there is an increase in the amounts of *Heterostegina sp. and Operculina* sp. which is accompanied by a gradual decrease in the amount of *Amphistegina sp.* and *Borelis Melo.*

## Interpretation

Facies D which has been interpreted as a fore-reef deposit grades into Facies C or B in the updip direction and Facies G in basinward direction. Subfacies $D_1$ and Subfacies $D_2$ were mainly deposited in the upper to middle fore-reef and the middle to lower fore-reef, respectively. Gorur (1994) described this facies as an off – reef deeper – water shoal deposits and similar facies in the adjacent Mut Basin is interpreted as shoal or channel fill deposits (Bassant, 1999).

The hydrodynamic energy is interpreted as low to moderate for the Subfacies $D_1$ because of its bimodal character, i.e. coarse skeletal clasts of coralgal debris and large benthic foraminifera floating in a mud dominated matrix. On the other hand, for the Subfacies $D_2$, deposition of grain dominated packstone indicates moderate energy environment. Large benthic foraminiferal facies is described as the deposits of the high energy environment adjacent the platform margin (Janson, 2010). During transgression, high-energy large benthic foraminiferal packstones or grainstones are deposited on the platform top by the oceanic currents and/or strong waves (Van de Weerd et al., 1987; Saller et al., 1992 and 1993; Saller and Vijana, 2002; Wilson and Vecsei, 2005). In the open shelf, large benthic foraminifera is also abundant (Beavington – Penney and Racey, 2004); however, the open shelf facies is included in Facies G because of the large amounts of planktonic foraminifers.

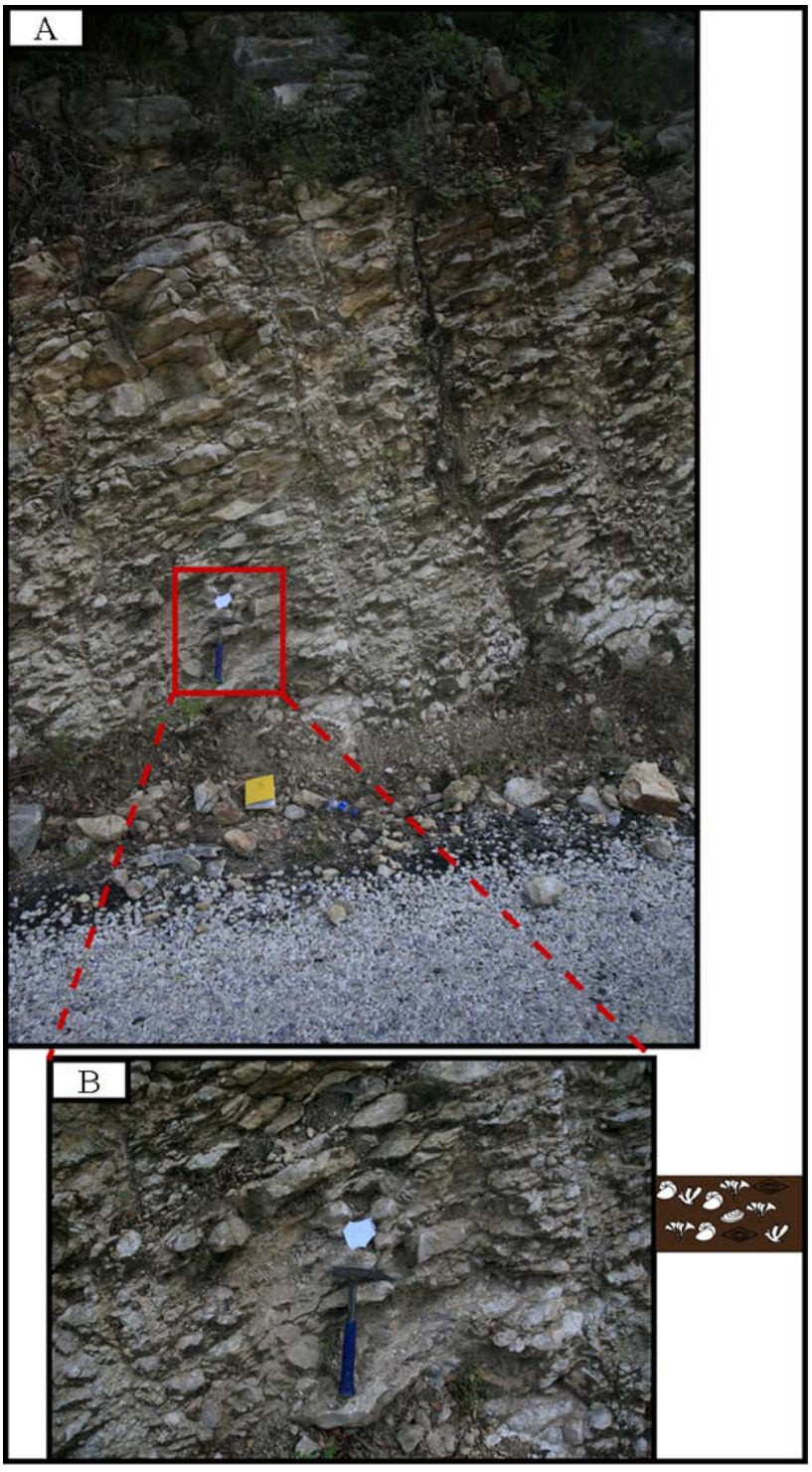


Figure 24: (A) Outcrop photo of large benthic foraminiferal packstone. (B) Close up view of (A).


Figure 25: Thin section photomicrographs of large benthic foraminiferal packstone (O: *Operculina sp.*, A: *Amphistegina sp*, L: *Lepidocyclina sp.*).

### 3.3.5 Facies E: Small Benthic Foraminiferal Packstone

The light gray to brownish gray moderately to well sorted facies is medium to thick bedded and occasionally thin bedded; especially, in the reef core. Facies E is composed of *Borelis melo,* other Alveolinidae, *Spiroloculina sp., Triloculina sp.,* other miliolids, Soritidae, *Rotalia sp.,* Textulariids, reef debris, and minor amounts of mollusks, bryozoan, and large benthic foraminifera.

Facies E exhibits a slight difference in fauna between the backreef, reef-front, and uppermost fore-reef. The reef core and backreef subfacies are richer in miliolids, whilst the reef-front to the uppermost fore-reef subfacies are enriched in Alveolinidae. Soritidae, which includes peneroplids and soritids, is a typical restricted platform or open platform skeletal allochem (Bassant, 1999; Beavington – Penney and Racey, 2004).

**Interpretation**

Depositional environment of Facies E is interpreted as low energy considering both the fauna and the mud content. However, as the grain supported subfacies deposited in the uppermost fore-reef includes mixture of restricted platform, shallow water, and deeper fore – reef skeletal allochems (Figure 26), these subfacies are likely to be deposited in a relatively moderate energy settings. All of the other subfacies of Facies E are deposited in quiet environments, either in the sheltered and baffled zone of the reef core, in the backreef or in a restricted platform. Hence, the fauna of these settings shows uniform shallow water bioclasts and mud dominated fabric (Figure 26).

The micritic envelopes developed around sea grass communities - soritids, peneroplids, miliolids, Alveolinidae, and Textulariids are the demonstrative forms for the recognition of the ancient sea grass habitat (Perry, 1999).

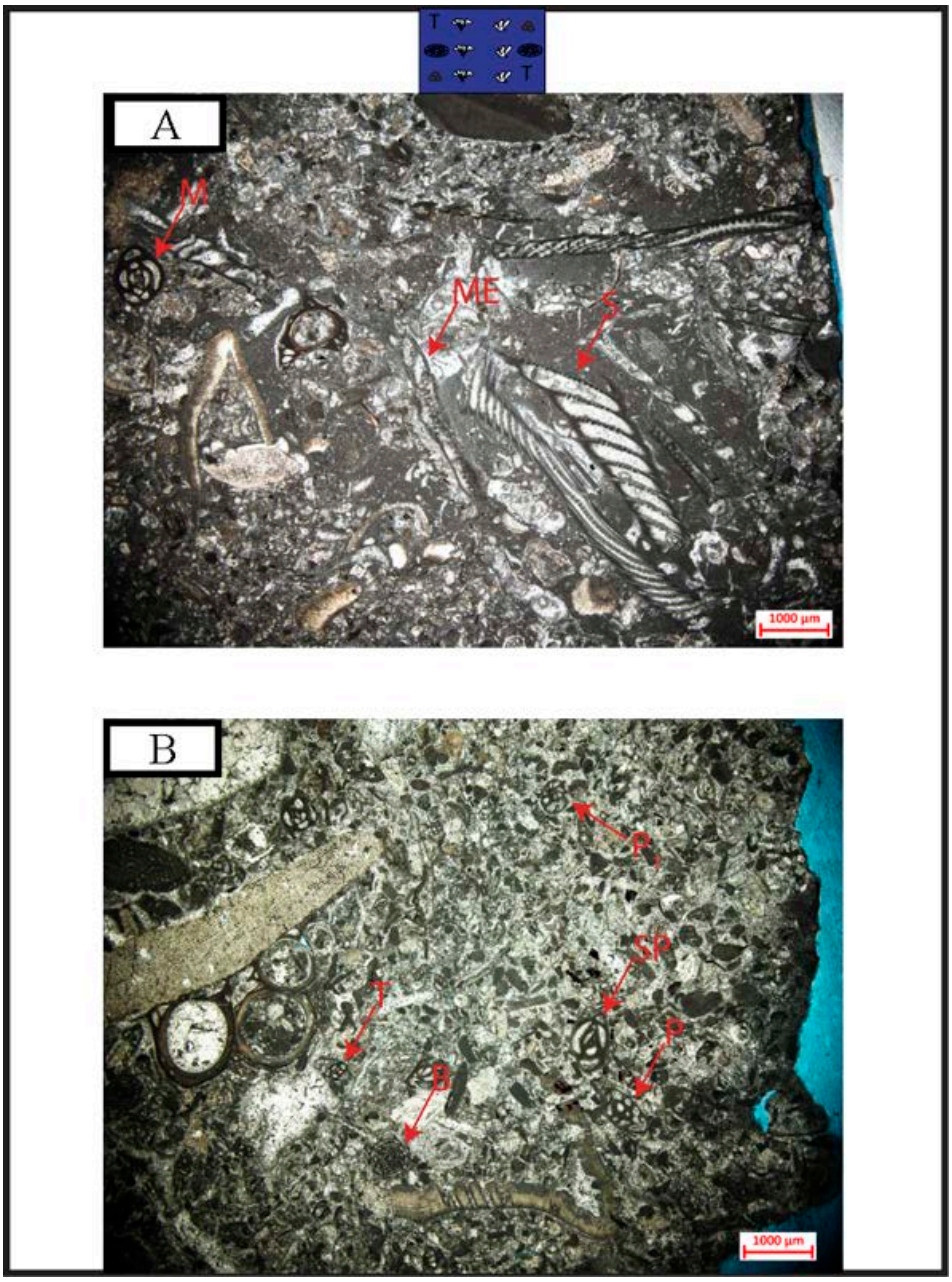


Figure 26: Thin section photomicrographs of small benthic foraminiferal packstone (S: Soritidae, M: Miliolid, SP: *Spiroloculina sp.*, B: *Borelis melo melo,* $P_1$: *Peneroplis farsensis* or Cibicides, T: *Triloculina sp.*, P: Peneroplid, ME: Micritic envelope).

### 3.3.6 Facies F: Planktonic Foraminiferal Coralgal Packstone

Facies F features light gray to yellowish gray colored massive to locally ripple laminated thin to medium beds (Figure 27). The skeletal assemblages consist of mixed reworked coral algae debris with considerable amounts of planktonic foraminifera, fewer amounts of large benthic foraminifera, and trace amounts of small benthic foraminifera. Globigerinidae foraminifers (Beavington – Penney and Racey, 2004; Wilson and Vecsei, 2005) are interpreted as autochthonous skeletal allochems at depths of 120 - 200 meters in the sub - euphotic zone, whilst the photosynthetic organisms, such as coral and crustose red algae, are interpreted as allochthonous at same water depths. Facies F exhibits moderate to occasionally poor sorting. The average grain sizes for the packstone and locally floatstone are ~ 1 mm and ~ 2-3 mm, respectively.

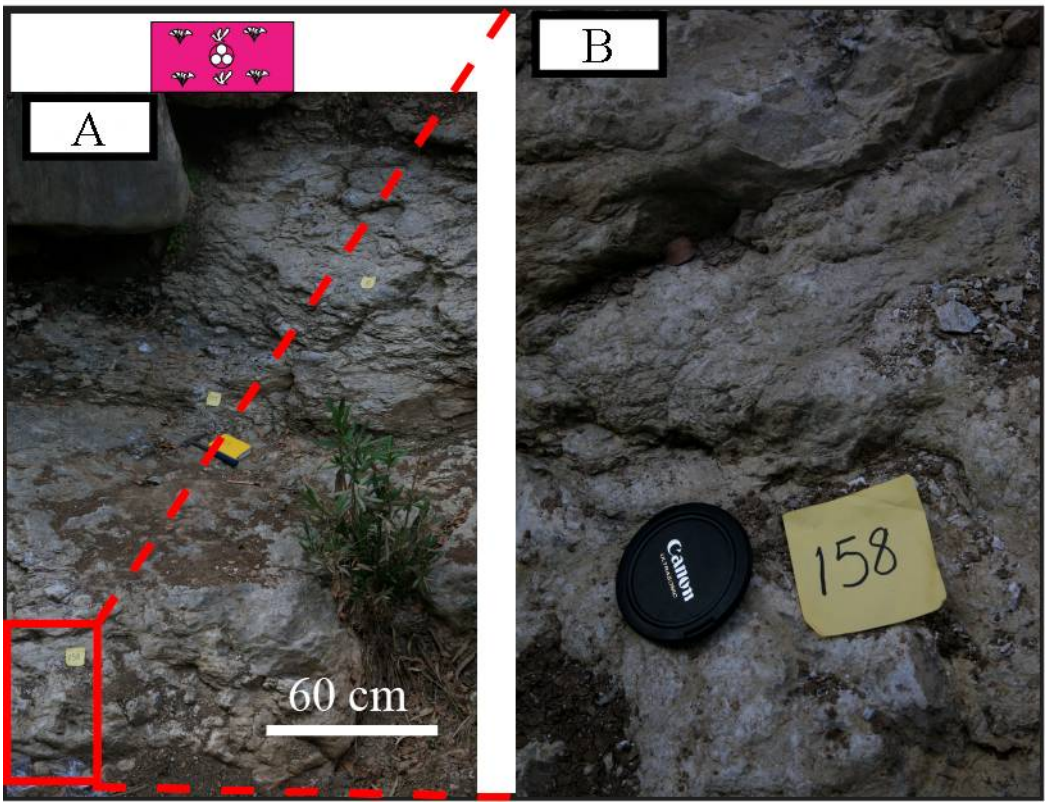


Figure 27: (A) Outcrop photo of planktonic foraminiferal coralgal packstone. (B) Close up view of (A).

## Interpretation

Abundance of mud and planktonic foraminifera indicates low energy setting. Facies F grades into Facies G – planktonic large benthic foraminiferal coralgal packstone – in basinward direction and Facies C or Facies D in landward direction (Figure 28). Facies F is interpreted to be deposited in a lower fore – reef environment. Gorur (1994) described this facies as inter–reef depression deposits. The facies that are enriched in the reworked red algae debris and in situ planktonic foraminifera are interpreted to be deposited in the lower fore-slope with water depths between 40 and 100 m or more (Pomar et al., 1996; Franseen and Goldstein, 1996b).

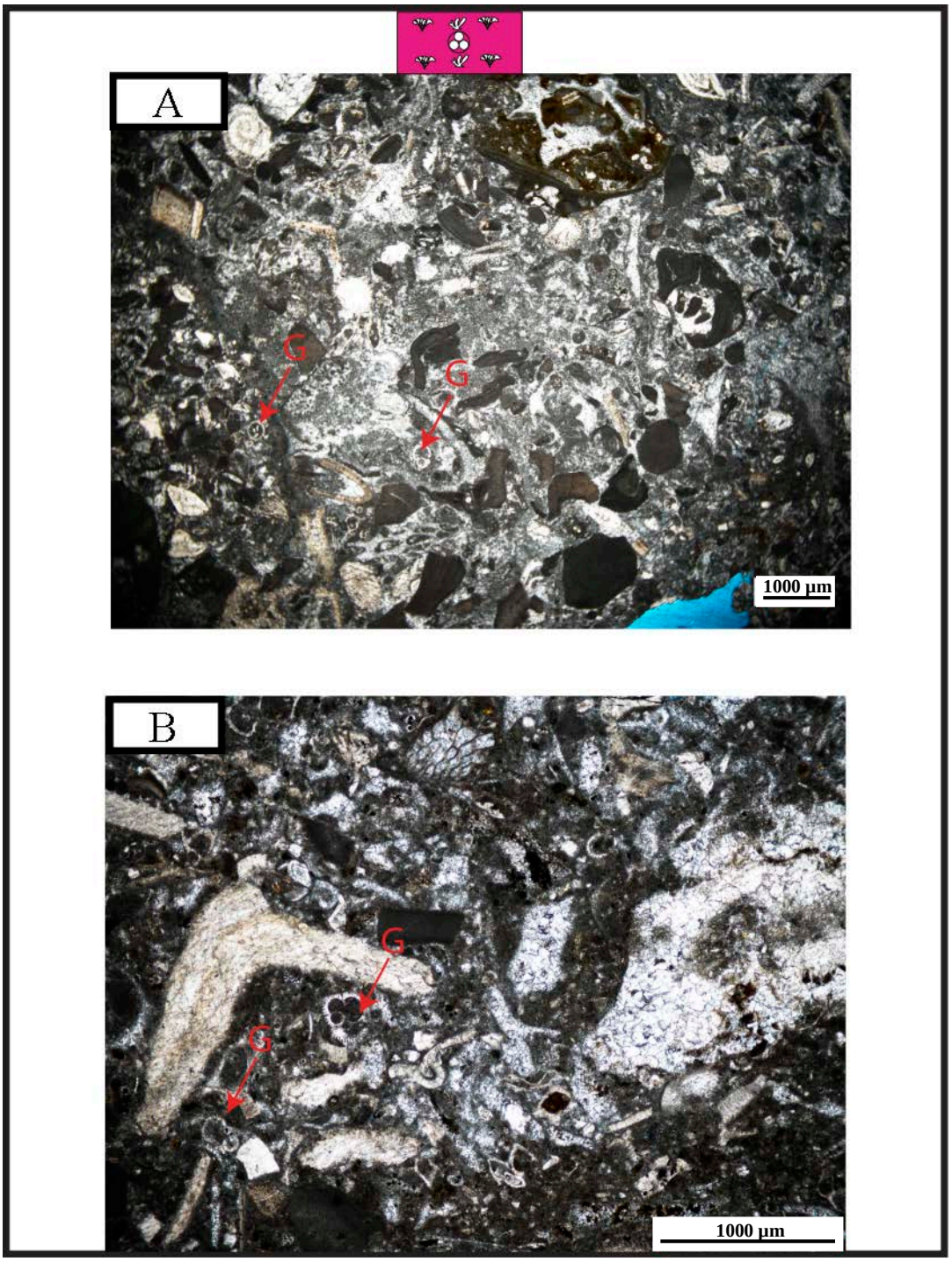


Figure 28: Thin section photomicrographs of planktonic foraminiferal coralgal packstone (G: Globigerinidae).

### 3.3.7 Facies G: Planktonic Foraminiferal Large Benthic Foraminiferal Coralgal Packstone

Facies G is composed of light to dark gray, thin to thick commonly nodular beds consisting of reworked coral algae debris, in situ large benthic foraminifera, Globigerinidae, echinoderms, sponge, mollusks, and Bulminid foraminifera with fewer amounts of bryozoan and Serpulid worm tubes (Figure 29). The fragments of reworked coral and algae debris are relatively small in size and have subangular to rounded edges. The amounts of reworked algae fragments are more than those of coral which are absent at downdip. The diagnostic faunal assemblages of Facies G are *Operculina sp.* and Globigerinidae with lesser amounts of *Amphistegina sp., Heterostegina sp.,* and *Lepidocyclina sp*. (Figure 30). The clay content varies between 5% and 25%.

Facies G exhibits 2 distinct subfacies, namely as planktonic foraminiferal large benthic foraminiferal coralgal packstone and floatstone. The packstone is characterized by light to dark gray colored, centimeter to decimeter thick beds with centimeter – scale ripple laminations, whilst the floatstone is composed of light gray colored, meter - scale thick beds forming massive benches (Figure 29). The dip angle ranges from $0^0$ to $10^0$ with the dip direction consistently to ENE or ESE.

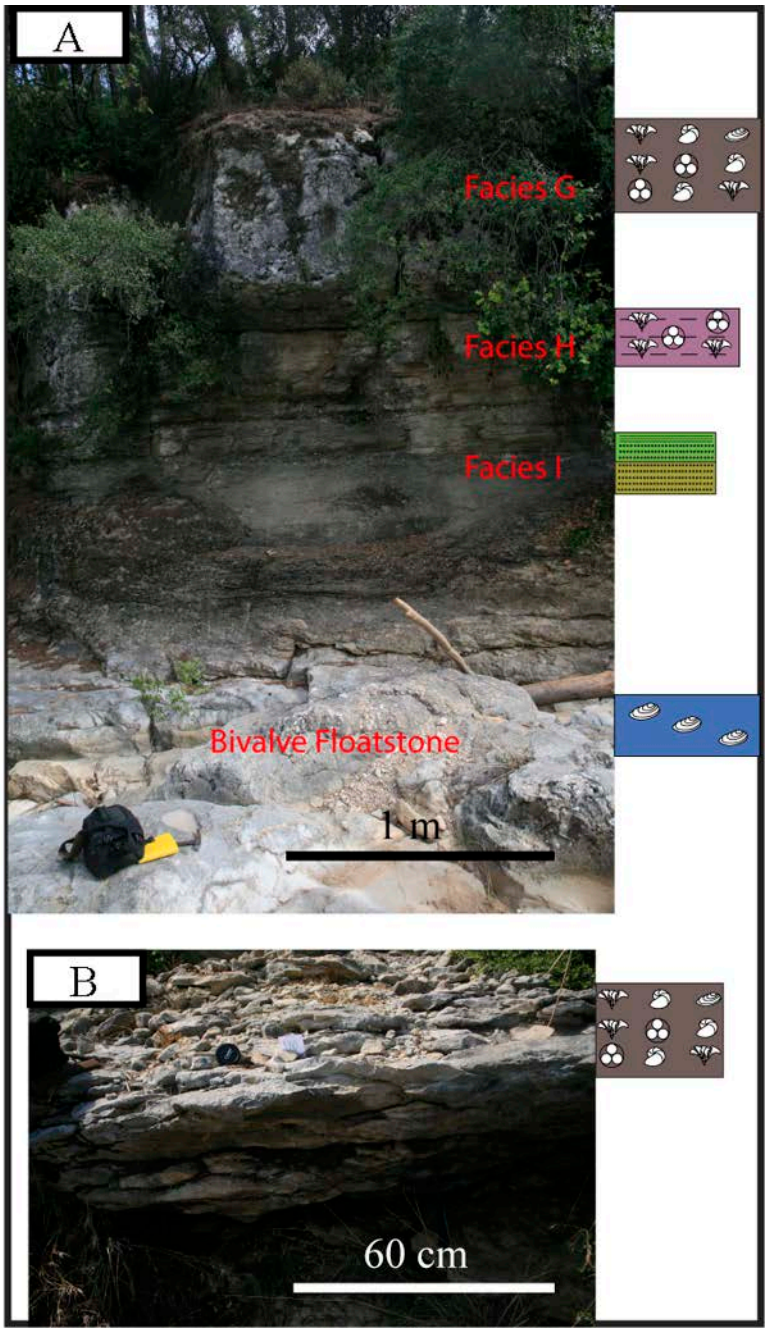


Figure 29: (A) Outcrop photo of planktonic and large benthic foraminiferal coralgal floatstone (Facies G), argillaceous coralgal wackestone (Facies H), marl/shale/siltstone (Facies I), and underlying bivalve floatstone of the Kaplankaya Formation. (B) Outcrop photo of planktonic and large benthic foraminiferal coralgal packstone.

## Interpretation

Facies G is interpreted to be deposited in a low energy environment because of its high mud content and large percentage of planktonic foraminifera (Saller et al., 1992 and 1993; Beavington – Penney and Racey, 2004). It passes laterally and vertically into Facies H – argillaceous coralgal wackestone – in basinward direction and Facies F or Facies D in landward direction.

Facies G was deposited in the lowermost fore–reef (toe of slope) and open shelf – transition zone of fore–reef to deep basin. Furthermore, during the drowning of the east platform, Facies G and Facies F were deposited on the uppermost fore-reef and top of the platform, respectively.

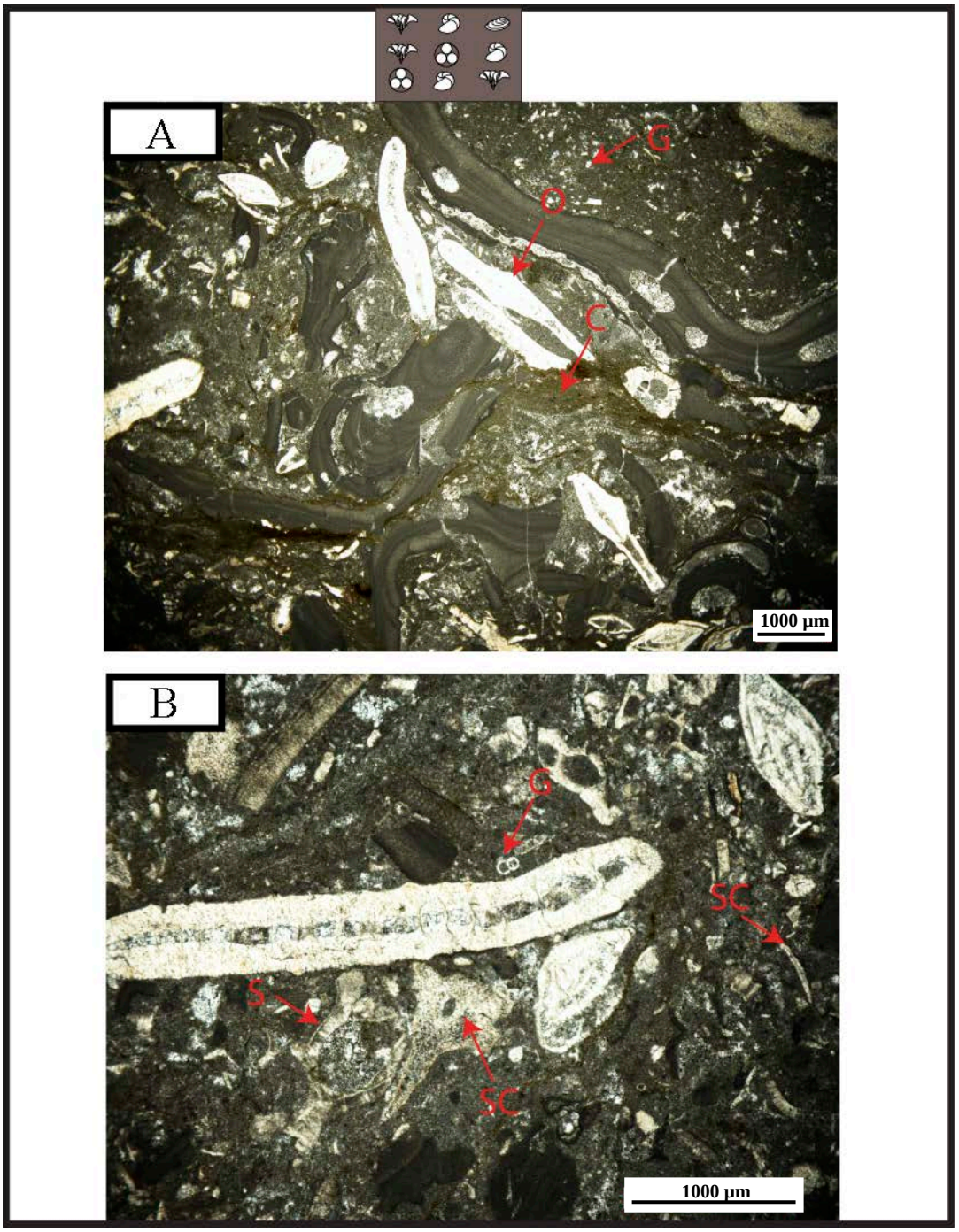


Figure 30: Thin section photomicrographs of planktonic and large benthic foraminiferal coralgal packstone (G: Globigerinidae, O: *Operculina sp.*, SC: Sponge Spicule, C: Clay).

### 3.3.8 Facies H: Argillaceous Coralgal Wackestone

Facies H is characterized by yellowish light to dark gray thin to medium beds with locally ripple laminations. This facies contains the skeletal grains of Globigerinidae, echinoderms, mollusks, and Bulminid foraminifera with minor or trace reworked algae debris and benthic foraminifera. The diagnostic features of Facies H are large amounts of Globigerinidae and minor amounts of reworked clasts with an argillaceous micritic matrix (Figure 32). The beds of Facies H exhibit dip angle varying from $0^0$ to $5^0$ with the dip direction to ENE or ESE (Figure 29 and Figure 31).

**Interpretation**

Facies H was deposited in a low energy setting as indicated by its high mud and clay contents along with planktonic foraminifera. Facies H grades laterally and vertically into marl, shale, and siltstone in basinward direction and Facies G in landward direction. The depositional environment is interpreted as a transitional zone to the deep marine basin (Pomar et al., 1996; Beavington – Penney and Racey, 2004).

### 3.3.9 Facies I: Shale/Marl/Siltstone

Facies I is representing the Kopekli Formation which is the transitional facies between shallow marine reefal carbonates – the Karaisali Formation and deep basinal shale of the Guvenc Formation. This facies depicts light yellowish brown, greenish blue, or light greenish gray color thinly bedded calcareous silty marl (Figure 31). The beds of the Kopekli Formation are almost horizontal and thin out towards basinward.

Facies I was deposited in a low energy setting in the transitional zone adjacent to the deep basin and include the pelagic bioclasts; planktonic foraminifera and Pteropoda (Gorur, 1994).

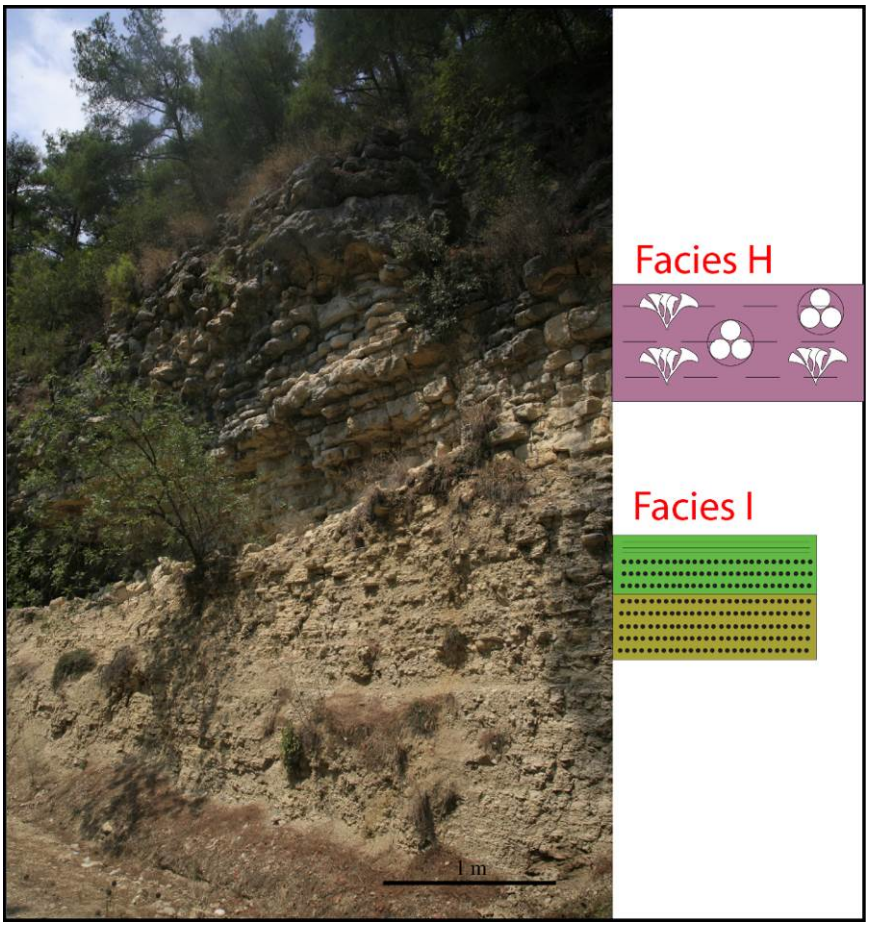


Figure 31: Outcrop photo of argillaceous coralgal wackestone (Facies H), marl/shale/siltstone (Facies I).

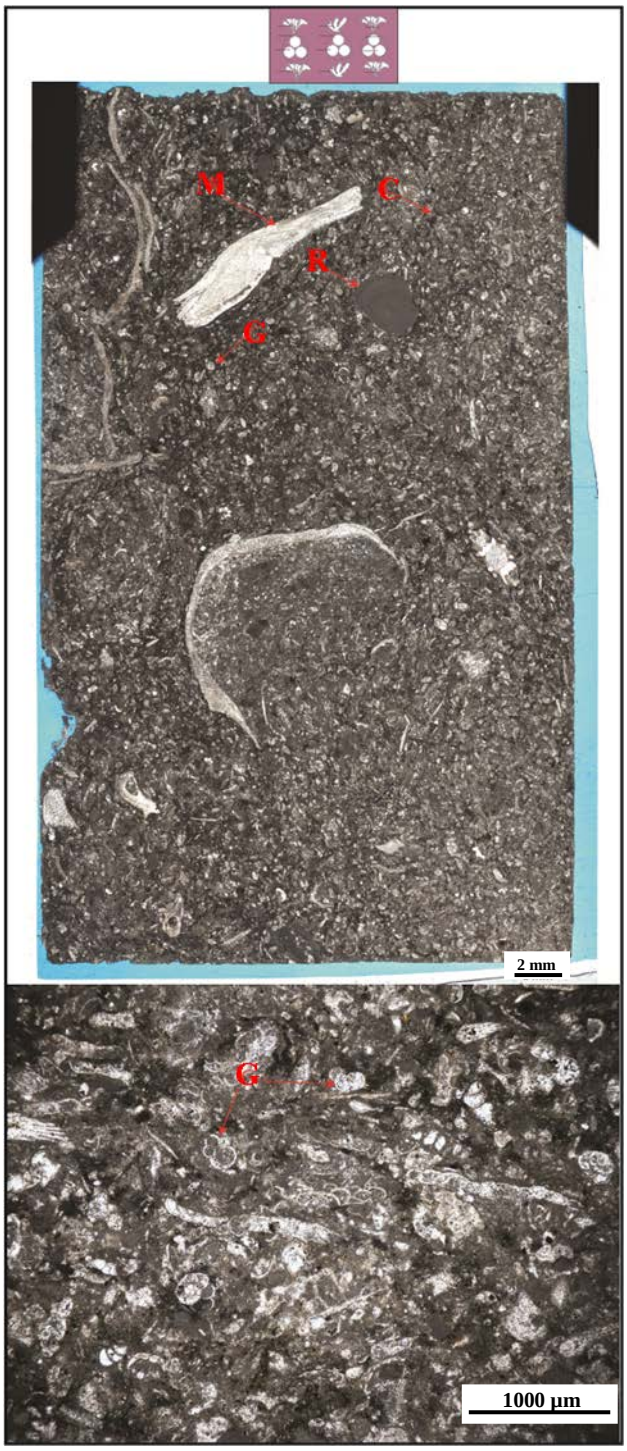


Figure 32: Thin section photomicrographs of argillaceous coralgal wackestone (G: Globigerinidae, M: Mollusk, C: Clay, R: Red Algae).

### 3.3.10 Facies J: Debris Flow/Slumps/Rock Fall

Facies J is restricted to certain areas in the study area. Debris flow developed in the lower part of the middle fore–reef, whereas the rock fall or olistolith was observed in the lowermost fore–reef settings (Figure 33).

Debris flow apron consists of 60% pebble – boulder sized poorly sorted angular shaped reef debris and 40% mud. Submarine rock falls/olistoliths are larger sized blocks of reef debris (Figure 33).

Figure 33: Outcrop photo of rock fall and olistoliths (indicated by red lines) (Facies J).

### 3.3.11 Facies K: Bivalve Floatstone

Facies K features yellowish light gray decimeter scale beds enriched in mollusks. This facies consists of mostly *Pecten sp.*, oysters, poorly sorted red algae fragments, and echinoderms. Well-preserved shells are common in the upper to middle fore-reef, whilst in the open shelf, the mollusks are reworked and fragmented.

## Interpretation

Facies K was interpreted to be deposited mainly in low energy and locally in moderate energy settings in the deep shelf and upper to middle fore-reef, respectively (Flugel, 2009). This facies is very similar to the bivalve floatstone (Figure 34) of the underlying Kaplankaya Formation in terms of its mud dominant fabric and color; however, Facies K includes occasionally coral, red algae, and benthic foraminifera.

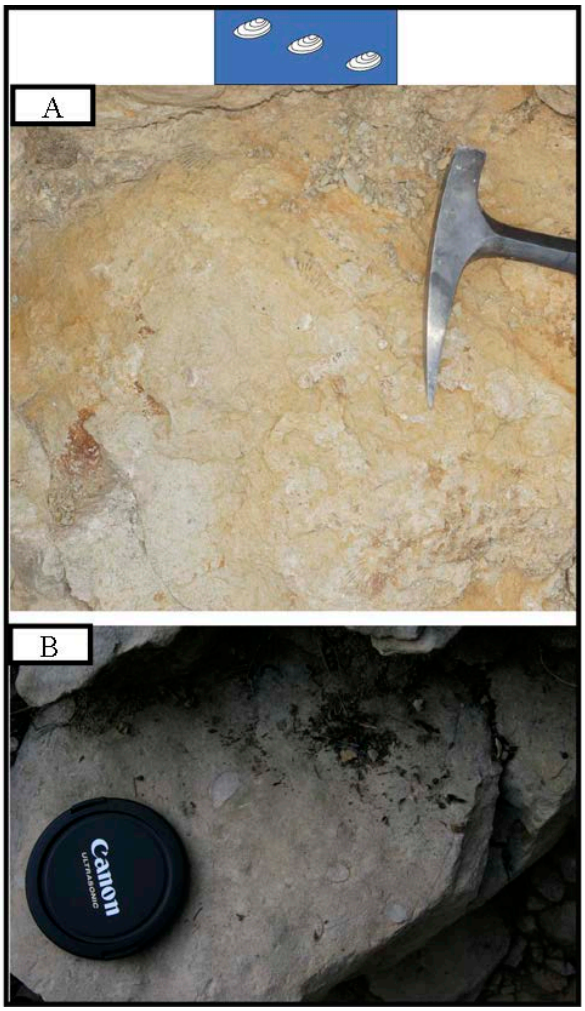


Figure 34: Outcrop photos of bivalve floatstone (B) enriched in echinoderms (Facies K).

### 3.12 Comparison of the Facies Model with Previous Studies

Figure 35 illustrates the facies distribution of the research field. Although certain discrepancies exist, facies descriptions of the Karaisali Formation described in the current study are mostly consistent with the previous descriptions reported by Gorur (1978 and 1994). Based on the detailed field mapping and the petrographic studies conducted in this study, aforementioned six facies assemblages (Gorur, 1978 and 1994) of the Karaisali Formation have been expanded to ten facies and eight subfacies.

Gorur (1994) defined the coral algal boundstone-packstone and small benthic foraminiferal packstone as the facies assemblages deposited in the reef core. However, reef framework does not only exhibit the boundstone fabric, but framestone and locally bafflestone fabrics are also observed in the reef core. Platey coral framestones are distributed from the reef core to the fore-reef. Moreover, the boundstones are not only developed in the reef core, i.e. argillaceous boundstone/framestone has also been observed in the fore-reef. Gorur (1978, 1994) reported that back-reefs were not developed in the Karaisali Platforms, whilst the back-reefs are developed in the landward side of the reef cores and characterized by the abundant small benthic foraminifers.

The coralgal wackestone-packstone deposited on the uppermost slope adjacent the reef core with the initial slopes of $30^0$; and the matrix and grain size increases further downdip (Gorur, 1994). Although there are some exceptions, this observation shows the general trend in the reef-front and upper-fore slope depositional environments of the Karaisali Formation.

Moreover, inter-reef depressions were characterized by the Globigerinid-algal packstone (Gorur, 1994). However, the field observations show that inter-reef

depressions are dominated by planktonic foraminiferal coralgal packstone, planktonic and large benthic foraminiferal coralgal packstone, argillaceous coralgal wackestone, marl, shale, and siltstone.

Finally, the transitional zone between the Karaisali reefal carbonates and basinal shales of the Guvenc Formation was suggested to consist of Globigerinid argillaceous wackestone (Gorur, 1994), whilst the transitional zone is characterized by the Kopekli Formation that includes the marls, siltstones, and shales.

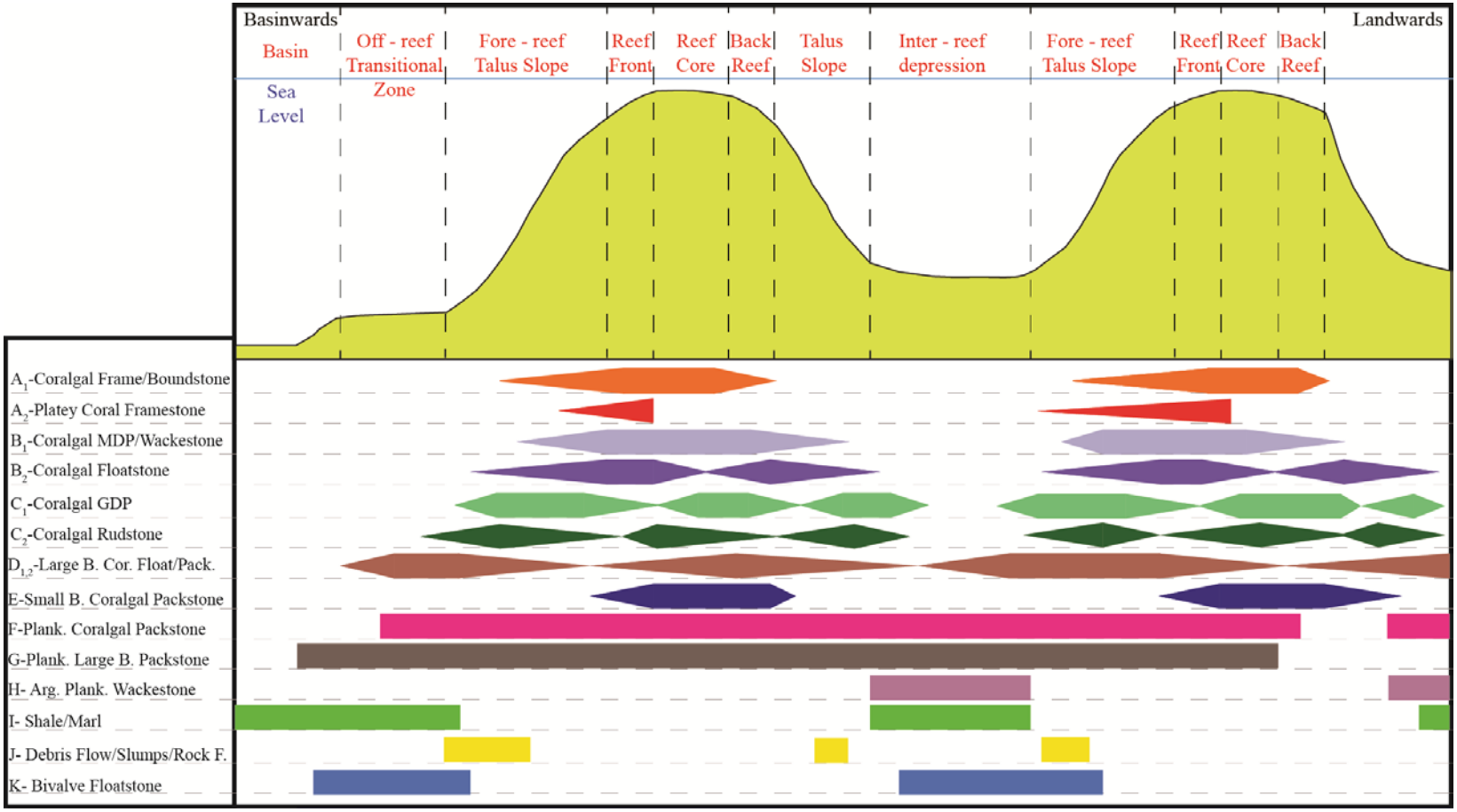


Figure 35: Facies distribution of the study area.

# Chapter 4 – Stratigraphic Architecture and Platforms Evolution Model

## 4.1 STRATIGRAPHIC ARCHITECTURE

In the study area, three small carbonate platforms developed along the paleo-topographic highs. On the geological map, illustrated in Figure 2, three geologic units were distinguished: (1) reef core, (2) proximal and distal slope, and (3) transitional zone to the deep basin corresponding to the following facies association:

1. Reef Core: coralgal boundstone/framestone, platey coral framestone, coralgal MDP/wackestone, coralgal floatstone, coralgal GDP, and small benthic foraminiferal coralgal packstone
2. Proximal and Distal Slope: platey coral framestone, coralgal MDP/wackestone, coralgal floatstone, coralgal GDP, coralgal rudstone, large benthic foraminiferal coralgal floatstone, large benthic foraminiferal coralgal packstone, planktonic foraminiferal coralgal packstone, planktonic and large benthic foraminiferal coralgal packstone, debris flow/slumps/rock fall, and bivalve floatstone
3. Transitional Zone: planktonic foraminiferal coralgal packstone, planktonic and large benthic foraminiferal coralgal packstone, argillaceous planktonic foraminiferal coralgal wackestone, and shale/marl/siltstone

The legend of the lithofacies and the mapped symbols are illustrated in Figure 36 and Figure 37.

### 4.1.1 Vertical Facies Succession

Locations of the measured sections were determined based on the following reasons:

- Accessibility of the outcrops to measure sections because of the steepness of the thick vertical cliffs

- Usefulness for correlating facies succession between adjacent platforms andbasinal deposits
- Ability to trace bedding planes and to see the transition between different facies and to capture stratal terminations

Measured sections were labeled using the numerical values considering their locations, i.e. sections of the East Platform were labeled as E1 – E4, the Middle Platform was labelled as M, transitional between carbonates and mixed carbonates and shales were labelled as T and the labels W1 - W3 was used for West Platform (Figure 38).


Figure 36: Legend of the lithofacies.

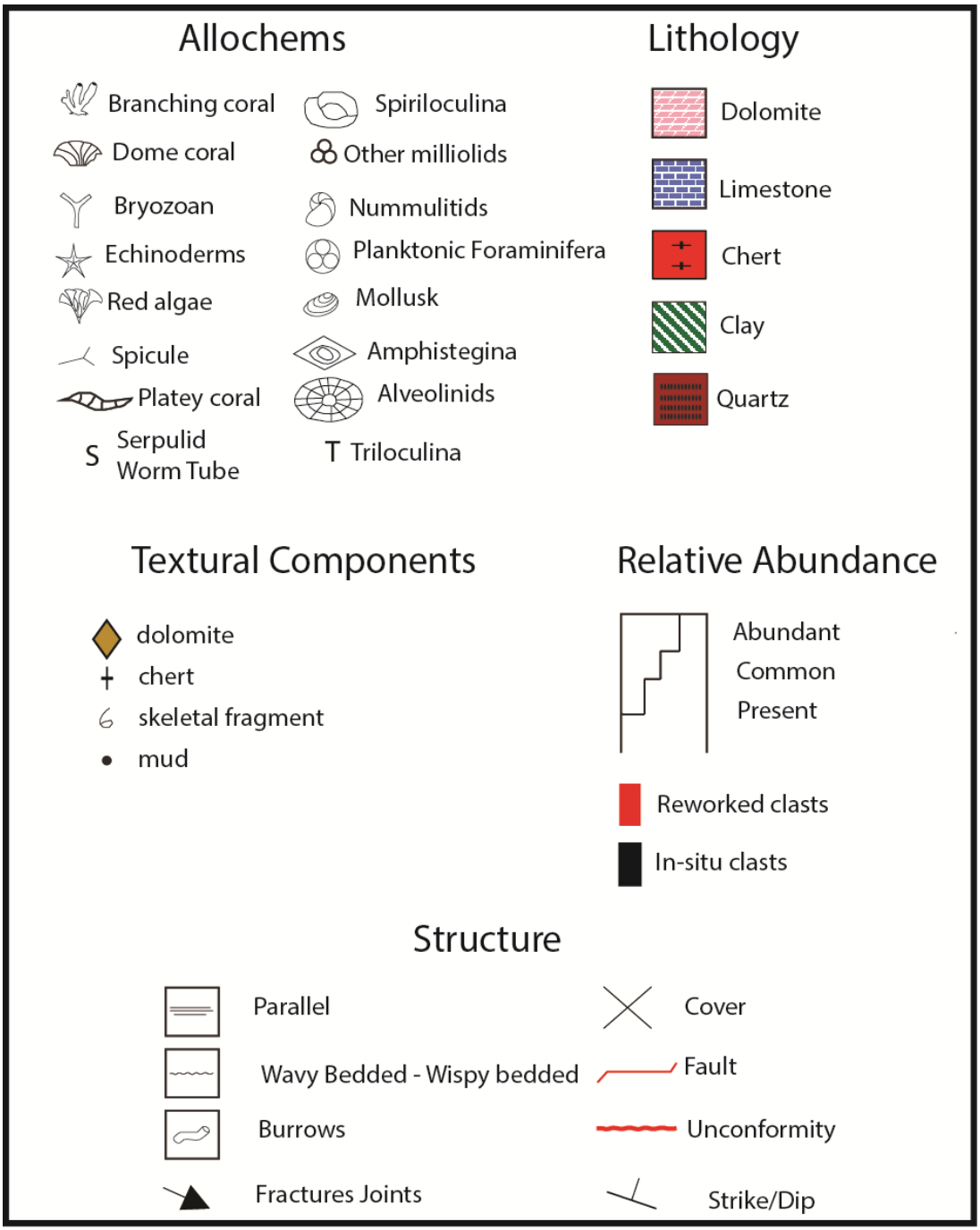


Figure 37: Legend of the allochems, lithology, textural components, and structure for the measured sections.

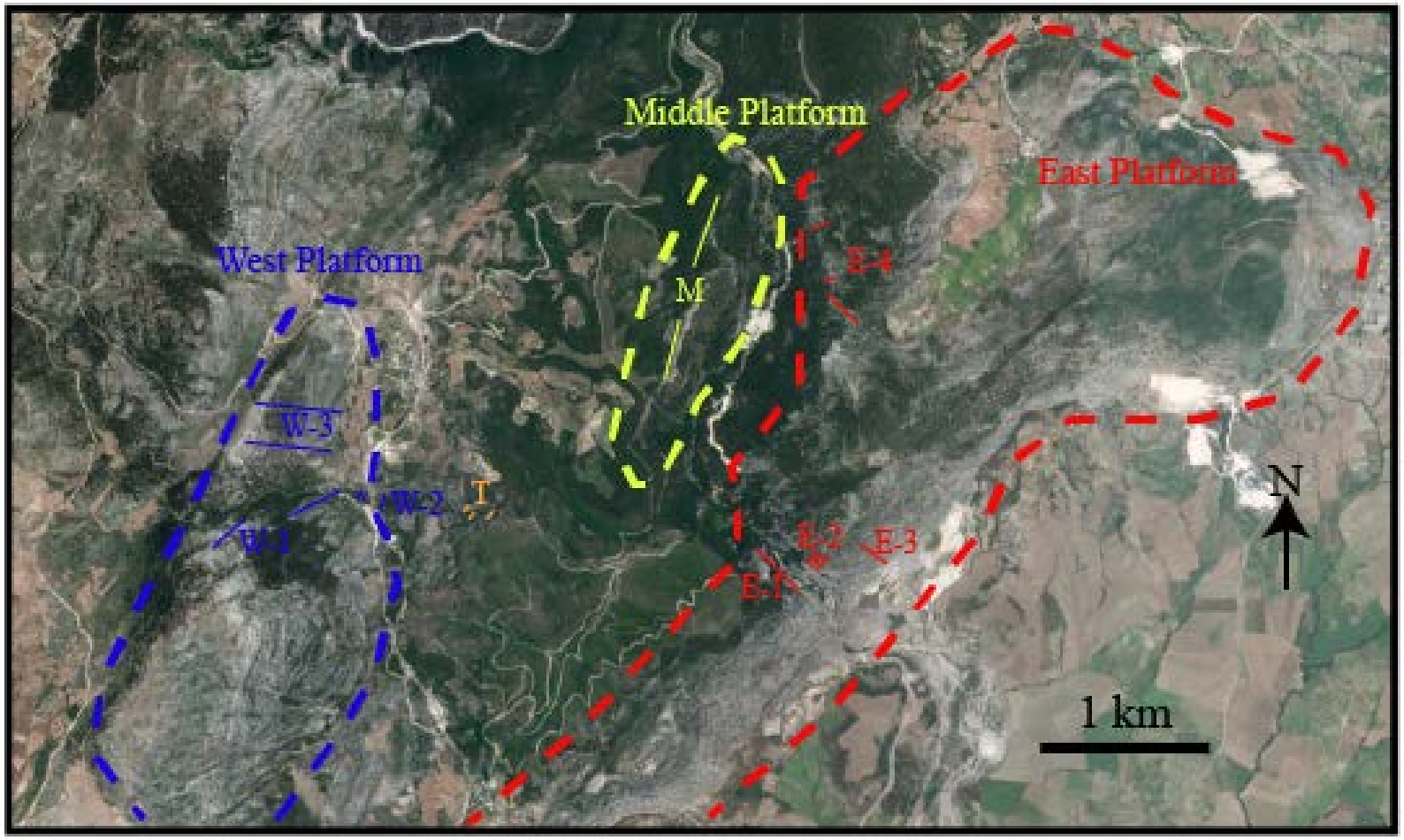


Figure 38: Platform and measured section locations (dash lines represent the platform locations and the solid lines show the locations of the measured sections; E: East Platform, M: Middle Platform, W: West Platform, T: Transitional zone).

#### *4.4.1.1 East Platform*

The East Platform is located in the most basinward direction. Samples were collected from eight sections; one section from E-1, three sections from E-2, one section from E-3, and three sections from E-4. These sections are shown in Figure 38.

The interbedded coralgal MDP/wackestone, small benthic foraminiferal coralgal packstone, and coralgal GDP are located in the most lowermost landward slope of the East Platform (Figure 39 and Figure 40). The clinobeds in this section have the average orientations of the beds of $300^0/12^0$. These facies are followed by locally argillaceous large benthic foraminiferal coralgal packstone dominated by *Amphistegina sp.* and *Heterostegina sp*. with the gradual decrease in the dip amounts. To sum up, the facies of the back-reef and reef core are succeeded by the upper fore-reef facies; hence, the facies succession records the gradual deepening (Figure 35). The interbedded coralgal GDP and large benthic foraminiferal coralgal floatstone are succeeded by coralgal framestone/boundstone which is locally intensely burrowed and dominated by encrustations. This depicts the lateral and vertical interfingering facies of the reef core and adjacent reef-front and upper fore-reef. This interval is capped by planktonic foraminiferal coralgal packstone that marks the deepening of the platform top. The beds of planktonic foraminiferal coralgal packstone are dipping $6^0$ towards NNE. The measured section E-1 moves overall about 200 meter in the basinward direction and shows the overall facies transition from the back-reef to the upper fore-slope and further to the off-reef/transitional zone (Figure 35).

The measured section E-3 is located in the most basinward and easternmost side of the East Platform. This section is parallel to the strike of the beds and has been taken from the lower paleo-slope towards the platform top. The lowermost section is a slope –

talus deposit consisting of red algae and coral fragments (Figure 41). This debris flow is followed by the coral algal floatstone and coral algal grain dominated packstone which are argillaceous at the bottom. The beds of these facies dip $30^0$ towards SSE. The planktonic and large benthic foraminiferal coralgal packstone is followed by the the argillaceous coral algal boundstone consisting of thin branching Porites coral with encrusting red algae. The planktonic coral algal packstone and floatstone is a poorly sorted rhodolithic limestone with common planktonic foraminifera. Thus, this vertical succession shows upward deepening from the middle fore-slope to the off-reef/transitional depositional environments with locally abundant clay minerals. All of the sequences mentioned above include the coral and red algae debris of the reef core that were bypassed, reworked by the currents, and deposited to the lower paleo-slope because of the steep angle of the upper paleoslope. The dolomitic basement is exposed in the middle to upper paleoslope that is interpreted as non-depositional and bypass zone. The substratum was overlain by the Kaplankaya Formation which is transgressive basal conglomerates and mudstones enriched in algal clasts at the top. The moderately sorted coralgal wackestone/mud dominated packstone is succeeded by the dark gray argillaceous platy coral framestone, the coralgal floatstone, and interbedded bioturbated coralgal mud dominated packstone. This vertical succession shows the overall aggradational trend of the uppermost fore-reef and reef-front facies. These were further overlain by the coralgal boundstone/framestone. These upper fore-reef, reef-front, and reef core facies depict the aggradational stacking patterns of the highstand system tract. The boundstone was further succeeded by the coralgal MDP, coralgal GDP, and coralgal floatstone which contain rhodoliths. This facies shift from the reef core to the upper to middle fore-slope indicates the upper deepening of the facies. The deposition of the

planktonic foraminiferal coralgal packstone over the platform top marked the certain deepening from the reef core to the off-reef/transitional depositional environments (Figure 35).

The overall vertical succession in the East Platform shows that the Karaisali Formation developed unconformably over a deformed dolomitic Mesozoic basement during the initial marine transgression in the Burdigalian (Gorur, 1994). The reef debris was transported down the slope and deposited as the coralgal packstone and small benthic foraminiferal packstone in the back-reef settings and as the coralgal packstone and floatstone in the basinwards (Figure 16 and Figure 35). The relative sea level rise resulted in the deposition of the deeper fore-reef and off-reef/transitional facies over the reef core and upper fore-reef or back-reef facies. The East Platform was eventually drowned as shown by the sharp transition from coralgal framestone/boundstone to planktonic foraminiferal coralgal packstone (Figure 35, Figure 42, and Figure 43).

The main evidence to support drowning is the abundance of rhodoliths over the coral algal boundstone/framestone and followed by Globigerina-rich facies indicating a clear change from the reef core to the off-reef/transitional zone and similar to other example of platform drowning in the Miocene (Sattler et al., 2009) (Figure 35 and Figure 44).

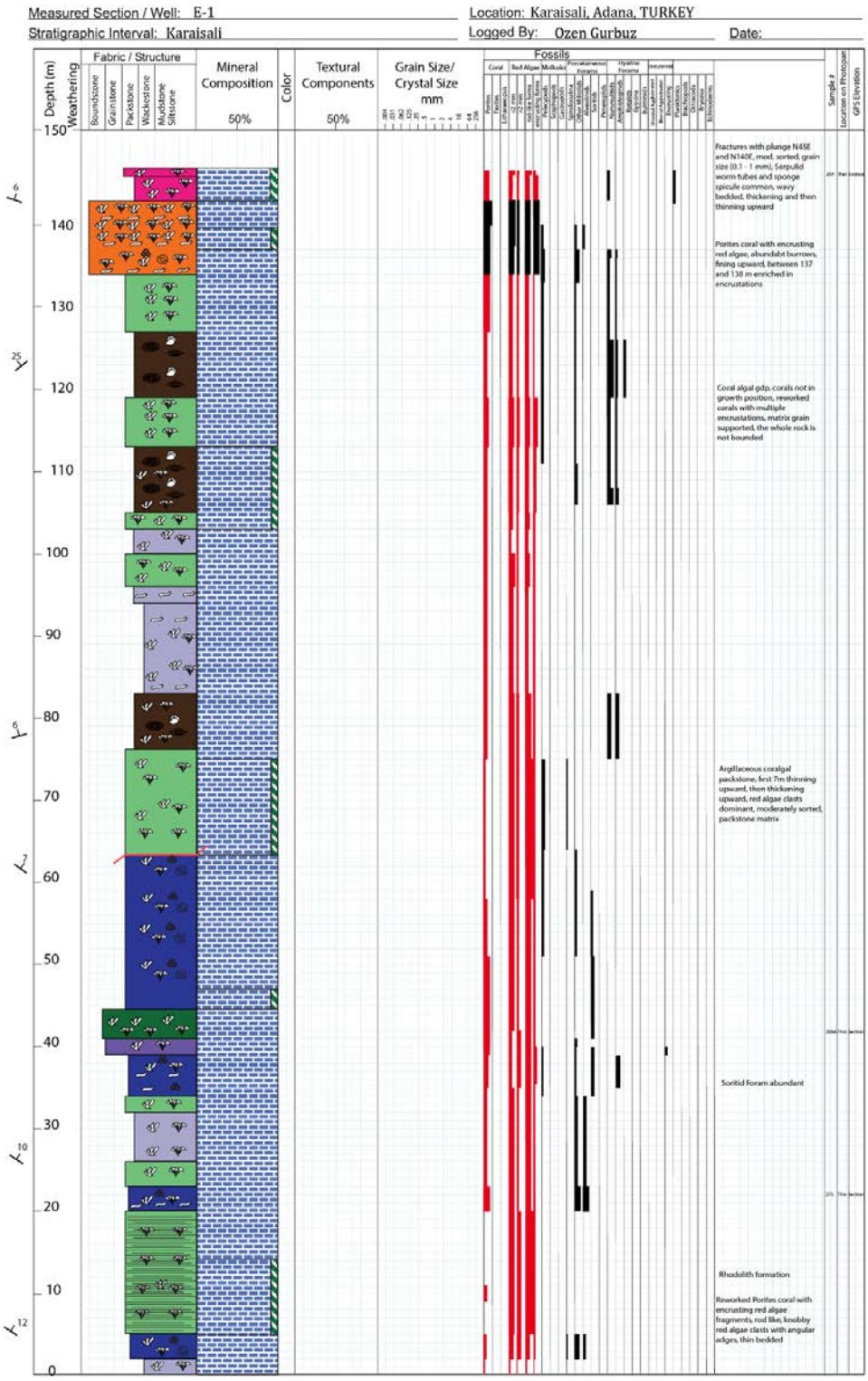


Figure 39: Measured section E-1.

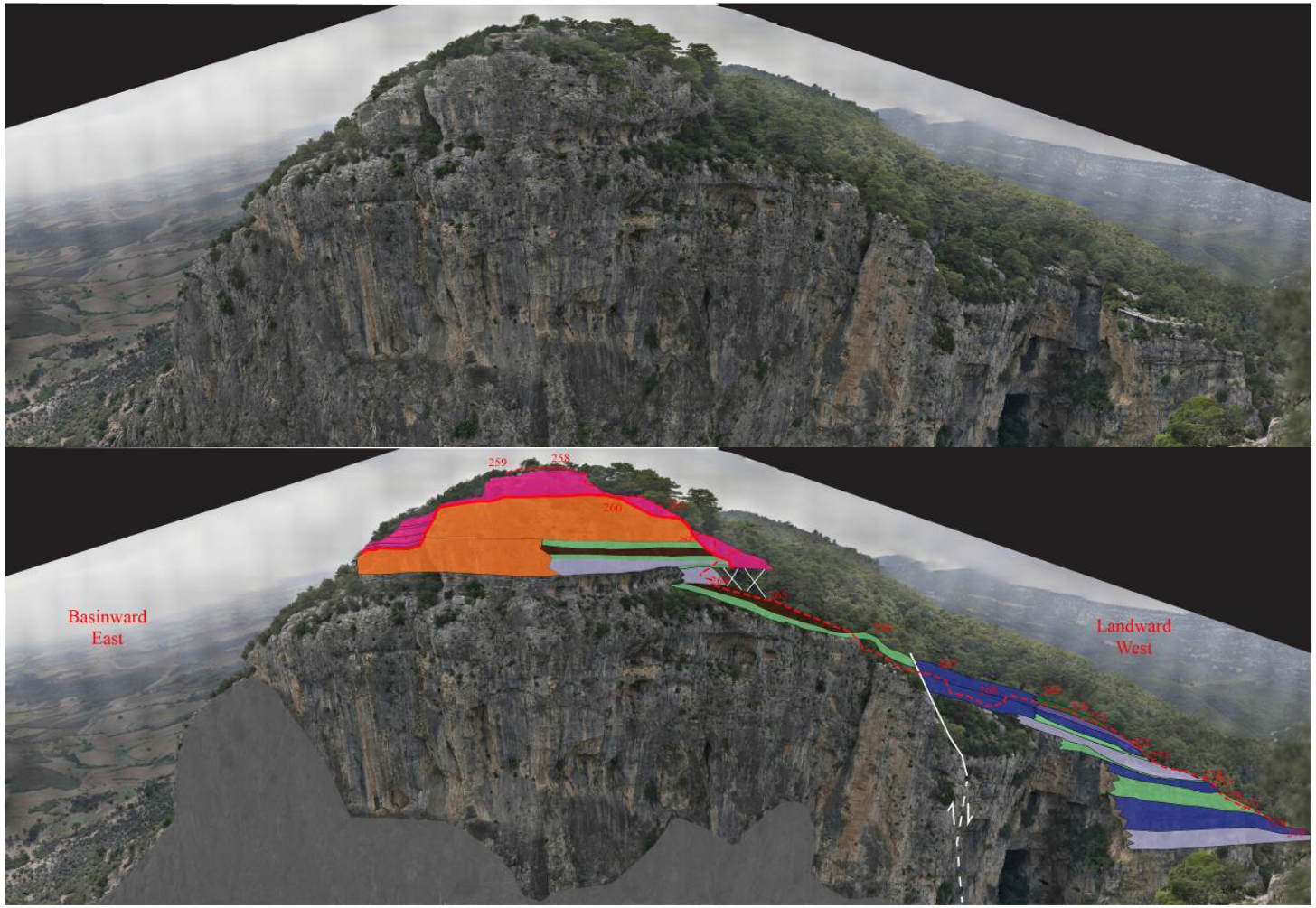


Figure 40: Interpreted ground – based photomosaic of north face of the East Platform (dash red line is the E-1 logging path, solid red line represents the drowning unconformity, and sample numbers are labeled).

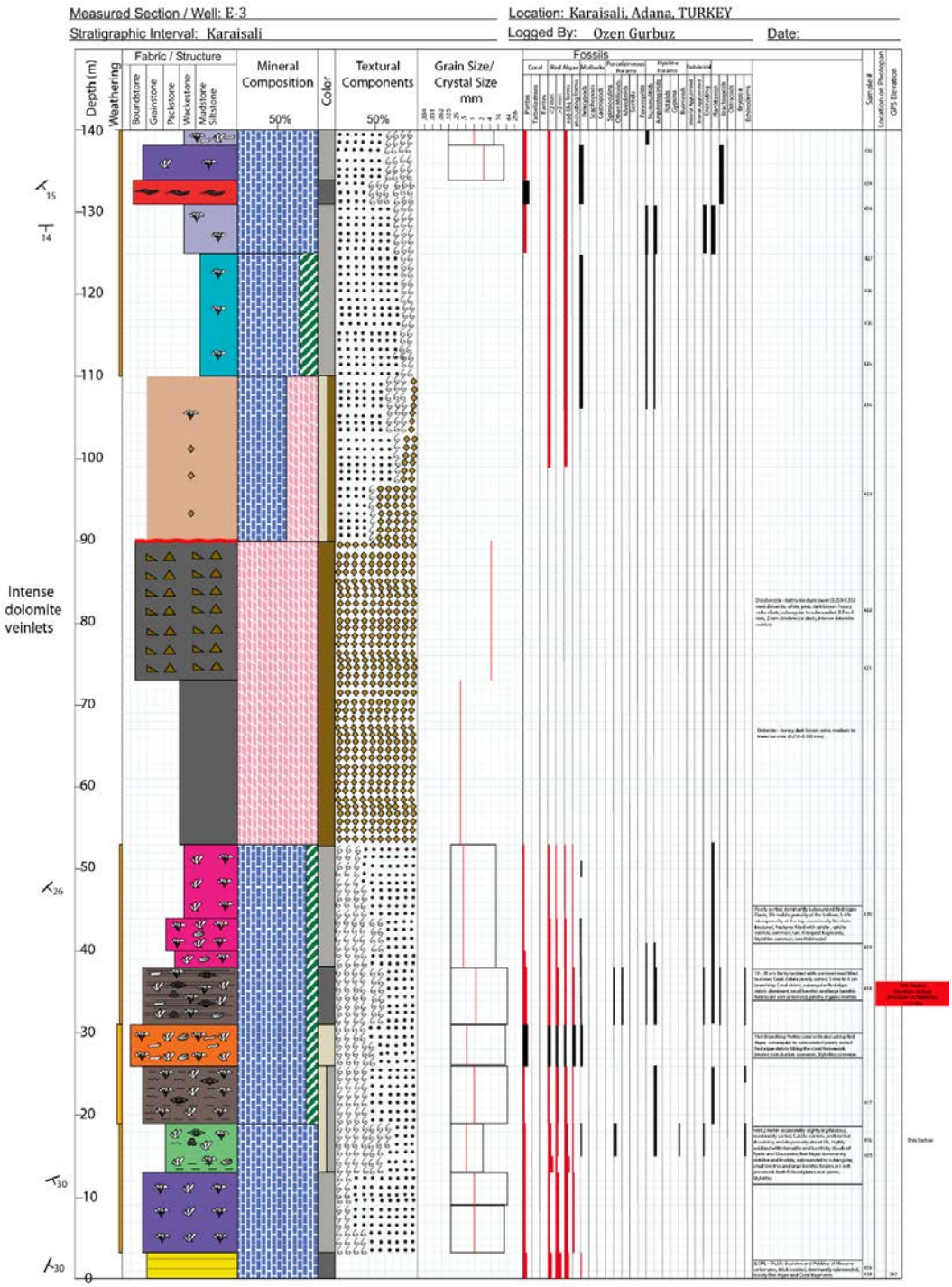


Figure 41: Measured section E-3.

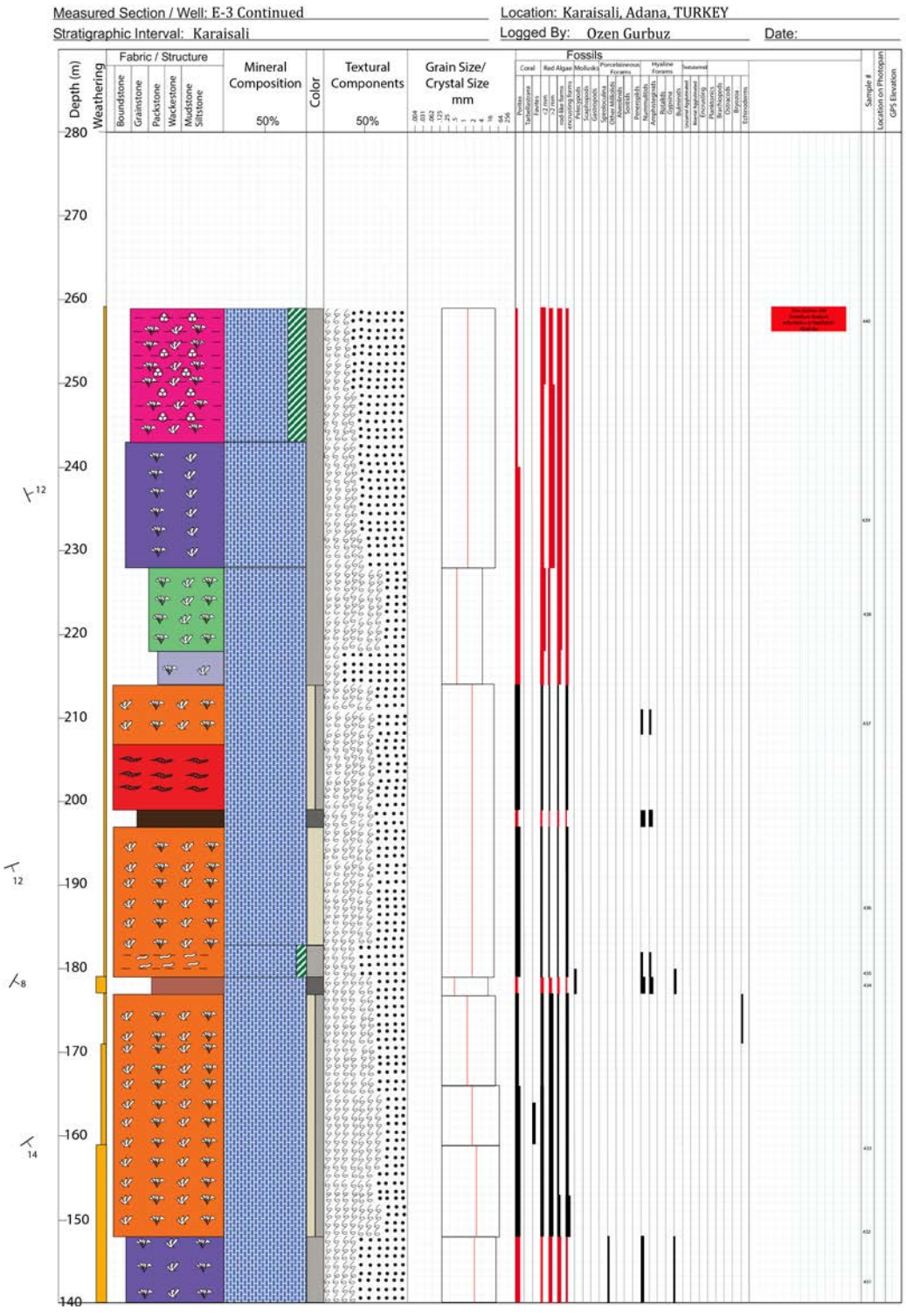


Figure 41: cont.

Figure 42: Interpreted ground – based photomosaic of south face of the East Platform (dash red line is the E-2-1, E-2-2, and E-2-3 logging paths, solid red line represents the drowning unconformity and thinner solid red line is the angular unconformity between dolomite basement and Miocene deposits).

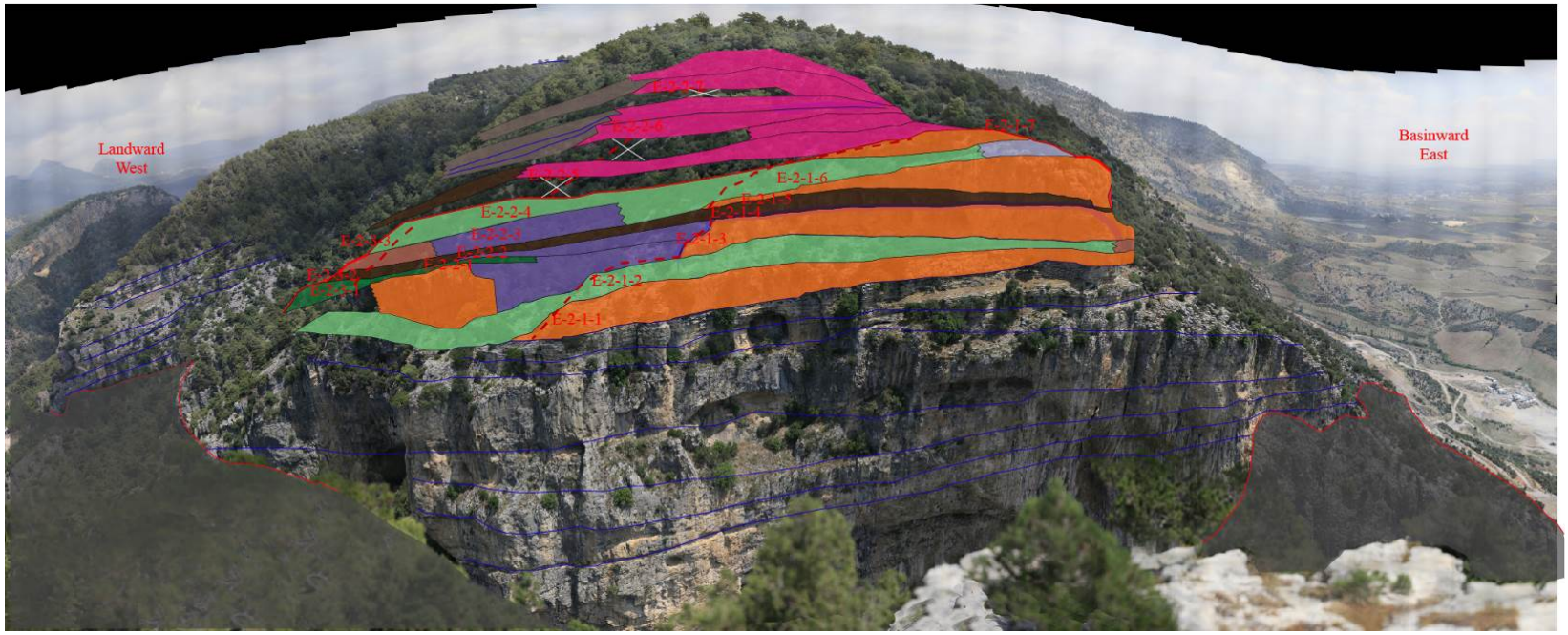


Figure 42: cont.

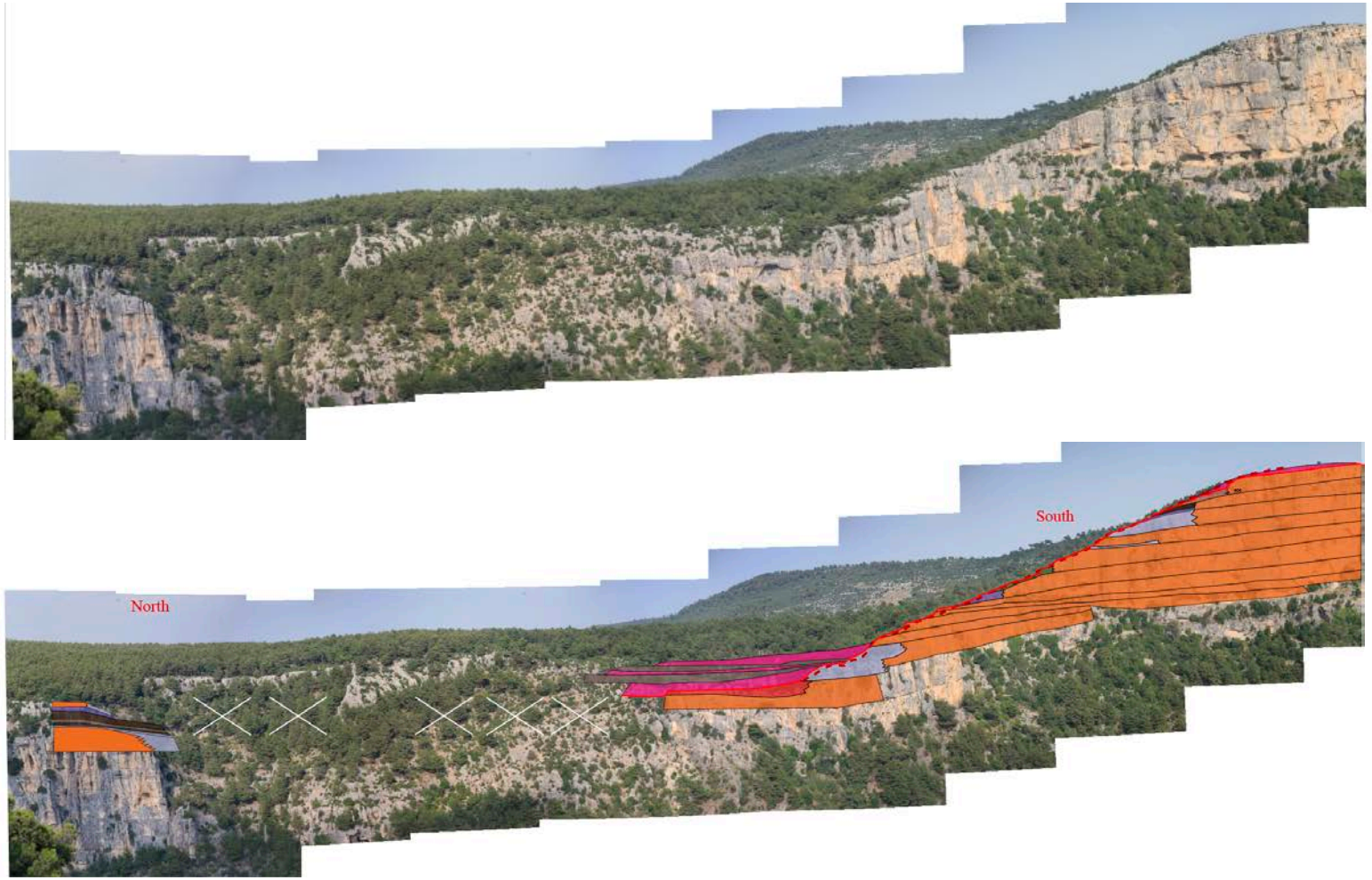


Figure 43: Interpreted ground – based photomosaic of east face of the East Platform (dash red line is the E-4-1, E-4-2, and E-4-3 logging paths, solid red line represents the drowning unconformity).

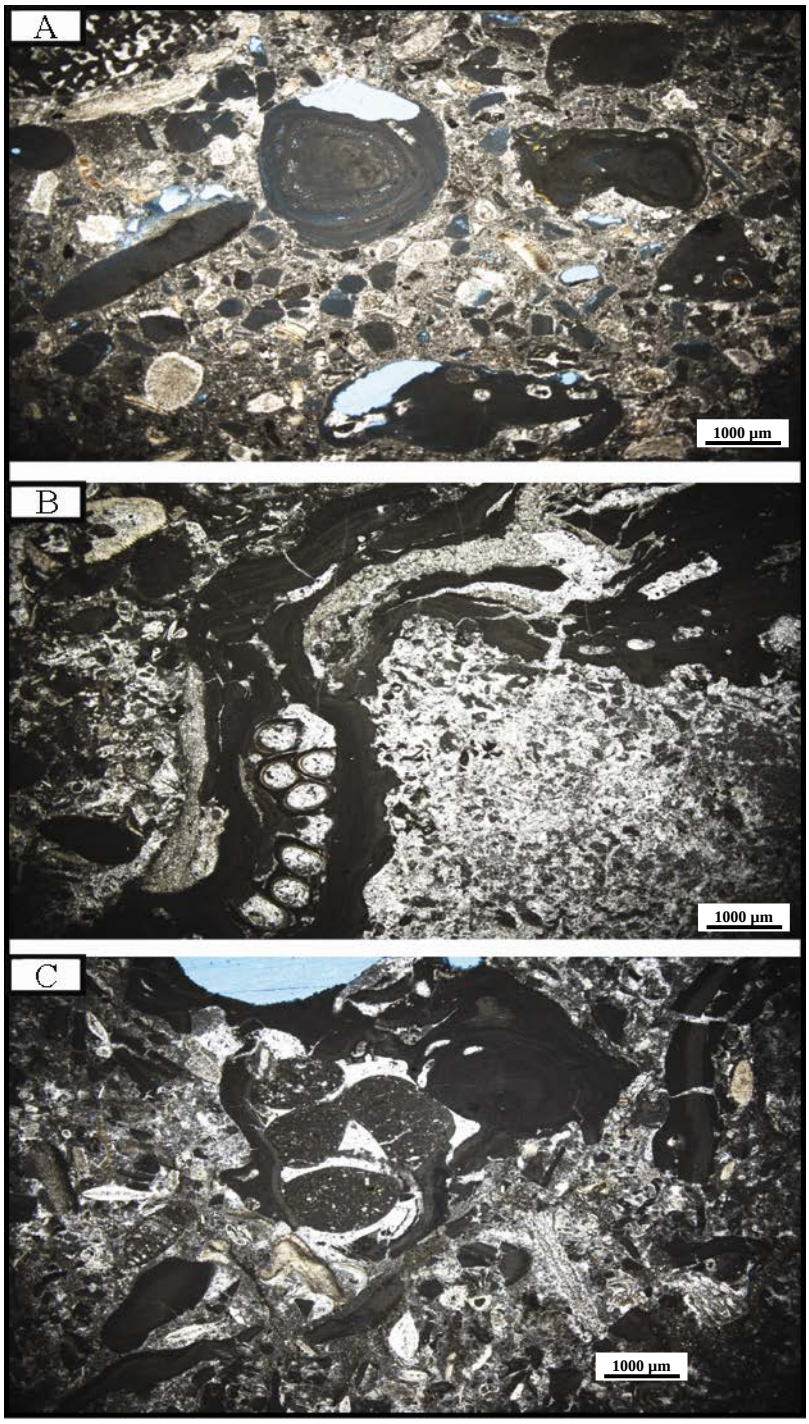


Figure 44: Drowning Signals (A) formation of rhodoliths and leaching (B) early marine cementation (C) planktonic depth zone.

#### *4.1.1.2 Middle Platform*

The Middle Platform is situated at the center of the East and West Platforms (Figure 38 and Figure 45). Two measured sections (M-1 and M-2) were collected from the north side of the platform. The facies in the south side of the platform were observed directly in the field during mapping and bed tracing has been done on the high-resolution photomosaics.

The measured section M-1 starts with coralgal GDP and coralgal rudstone (Figure 46). The beds of these grain dominated subfacies dip towards north with the dip magnitudes of $20^0$. These subfacies are overlain by interbedded coralgal floatstone and small benthic foraminiferal packstone. This facies evolution shows a change from the talus-slope to the back-reef and reef core environments. The platform top was covered by the planktonic foraminiferal coralgal packstone that represents a clear deepening from the reef core to the off-reef/transitional environments (Figure 35).

The Middle Platform presents the lateral transition from the reef core to the shales further in the south direction with aggradational stacking pattern geometry.

In the lower parts of the platform, rotational slide deposits were observed in the photomosaics which are the downslope movement of the blocks along a slippage plane that was created by the oversteep fore-reef slope (Flugel, 2009) (Figure 45). The reefal carbonates in the Middle Platform were interpreted to be developed in the HST because the overall sequence in the Middle Platform mainly shows an aggradational character and the coralgal boundstone and framestone were relatively thinner and not well-developed with respect to the ones in the East Platform; hence, the Middle Platform misses the transgressive reefal carbonates that were observed in the East Platform. The reef core facies grades laterally into reef-front and fore-reef facies which further interfingers the lower fore-reef facies. The deep marine shales and marl were located further downdip in

south (Figure 45). Thus, the Middle Platform shows the lateral facies transitions from the reef core to the off-reef/transition and basin settings (Figure 35). These units were overlain by the planktonic foraminiferal coralgal packstone that shows a clear deepening of the Middle Platform from the reef core and fore-slope to the off-reef/transition environments (Figure 35).


Figure 45: Interpreted ground – based photomosaic of west face of the Middle Platform (dash yellow and black lines are the M-1 and M-2 logging paths, respesctively, yellow units are the rotational slides, and solid red line represents the drowning unconformity).

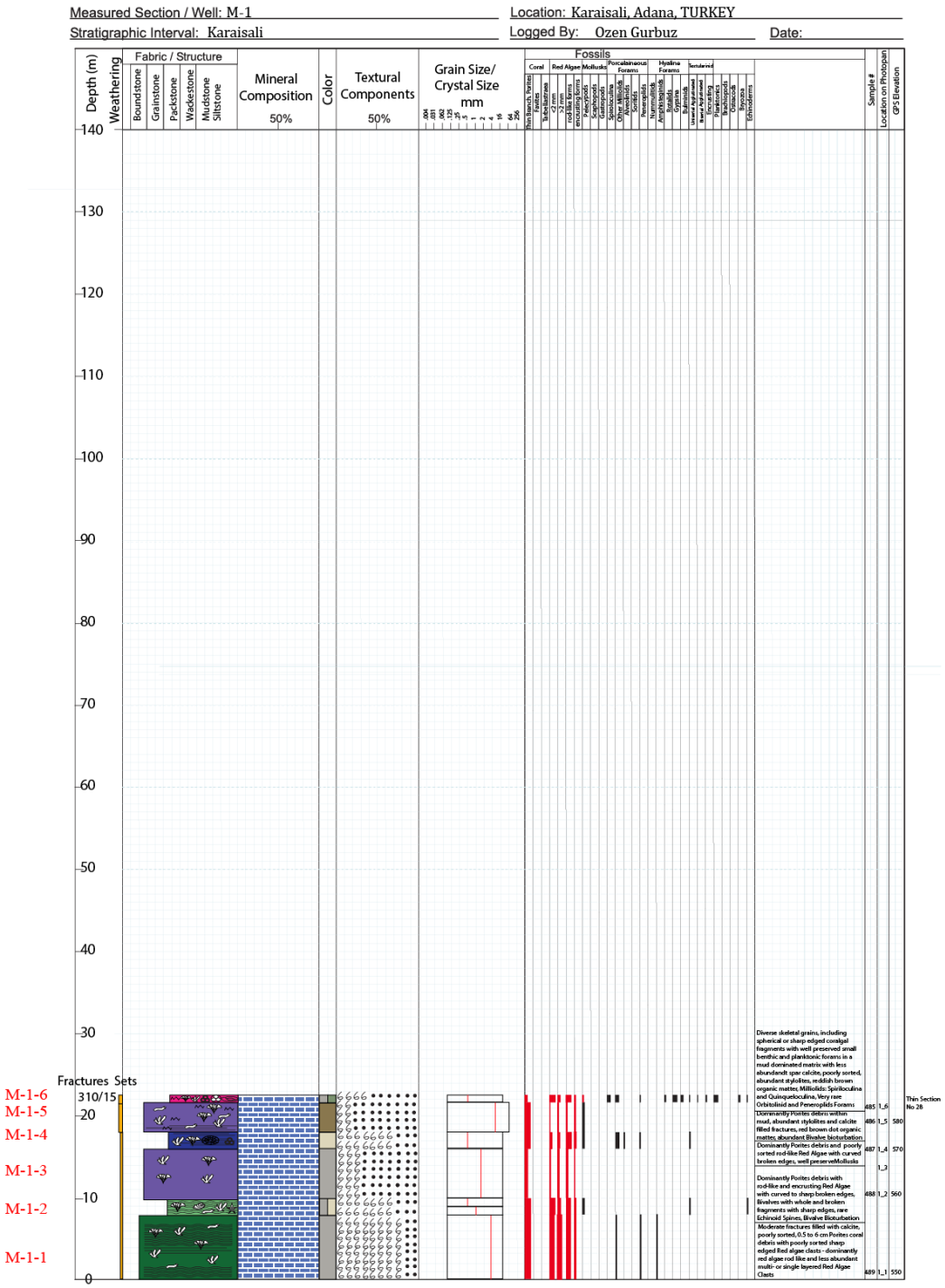


Figure 46: Measured section M-1.

#### *4.1.1.3 West Platform*

The West Platform which is located in the most landward direction shows exceptionally well developed facies transition from the reef core to the lower fore-reef (Figure 38, Figure 47-Figure 50).

The basal conglomerate rests unconformably on the substratum of which beds dip towards SW with dip amount of $60^0$ and was overlain by the bivalve floatstone and coralgal floatstone with dip magnitudes of average $21^0$. Coralgal MDP and coralgal floatstone are interbedded with small benthic foraminiferal coralgal packstone and planktonic foraminiferal coralgal packstone which was interpreted as a maximum flooding zone (MFZ) because of the landward facies shift from the coralgal MDP towards the planktonic foraminiferal coralgal packstone. Hence, this indicates a change from the reef-front and upper fore-reef to the off-reef/transitional depositional environments (Figure 35). MFZ was overlain by the coralgal MDP and coralgal floatstone that are locally enriched in rhodoliths. This sequence records the progradational character of the stacking patterns above the MFZ and a change of the depositional environments from the off-reef/transitional to the upper fore-reef (Figure 35). The deposition of the locally bioturbated coralgal rudstone and coralgal GDP consisting of coral debris and rhodoliths in the middle fore-slope indicates the dominant aggradational with minor transgressive trend of the stacking patterns.

The basement rock in the upper paleo-slope settings was overlain by the transgressive basal conglomerate and mudstone of the Kaplankaya Formation. Interbedded coralgal boundstone/framestone and coralgal GDP are located in the reef core environment at the top of the West Platform (Figure 51). Thus, these units indicate the reef core depositional environments (Figure 35). These facies were overlain by the almost horizontal beds of planktonic and large benthic foraminiferal coralgal packstone that

marks the MFZ. Hence, the depositional environment shifted from the reef core to the lower fore-slope (Figure 35). The MFZ was overlain by the small benthic foraminiferal coralgal packstone, coralgal floatstone, coralgal GDP, and the coralgal boundstone/framestone, respectively. This sequence shows the first progradational and later aggradational stacking patterns of HST located in the top of the West Platform. The depositional environment changed from the lower fore-slope to reef-front and the reef core (Figure 35).

The coral algal boundstones/framestones overlay the substratum with the unconformity on the platform top. Hence, this indicates that the reefs were preferentially developed on the paleo-highs of the antecedent topography. The reef debris was transported downdip and deposited as the coralgal packstones forming well-developed clinobeds in the lower to middle fore-slope. With the increase in the rate of relative sea-level rise, the planktonic and large benthic foraminiferal coralgal packstone was deposited on the top of the platform (Figure 35).

The East, Middle, and West Platforms show overall similarities, such as, the development of the coral boundstone/framestone on the platform top, presence of reef-front, fore-reef, and transitional facies. The clinobeds in the West and Middle Platforms are well-developed in the lower fore-slope; however, they are absence or covered by the basinal shales in the East Platform. The coralgal boundstone/framestones are thickest in the East Platform, relatively thinner in the West Platform, and thinnest in the Middle Platform. The planktonic foraminiferal coralgal packstone is thick in the East Platform and thin in the Middle and West Platforms.

.

Figure 47: Interpreted ground – based photomosaic of south face of the West Platform (red dash lines are the W-1-1 and W-1-2 logging paths).

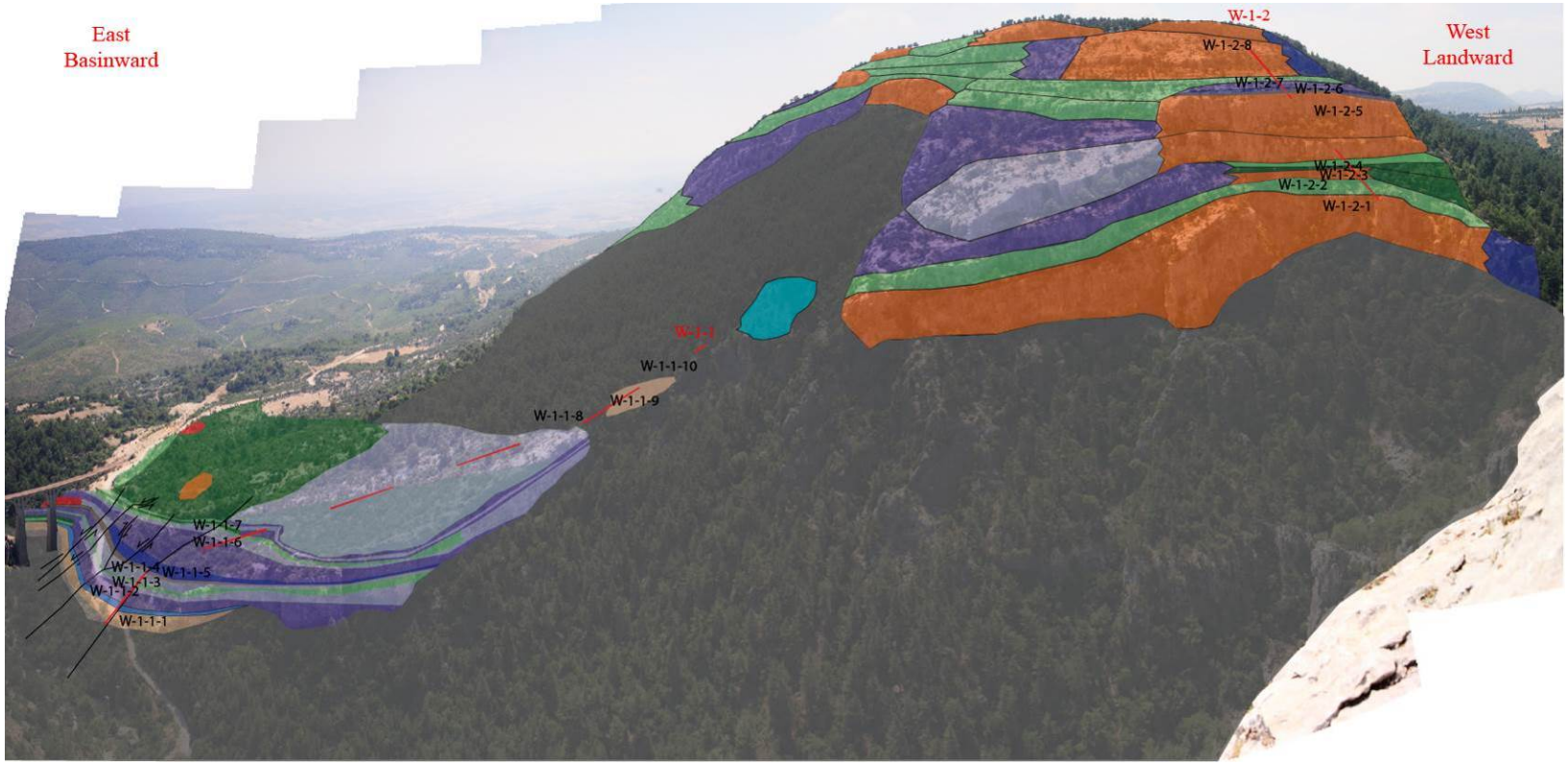


Figure 47: cont.

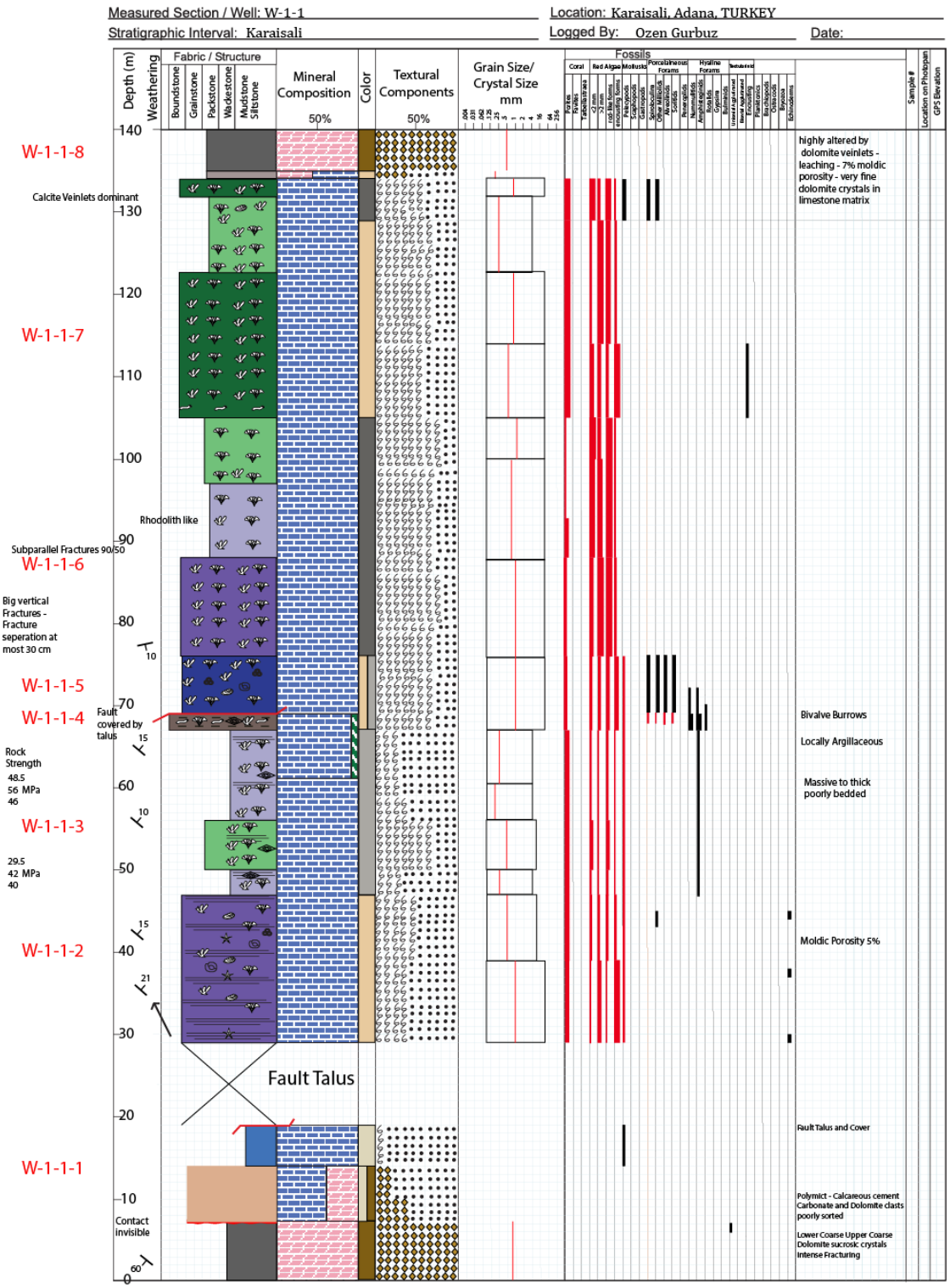


Figure 48: Measured section W-1-1.

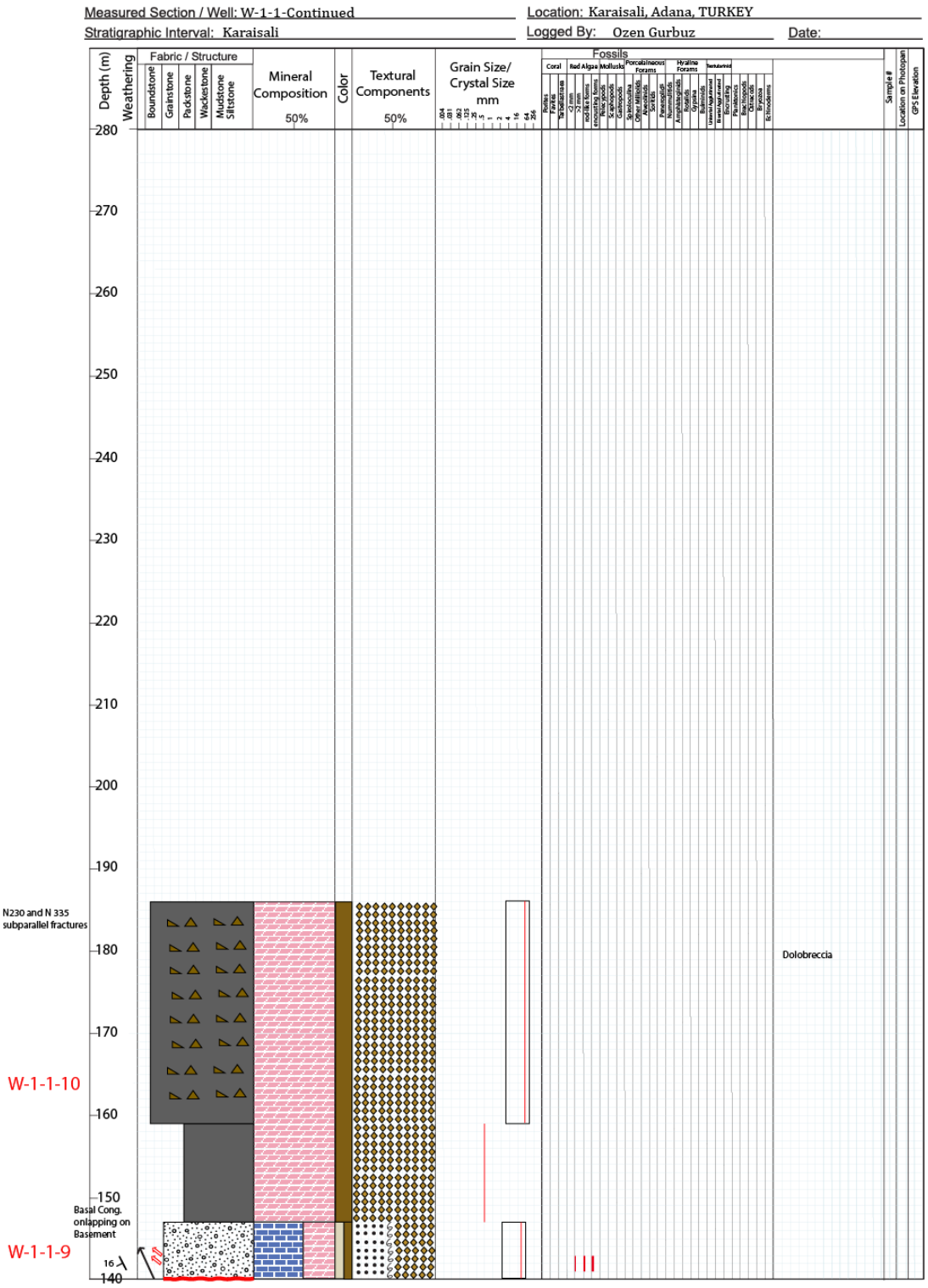


Figure 48: cont.

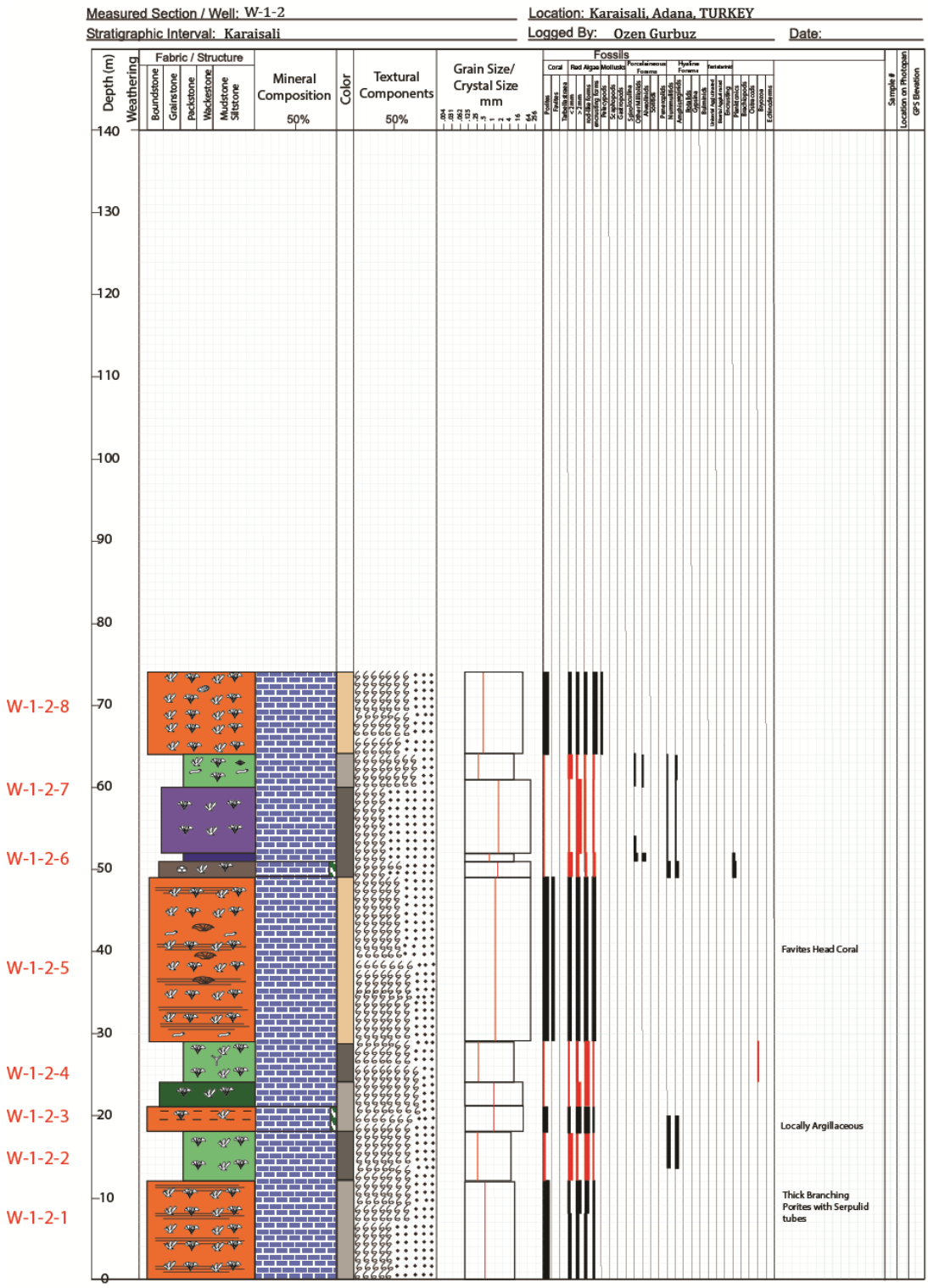


Figure 49: Measured section W-1-2.

Figure 50: Interpreted ground – based photomosaic of south face of the West Platform (red lines are the W-1 and W-2 logging paths, yellow dash line shows the path of the rock sampling, red line represents the angular unconformity, blue dash line is the maximum flooding surface).

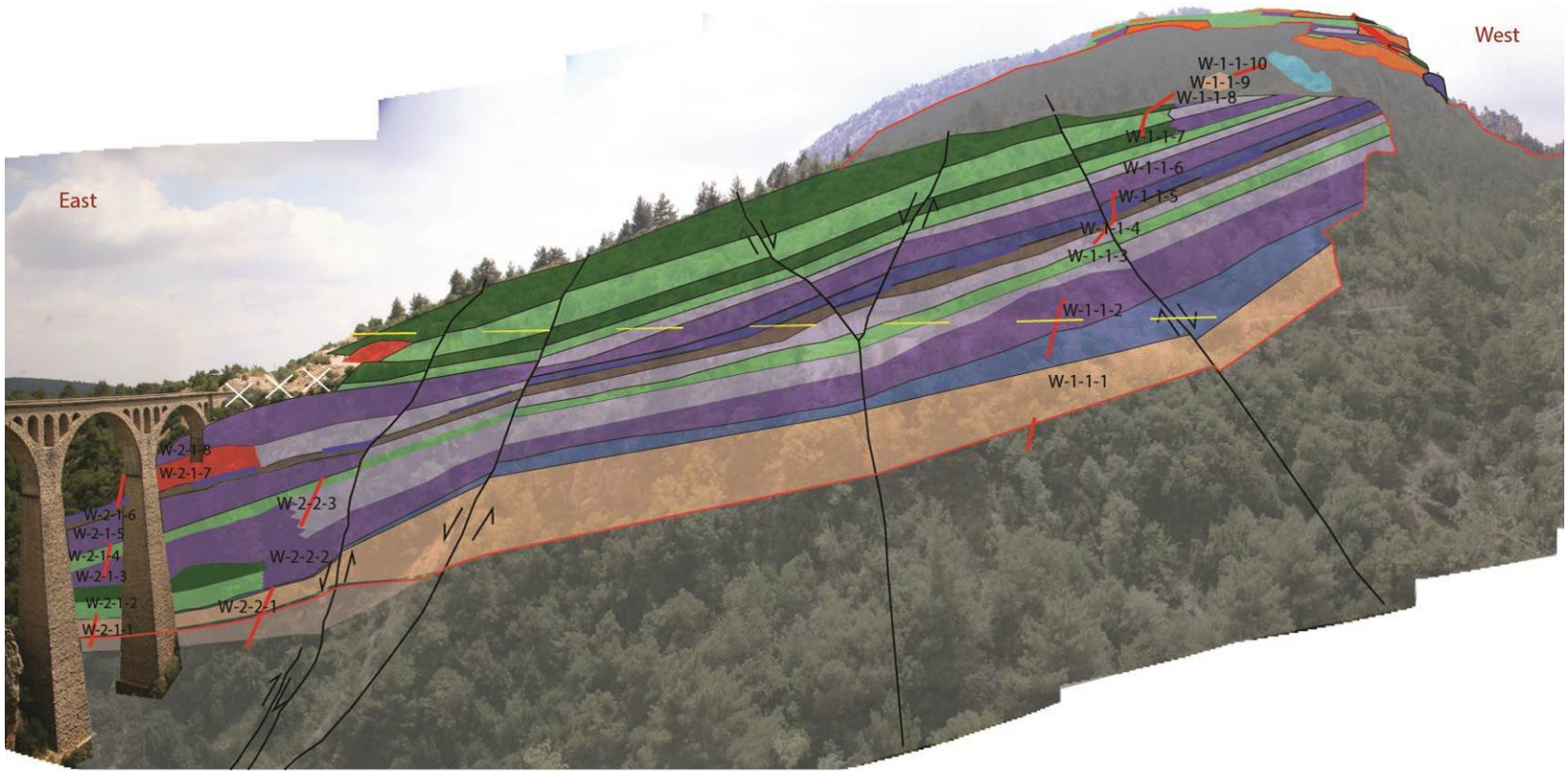


Figure 50: cont.

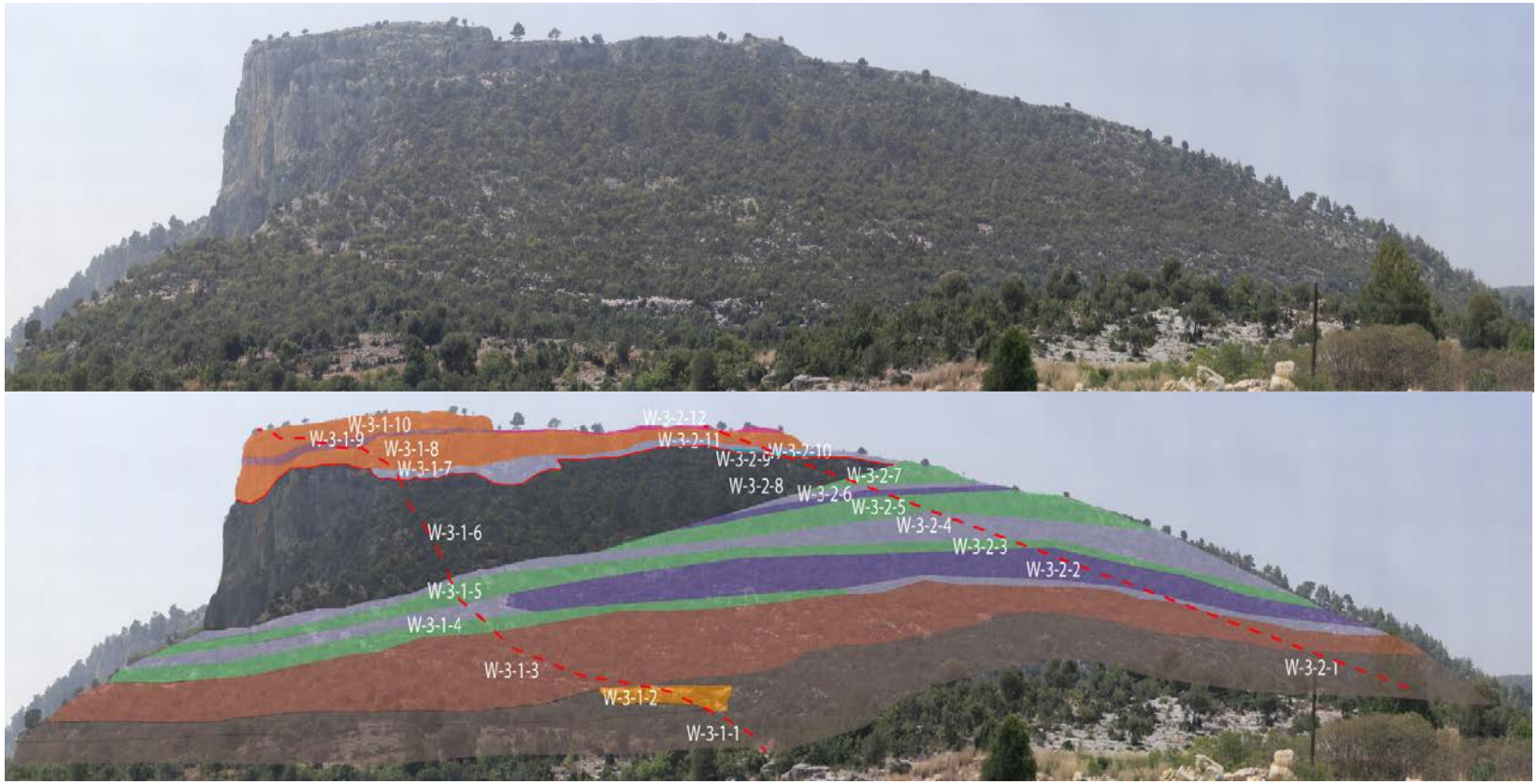


Figure 51: Interpreted ground – based photomosaic of the strike section of the West Platform (red dash lines are the W-3-1 and W-3-2 logging paths, red line represents the angular unconformity).

#### *4.1.1.4 Lower Fore – Reef and Transitional Environment*

Four logs have been taken in the transition of lower fore - reef carbonates and off – reef shales (Kopekli Formation) in order to document the lateral facies translations between the East and West Platforms (Figure 38). These logs were designated as T-1, T-2, T-3, and T-4 from east to west.

The measured section in the transition zone starts with shales/marls/siltstones which represents the open marine facies and was enriched in pyrite minerals at the lower sections (Figure 52 and Figure 53). Shale/marl grades vertically upwards into argillaceous planktonic foraminiferal coralgal wackestone and planktonic and large benthic foraminiferal coralgal packstone with a gradual decrease in quartz and clay minerals. These facies were followed by the planktonic foraminiferal coralgal floatstone, large benthic foraminiferal coralgal packstone, coralgal rudstone, and large benthic foraminiferal coralgal floatstone with the beds dipping towards northeast with the average dip amounts of $5^0$. The vertical facies succession shows first deepening and followed by the shallowing sequences. That is the lower fore-slope facies were first overlain by the transitional facies which were then followed by the lower to upper fore-slope facies.

The basinal shales/marls/siltstones are abundant in the basinward, whilst the coral algal packstone and large benthic foraminiferal packstone/floatstone are dominant in the landward direction of the transitional environment.

Figure 52: Measured sections T-1.

Figure 53: Measured sections T-2.

### 4.1.2 Depositional Model

The strontium isotope chronostratigraphy is an effective analytical method for the dating of lower to lowermost middle Miocene as $^{87}Sr/^{86}Sr$ ratios increase through time (Oslick et al., 1994).

In the scope of this study, strontium isotope analyses were performed on twenty samples. Strontium isotope age is estimated for nineteen of samples as Burdigalian (Figure 54). These estimated strontium ages are in good agreement with the stratigraphic position of the samples and the age analysis of Karaisali Platforms made by Turkish Petroleum Corporation.

$^{87}Sr/^{86}Sr$ ratios are converted to numerical values by using the look – up table of McArthur (2001). The numerical ages are derived using the linear regression in Oslick et al. (1994) in order to check the accuracy of the data. All of the derived ages are approximately similar, although there are slight differences in the third digits. The linear regression for the lower to lowermost middle Miocene section has a slope of 0.000068/m.y. This regression is valid from 15.5 Ma to 22.8 Ma (Oslick et al., 1994). The standard deviation of the analytical precision of the $^{87}Sr/^{86}Sr$ ratios of the nineteen samples is calculated to be 2.934E-05. Hence, the age error (precision) is +/- 0.43 m.y. (standard deviation/slope of linear regression) (Saller et al., 1993).

The strontium isotope analysis shows that the sediments are becoming progressively younger from east to west which is in agreement with the geological interpretation of platform backstepping from SE to NW driven by the relative sea level rise.

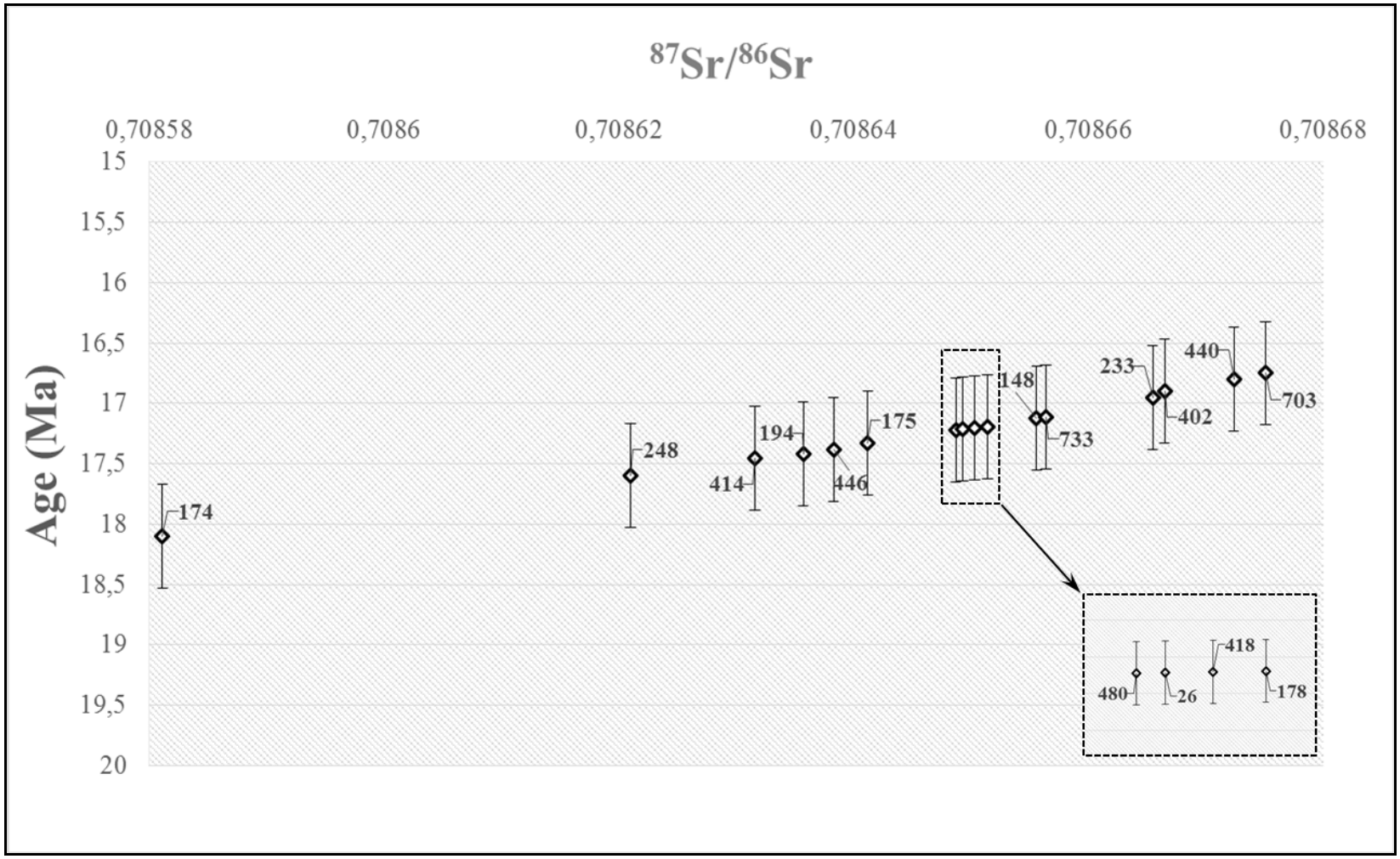


Figure 54: $^{87}Sr/^{86}Sr$ versus age (Age error = +/- 0.43 m/MA. The numbers in the chart indicate the sample IDs).

Based on the measured section, field mapping, and photomosaic, a regional cross section is built (Figure 55). The elevations and coordinates of the measured sections and rock samples have been located on the cross section using the field based gps measurements and topographic maps. Measured sections were correlated by bed-tracing in the field where possible and bed tracing on photomosaic elsewhere. A DEM of the study area shows about 480 meter topographic elevation difference between the East and West Platform (Figure 56).

The dip – parallel oriented cross section was built from the lower fore–reef facies of the East Platform to the transitional zone further up-dip to the back–reef of the West Platform (Figure 55).

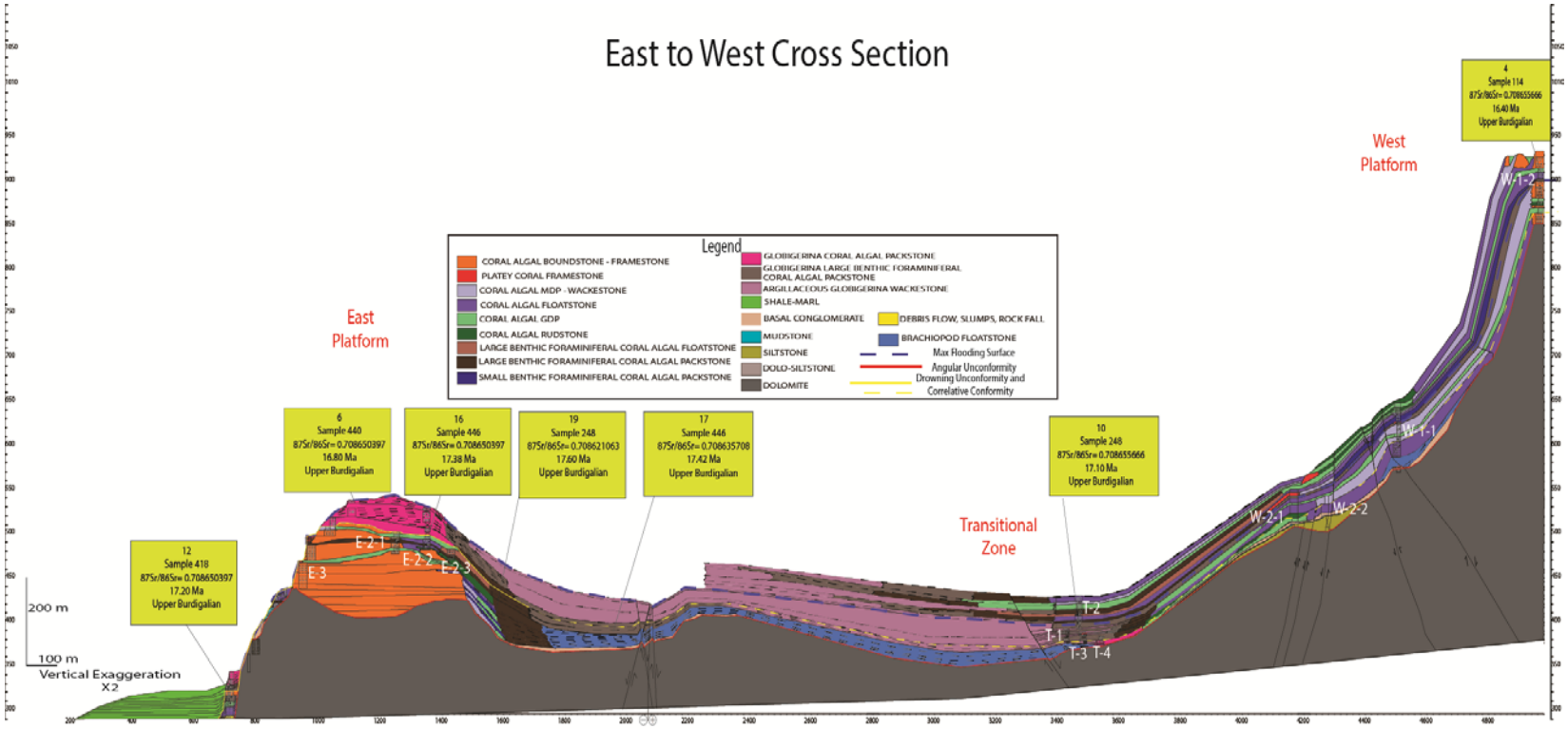


Figure 55: Cross section showing the facies distribution from the lower fore – reef of the East Platform to the reef core of the West Platform has been demonstrated using E-2, E-2-1, E-2-2, E-2-3, T-1, T-2, T-3, T-4, W-2-1, W-2-2, W-1-1, and W-1-2 measured sections and facies changes were walked out and recorded in the field. (Solid red line: angular unconformity overlying the substratum and underlying the Karaisali or Kaplankaya Formations, solid yellow line: drowning unconformity, dash yellow line: its correlative conformity, dash blue line: maximum flooding surface, yellow boxes: locations of the samples for the strontium isotope analysis and the results of the $^{87}Sr/^{86}Sr$ data).

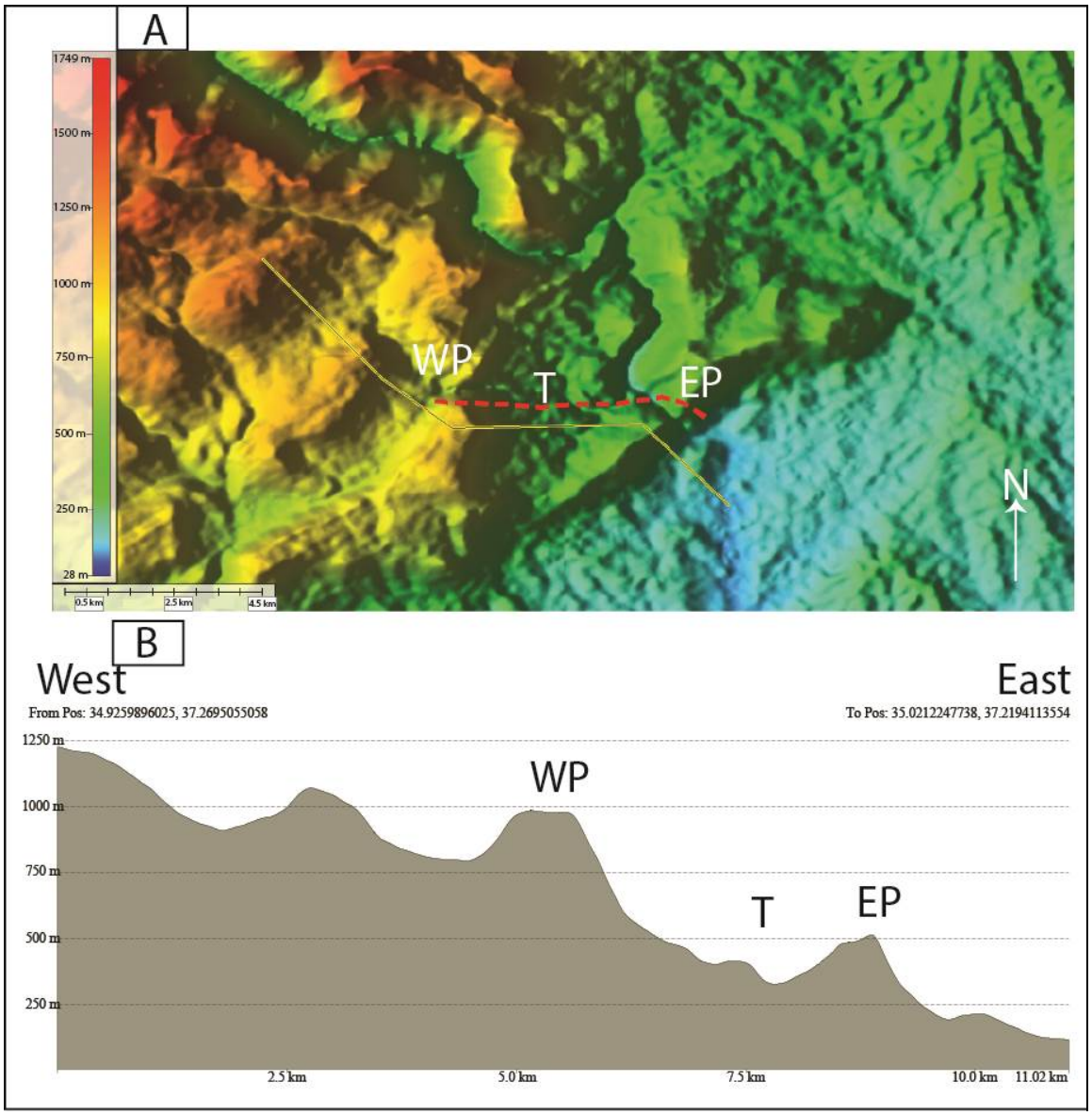


Figure 56: Digital elevation model of the study area (yellow solid line: location of the east to west profile illustrated in 68B, red dash line: location of the cross section represented in Figure 65, WP: Western Platform, T: Transitional Zone, and EP: Eastern Platform).

The cross section serves as a basis to develop a more general depositional model of the evolution of the small attached carbonate that developed in the study area (Figure 57).

The initial transgression during the Burdigalian resulted in the deposition of the basal conglomerates, mudstones, and bivalve floatstone of the Kaplankaya Formation unconformably into the paleo-depressions onto steeply dipping the substratum topography (Gorur, 1994). The shallow-water carbonates initially started to develop and onlap on the substratum paleo–slope in the East Platform. Small muddy and silty coral buildups backstepped against the steep substratum slope with the continued relative sea level rise. As relative sea level continue to rise, the shallow water carbonates could established on the substratum-high tops and allows a larger platform to develop and aggrade. The small carbonate platforms aggraded and built up vertically and laterally in the euphotic zone where the carbonate production is maximized. Periodically, the wave resistant reef margin collapsed and the rock falls/olistoliths were transported down to the toe of the slope and the basin. The middle slope was a zone of sediment bypass. Debris flows were observed in the updip position with respect to the rock falls. The size of the reworked clasts varies from a few microns to the boulder size. The coral algal floatstones in the uppermost fore-reef adjacent the reef - front exhibit dip angles of up to $36^0$. The clinoforms were not observed in the lower fore-reef of the East Platform. They might have been covered with the basinal shales of the Langhian Guvenc Formation (Ozcelik and Yetis, 1994) or they did not develop at all.

The basal conglomerates of the Kaplankaya Formation onlap the inherited topography of the substratum. The Karaisali Formation built up and tracked the sea level rise. These are interpreted to develop during the early and late transgression system tract

(TST). The coralgal boundstones/framestones were laterally and vertically well–developed during this phase. The overlying interval is dominated by debris flow in the middle to lower slope that contains boulders and cobbles of coral boundstone debris and carbonate mud. The presence of the mud in the matrix with the reworked coarse debris in the lower fore-reef is interpreted to develop during the highstand system tract (HST) (Brown and Loucks, 1993). Coralgal boundstone/framestone found in that HST only developed in the basinward (east) margin of the platform forming a raised rim.

The reefal carbonates in the East Platform could not keep-up with the relative sea level rise and the platform gradually drowned. The carbonate factory shut down as the reef was submerged beneath the euphotic zone. The drowning unconformity is not in the classical sense of the unconformities which include the hiatus and erosional surfaces related to the subaerial exposures (Schlager, 1992). The drowning interval on the platform exhibits a gradual vertical evolution of the facies from rhodolith bindstone with the moldic porosity forming during the initial drowning stage, followed by a thick succession of the planktonic coralgal packstone (Figure 44) finally overlain by thin planktonic-rich facies. That showed an increase in water depth on the platform top. The reef complexes in the easternmost margin of the East Platform then backstepped towards the northern-west margin that was topographically higher. The minimum and maximum age constraints for the initiation of drowning of the East Platform are 17.38 +/- 0.43 Ma and 17.60 +/- 0.43 Ma, respectively. The minimum age constraint for final drowning stage is 16.80 Ma +/-0.43 Ma.

The increase in the rate of sea-level rise resulted in the deposition of the planktonic coralgal packstone over the top of the East Platform and drowning of the

platform. This planktonic sequence is interpreted to represent the transgressive system tract (TST).

The reef complex in the Middle Platform was not well developed and relatively small in both lateral and vertical dimensions. Prograding clinoforms developed from north to south and rotational slides were observed in the lower slope. This aggradational character of the clinoforms resulted in the interpretation to represent HST. The drowning unconformity developed directly on the top of the coralgal boundstone/framestones that form the bulk of the Middle Platform. These boundstones were overlain by thin planktonic foraminiferal coralgal packstones. All of the above observations show that the reef complex was developed during the early highstand and drowned at the late highstand or early transgression.

The lower section of the transitional zone exhibits upward deepening and upward thickening trend of the high frequency cycles (HFC). These transgressive system tract deposits were overlain by the maximum flooding surface. The age data of the planktonic and large benthic foraminiferal packstone/floatstone underlying the maximum flooding zone (MFZ) points out that MFZ was developed later than 17.10 +/- 0.43 Ma which is consistent with the age estimation of MFZ in the top of the East Platform. The succession overlying the MFZ is characterized by the upward thinning and shallowing cycles consisting of large benthic foraminiferal coralgal packstone at the base and coralgal floatstone at the cycle top. This highstand system track succession depicts well–developed clinobeds in the lower to middle fore-reef of the West Platform. This clinobeds show lateral and vertical transition of the middle slope facies to the lowermost fore–reef facies.

The West Platform exhibits two distinct growth patterns of the reef complexes; the reef core underlying the MFZ developed as a laterally and vertically extensive coral algal boundstone/framestone. The sample taken from the planktonic and large benthic foraminiferal packstone/floatstone (MFZ) is dated of 16.40 +/- 0.43 Ma, which is in agreement with the age constraints in the East Platform and the transitional zone. Well–developed transgressive coral algal boundstones/framestones were partially drowned and overlain by the planktonic facies in the late TST or early HST. The basement-high top platform was then flooded resulting in the deposition of thick beds of coral algal floatstone/ grain dominated packstone (Brown and Loucks, 1993 and House et al., 2000). There, carbonate production once started and caught up with the relative sea level rise during the late HST; however, these coral-buildups were discontinuous and were never able to build up well–developed continuous reefal rimmed margin. Furthermore, they raised their rims and prograded and aggraded basinwards.

In conclusion, the development of the reefal carbonates - Karaisali Formation was initiated with the Burdigalian transgression (Gorur, 1994). These carbonates started to develop with the onlapping geometry on the paleo–slope. As they reached the paleo high, they unconformably overlay the dolomitic basement and built–up extensive reef frameworks in the transgression. The amount of reef debris transported to the slope was enhanced during the highstand and the East and Middle Platforms were drowned starting at 17.60 Ma in the late highstand and early transgression. The reefs backstepped towards west and MFS was developed at 16.40 Ma. The West Platform exhibits the transgressive well developed reef frameworks and discontinuous coralgal boundstones above the MFS in the early to late highstand.

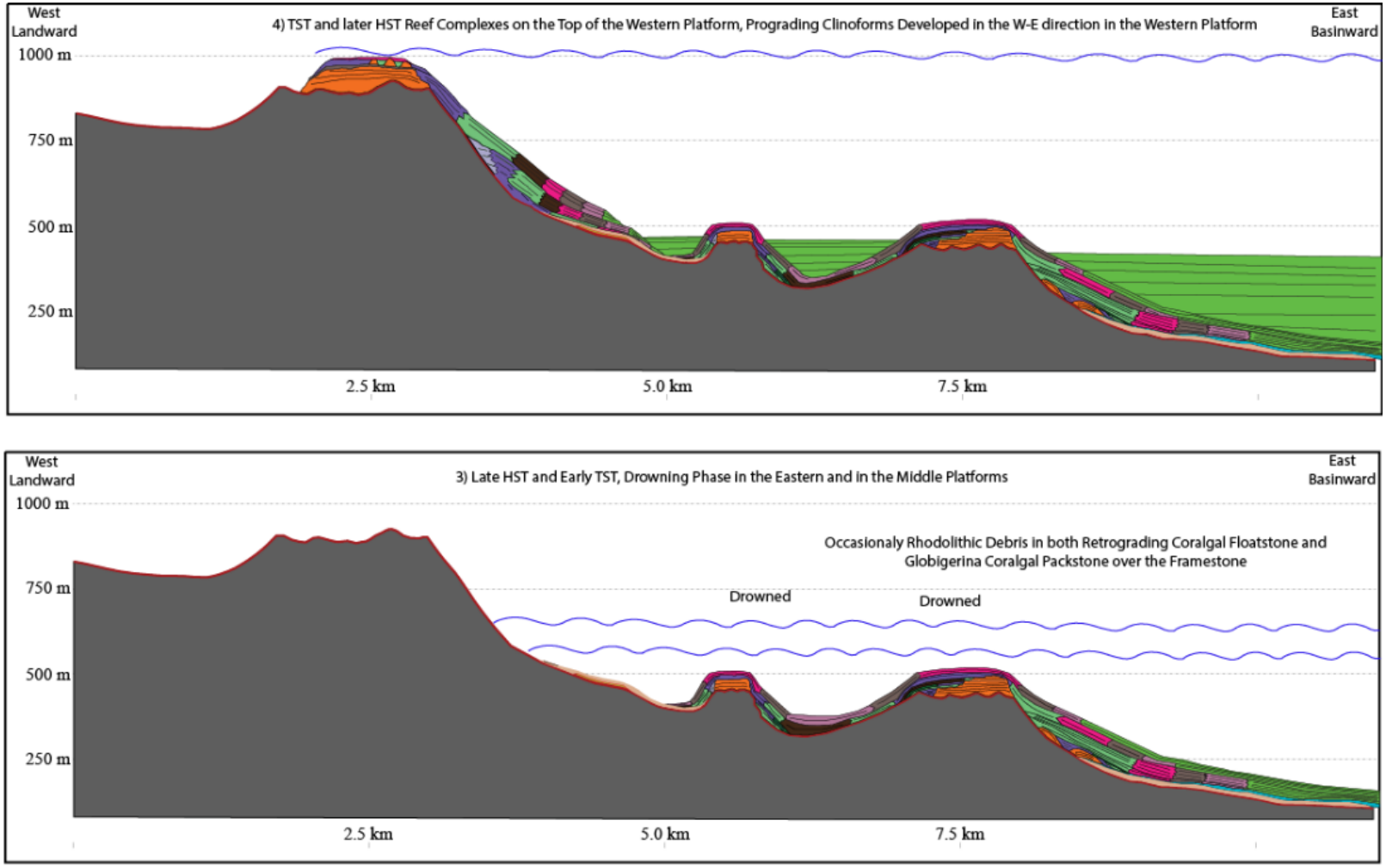


Figure 57: Generalized Depositional Model.

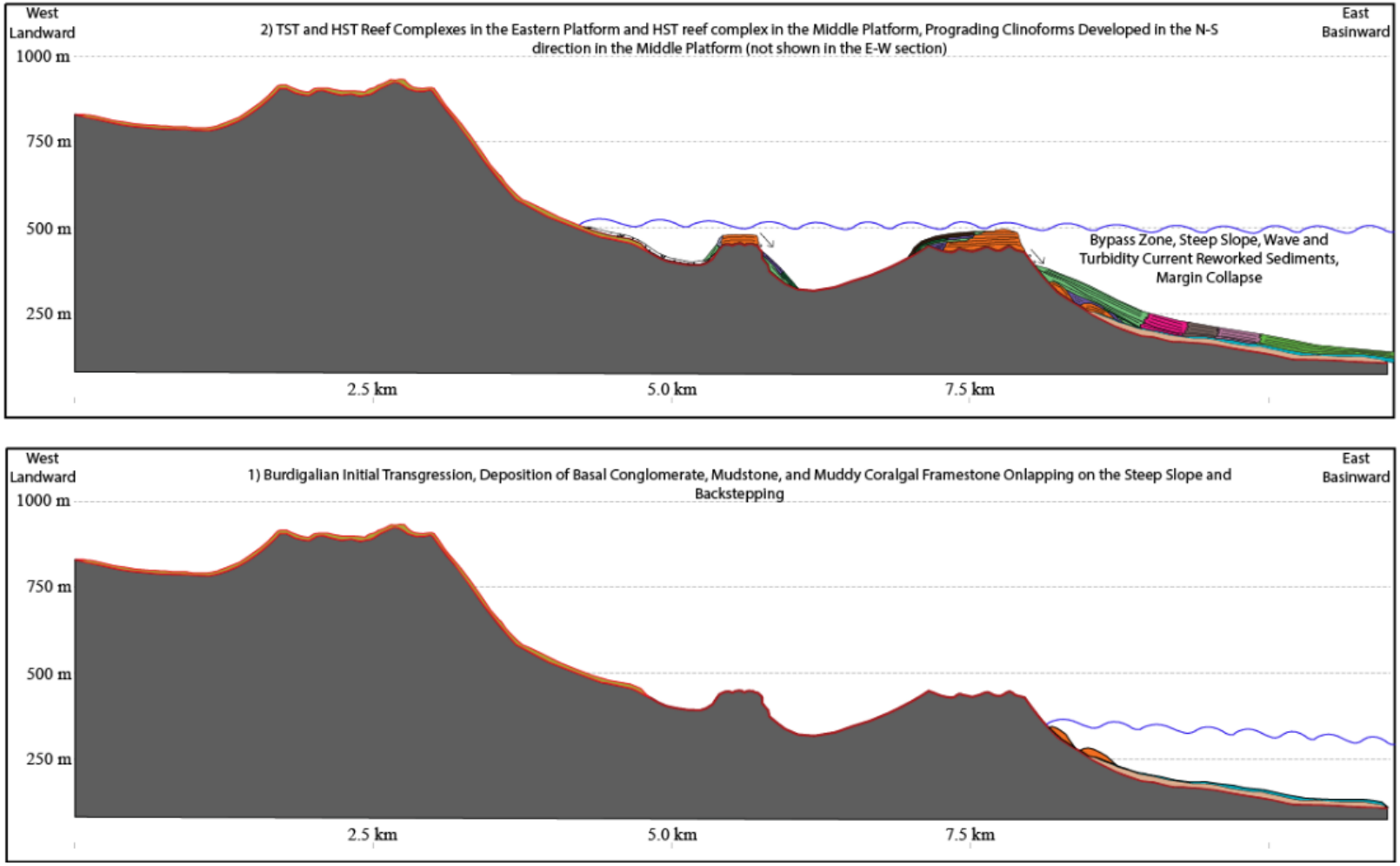


Figure 57: cont.

# Chapter 5 – Discussion

Two main questions need to be discussed to better understand the interaction between the structural framework and relative sea level fluctuations in creating the stratigraphic architecture of the Burdigalian carbonate platforms in the study area. These questions are: 1) Why did the platforms drown? and 2) Were the reef complexes in the East and West Platforms deposited contemporaneously?

## 5.1 Driving Mechanisms for Drowning

The growth, production, and termination of the hermatypic coral reefs are mainly controlled by the relative sea–level (eustacy and tectonics), nutrients, temperature, latitude, roughness of the substratum, intensity of light, and other environmetal factors (Schlager, 1992).

Chlorozoan associations (green algae and coral) grow in the temperature range between $15^0$ C and $30^0$ C. Thus, corals prefer warmer temperatures, although there exists an upper temperature limit (Schlager, 1992). The mean average temperature of the middle to late Burdigalian climate is about $20^0$ C for Turkey which is favorable for the coral growth (Figure 58) (Akgun et al., 2007). Hence, the temperature could not be the driving mechanism for the drowning of the platforms.

High nutrients are not favorable for the coral reefs since they can produce their own nutrients and recycle them within their systems, furthermore bio – erosion is enhanced with increasing nutrient supply (Schlager, 1992). The nutrients are often related with the arrival of terrigenous sediments (Bassant, 1999). The terrigenous inputs from the Tauride Mountains was deposited as deep marine channel turbidites in the Adana Basin during the late Burdigalian (Derman and Gurbuz, 2007; Blanco, 2014). However, the movement of the siliciclastic sediments towards the Karaisali reefal platforms was limited

during the Burdigalian and if terrigenous sediments existed, they confined to the depression between the platforms (Gorur, 1994 and Satur, 2004). Thus, external nutrient influx could not be the factor for drowning.

The average growth rate of the reefal platforms is 300 - 1000 m/Ma in the time range of $10^3 – 10^5$ years; moreover, the growth rate of the modern Caribbean reef corals is 5-10 mm/yr up to 10 meter water depth and decreases as the water depth increases (Schlager, 1992). Hence, the coral reefs keep up with the steady subsidence and third – order sea level fluctuations with both of 10 – 100 m/Ma (Schlager, 1992 and Kim et al., 2012). The drowning of the platform can occur with the relative sea – level rise whose rate outstrips the growth rate of the reefal platforms (Schlager, 1992 and Kim et al., 2012).

Rhodoliths and planktonic-rich facies, which are both interpreted as relatively deep water facies, were found overlying shallow water coralgal boundstone in the East Platform. The transition from the shallow water facies to deeper water facies is sharp possibly indicating a sudden deepening.

The successful drowning of the East and Middle Platforms in the study area is interpreted as being related to a sharp relative sea level change.

### 5.2 WERE THE EAST AND WEST PLATFORMS COEVAL?

The West Platform is located 480 meter higher than the East Platform in topographic elevation (Figure 56). To test whether this elevation difference represents the elevation difference in paleotopography and to check whether the carbonate complexes could have developed contemporaneously or be later faulted, both the strontium isotope analysis data and the stratigraphy are examined in this section to support that the

platforms were not coeval and that the successful drowning was mainly driven by a relative sea level rise.

The faults that were mapped in the study area have vertical offset of maximum 10 – 20 meter. In the geological map (Figure 2), the faults which are drawn with white lines have mostly small vertical offsets. These faults are dominantly NNE-SSW oriented extensional and transtensional structures that can be related to the sinistral strike slip Kozan and Ecemis Fault Zones due to their similar trends and slip characters (Kocyigit and Beyhan, 1999; Jaffey and Robertson, 2001; Piper et al., 2010). Most of the faults are post-depositional (post-Burdigalian) extensional stuctures since the growth strata, growth of the fault with sedimentation, and facies patterns related to syndepositional faults were not observed along these structures (Cross et al., 1998 and Wilson, 1999). Few small sydepositional faults tip out below the growth folds with 40 to 100 cm vertical offsets. The vertical offsets could not be measured in the other faults because either the fault planes were eroded or marker beds can not be found. The main problem encountered in observing the record of the faults in the successions is the absence of the post–Burdigalian deposits in the study area.

The black lines in the geological map (Figure 2) represent the main faults which were compiled from General Directorate of Mineral Research and Exploration (MTA) N33 and N34 geological maps. Three easternmost faults cannot create a large topographic elevation difference between the East and West Platforms because either their fault planes are passing through the top of the East Platform with smaller fault throws or the platform is located on the up-thrown block of the most easternmost fault that is not increasing the elevation difference between the East and West Platforms. The westernmost faults are also unlikely to create a large vertical offset, such as, 300 – 500 m, a sharp change in the facies

along the fault planes was not observed in the field. Hence, most of the faults in the study area are post-depositional and do not have large vertical throws that can result in a large topographic elevation difference between the platforms.

Assuming that, to create a topographic elevation difference between the platforms located about 3 km apart from each other, platforms were subjected to differential subsidence and the hinge line was located in the West Platform. In order to create a tilt of 300 meter over 3 km, the beds would have been tilted about $5.8^0$. However, the beds are almost horizontal at the platform tops and in the transitional zone.

Established eustatic curves from Miller et al. (2005) and Komintz et al. (2008) do not show any significant sea level rise during middle to late Burdigalian (Figure 58). The eustatic curve of Haq et al. (1987) exhibits a total of 100 meter sea level rise during the entire Burdigalian. In the adjacent Mut Basin, Bassant (1999) reported relative sea level rise of 200 meter within 1.7 Ma in the Burdigalian and concluded that this rise is related to the basinwide post–extensional subsidence plus the eustatic sea level rise reported by Haq et al. (1987). Gorur (1994) constructed a relative sea level curve for the Adana Basin and pointed out that this relative sea level curve resembles to the eustatic curve constructed by Haq et al. (1987) during Burdigalian. However, there exists a discrepancy between the relative and eustatic curves in Langhian to Serravalian.

The subsidence in the Adana Basin initiated in late Oligocene to earliest Miocene (Kelling et al., 1987). Total subsidence in the Adana Basin during Oligocene to Serravalian is about 4.0 km of which 2.5 km is the tectonic subsidence (Radeff, 2014). Assuming the constant subsidence during this interval, the rate of total subsidence (the amount of total subsidence/total time duration between Oligocene and Serravalian) and tectonic subsidence rate (the amount of tectonic subsidence/total time duration between

Oligocene and Serravalian) is 243 m/MA and 152 m/Ma, respectively. This assumption is made due to the fact that the total and tectonic subsidence curves of the Adana Basin have been drawn as linear (Radeff, 2014). Although these overall subsidence rates are relatively high enough to depict the rise of the relative sea level, they are not high enough on their own to drown a coral dominated carbonate platform (Schlager, 1992).

For calculation of the local subsidence rate, the following assumptions have been made:

1. An increase in the subduction rate caused the drowning of the East Platform.
2. The rise of subsidence rate was continuous within 1 Ma.

Sample 446 (just above the drowning unconformity) and Sample 114 (within the top of the MFZ sequence) represent the base and top of the transgressive sequence in which the rate of subsidence increased. This interval recorded the variation in the relative sea level (subsidence and eustacy). Since the sediments (Sample 446 and Sample 114) were deposited at the same water depth (both samples include planktonic foraminifera), the current topographic elevation difference indicates the relative sea level rise. The elevation difference between the sample 446 and sample 114 is 434 m. The overall total eustatic sea level during the Ottnangian and Karpatina is almost constant and fluctuates between +10 and 0 m; and -10 and +10 m in the eustatic curves constructed by Miller et al. (2005) and Komintz et al. (2008), respectively. The sea level curve of the adjacent Mut Basin shows that relative sea level of the Mut Basin fluctuates between 0 and 40 m during this time interval (Figure 58). We assume that the rate of the relative sea level rise equals the rate of total subsidence in the study area because of the relatively constant eustacy during middle and late Burdigalian. $^{87}Sr/^{86}Sr$ ratios indicate that these samples were deposited at 17.38 and 16.40 Ma, respectively. The total duration of the

transgressive sequence is 0.98 Ma +/- 0.43 Ma. The ratio of the rate of total subsidence to the total duration of the increase in the rate of total subsidence is 434 meter / 0.98 Ma. Thus, the rate of total subsidence ranges from 301 and 856 m/Ma using the age error of +/- 0.43 Ma with the mean value of ~ 443 m/Ma.

To calculate the tectonic subsidence rate, the values of the decompaction and the change in paleobathymetry of the Adana Basin have been determined using the linear subduction graphs of Radeff (2014). The rate of the sum of decompaction and the change in paleobathymetry is found as 91 m/MA (the sum of decompaction and the change in paleobathymetry = 1.5 km between Oligocene and Serravalian (Radeff, 2014)). The tectonic subsidence rate, calculated by subtracting the rate of the sum of decompaction and the change in paleobathymetry from the rate of total subsidence, is found as 352 m/Ma which can easily outpace the growth rate of the coral reefs (the mean growth rate of the corals ~ 300 m/Ma (Schlager, 1992. The rate of tectonic subsidence ranges from 210 and 765 m/Ma using the age error of +/- 0.43 Ma with the mean value of ~ 352 m/Ma. The rate of tectonic subsidence is high enough to drown the coral reefs including the age errors, even if the minimum rate of total subsidence = 301 m/Ma (rate of tectonic subsidence + decompaction + the change in paleobathymetry) can readily drown the reefal platforms; in addition, other factors, such as, the decrease in the surface area of the platform top and in the light intensity had stressed the corals out.

In conclusion, the increase in the rate of tectonic subsidence rate at approximately 17.38 Ma in Karaisali resulted in certain deepening and drowning of the East and Middle Platforms within 0.98 Ma. The reef carbonates in the East and West Platforms are not contemporaneous, which can also easily be detected because of the thick and relatively very thin planktonic facies in the top of the East and West Platforms, respectively. This

increase in the rate of subsidence might be related with the uplift at the basin margin (Tauride Mountains) and resulting subsidence in the basin interior. Furthermore, an increase in the rate of total subsidence in the eastern regions of the Mut Basin adjacent the Adana Basin was detected in the late Burdigalian (Blanco, 2014).

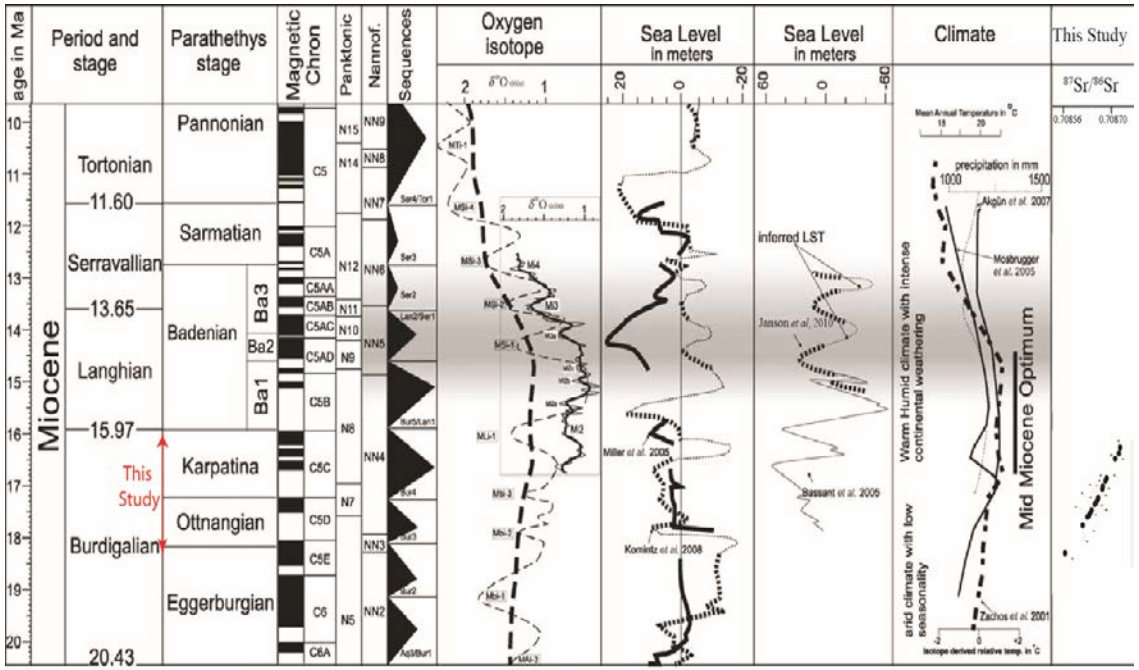


Figure 58: Early to middle Miocene age, stages, biozonation, sequences, isotopic curves and sea-level reconstruction modified after Janson et al. (2010) and Piller et al. (2007). Geochronology, geomagnetic polarity chrons, biozonations of planktonic foraminifers and calcareous nannoplankton modified after Lourens et al. (2004). Sequence stratigraphy and sea-level curve (after Hardenbol et al. (1998) and oxygen isotope stratigraphy (dashed curve after Abreu & Haddad (1998) partly recalibrated and correlated to regional chronostratigraphy of the Central ParaTethys from Piller et al. (2007). The solid oxygen isotope curves come from Miller et al. (1998). The sea-level reconstructions come from the New Jersey continental margin (solid line from Kominz et al. (2008) and dashed line from Miller et al. (2005)). Sea-level curves for the Mut basin from Bassant et al. (2005) and from this study. The climate column contrast an oxygen isotope derived relative temperature curve from Zachos et al. (2001) with two mean annual temperature curve for Germany (Mosbrugger et al. 2005) and Turkey (Akgun et al. 2007).

# Chapter 6 – Conclusion

The relative sea level rise (dominantly governed by the tectonic subsidence) and steep-rugged antecedent topography mainly control the initiation, architecture, facies distributions, and drowning of the Miocene reefal platforms in the Adana Basin. In this work, the sedimentological and structural analysis supplemented by strontium isotope dating lead to a better understanding of the reefal carbonates – Karaisali Formation developing in a strongly subsiding basin.

The facies assemblages of the previous works have been expanded as a result of field mapping and microscopic studies. Platey coral framestone, coralgal rudstone, coralgal flatstone, planktonic and large benthic foraminiferal packstone/floatstone, bivalve floatstone, and slumps/debris flow/rockfalls were created based on the faunal content, sedimentary structures, and the depositional environments.

The correlation of depositional environments of two adjacent Karaisali reefal platforms were provided in detail. Two transgressive and two highstand system tracts were detected in the Burdigalian Karaisali Formation. The age of the drowning unconformity and the later MFZ are 17.38 +/- 0.43 Ma and 16.40 +/- 0.43 Ma, respectively. The depositional model depicted that the Karaisali Platforms were developed in a rapidly subsiding basin without any significant syn-sedimentary movement associated with the substratum topography.

The relative sea level rise was found as regional in the Adana Basin and mainly governed by the tectonic subsidence. The rate of local tectonic subsidence increased at 17.38 +/- 0.43 Ma. The rate of mean total subsidence and tectonic subsidence, ~ 443 m/Ma and ~ 352 m/Ma, respectively, resulted in drowning and backstepping of the Karaisali reef complexes towards northernwest.

The Karaisali reefs preferentially developed on the paleo-highs of the antecedent topography. These grow patterns are similar to the ones of the Burdigalian Mut Platform, Mersin, Turkey (Bassant, 1999 and Bassant et al., 2005), the Miocene reefs in Cyprus (Follows, E.J. et al., 1996), the upper Miocene reefal platform of Las Negras area, southern Spain (Franseen and Goldstein, 1996b), and Jurassic Carbonates of the Venetian Alps, Italy (Zempolich, 1993).

# Appendix A

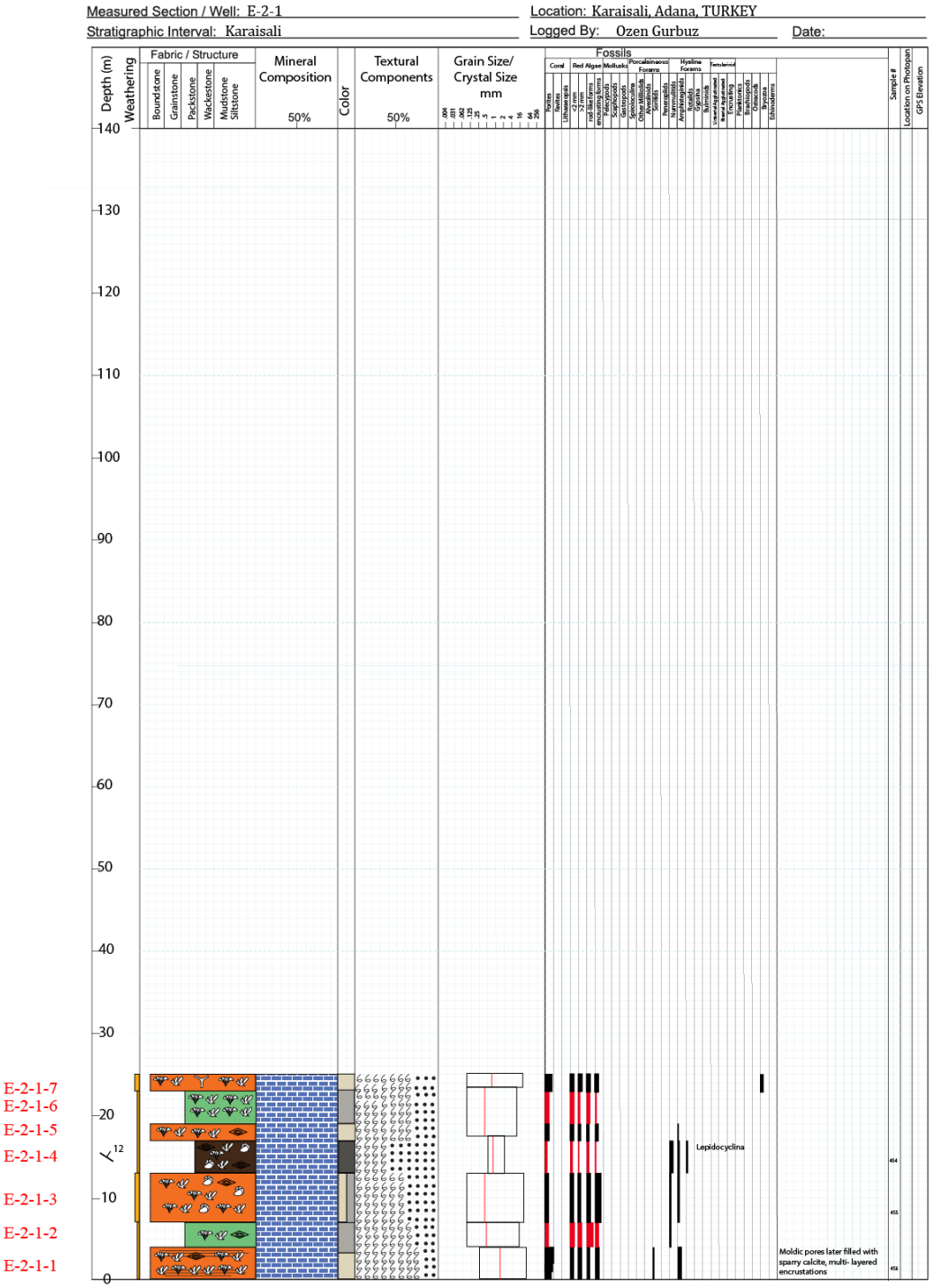


Figure 59: Measured section E-2-1.

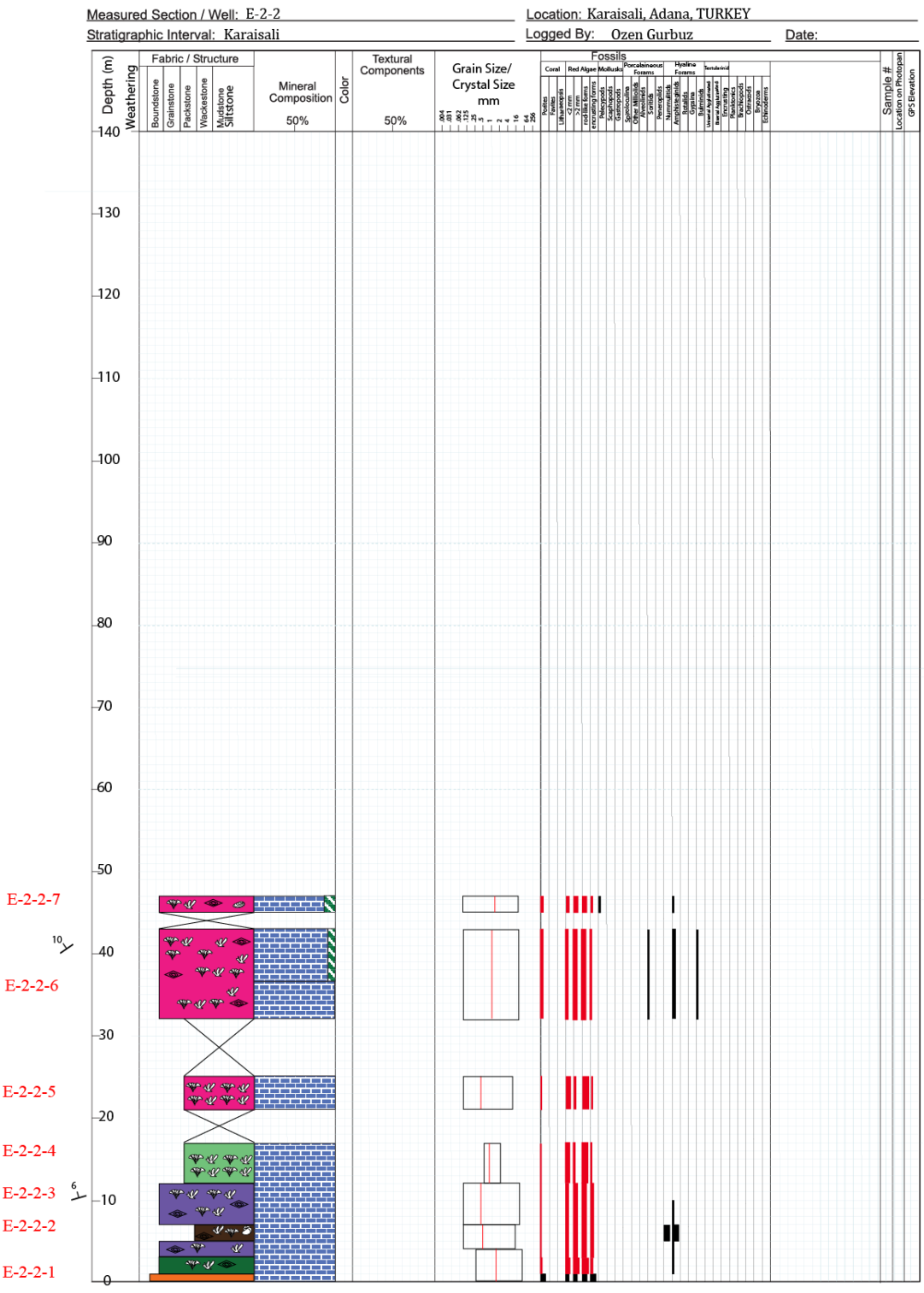


Figure 60: Measured section E-2-2.

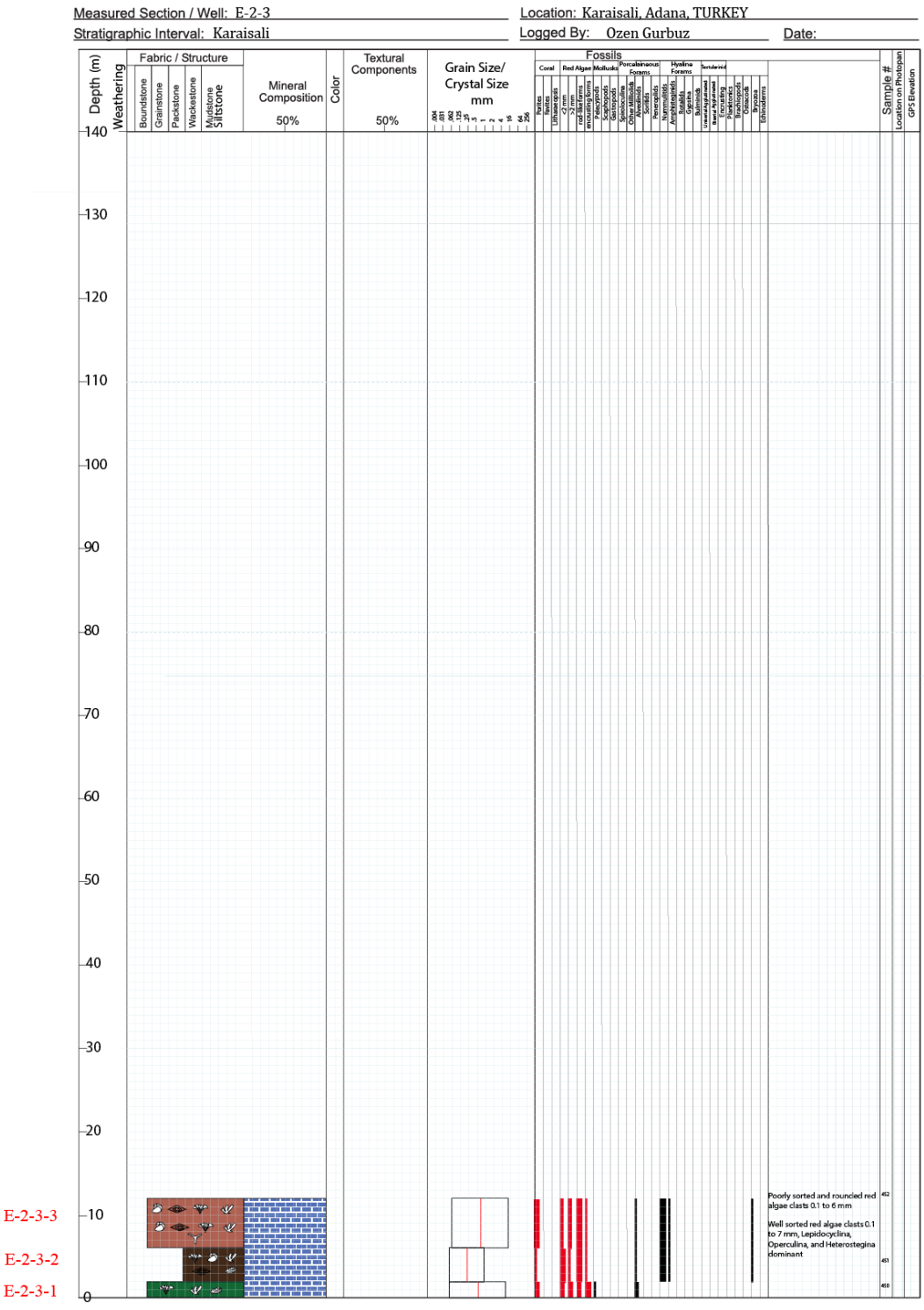


Figure 61: Measured section E-2-3.

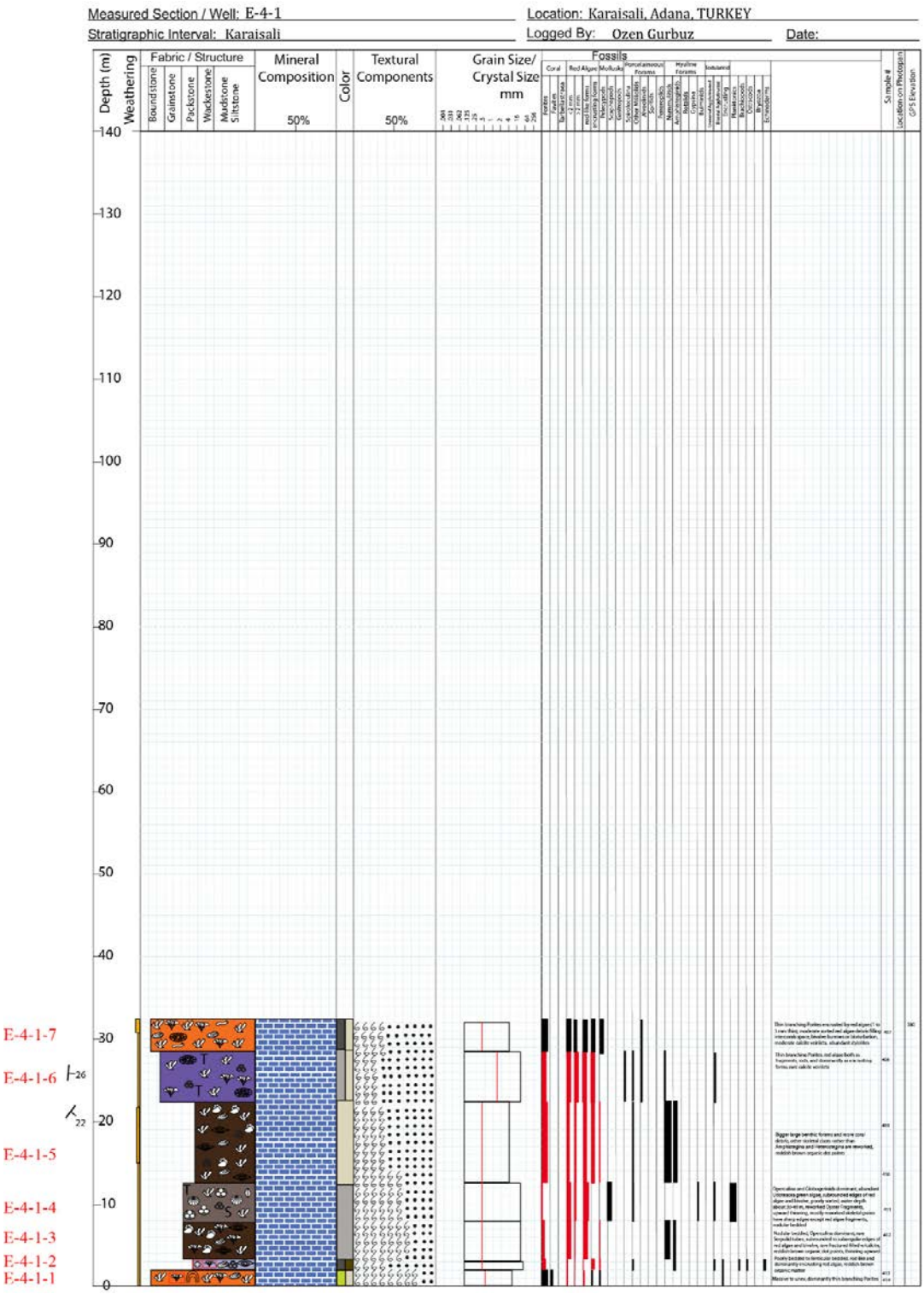


Figure 62: Measured section E-4-1.

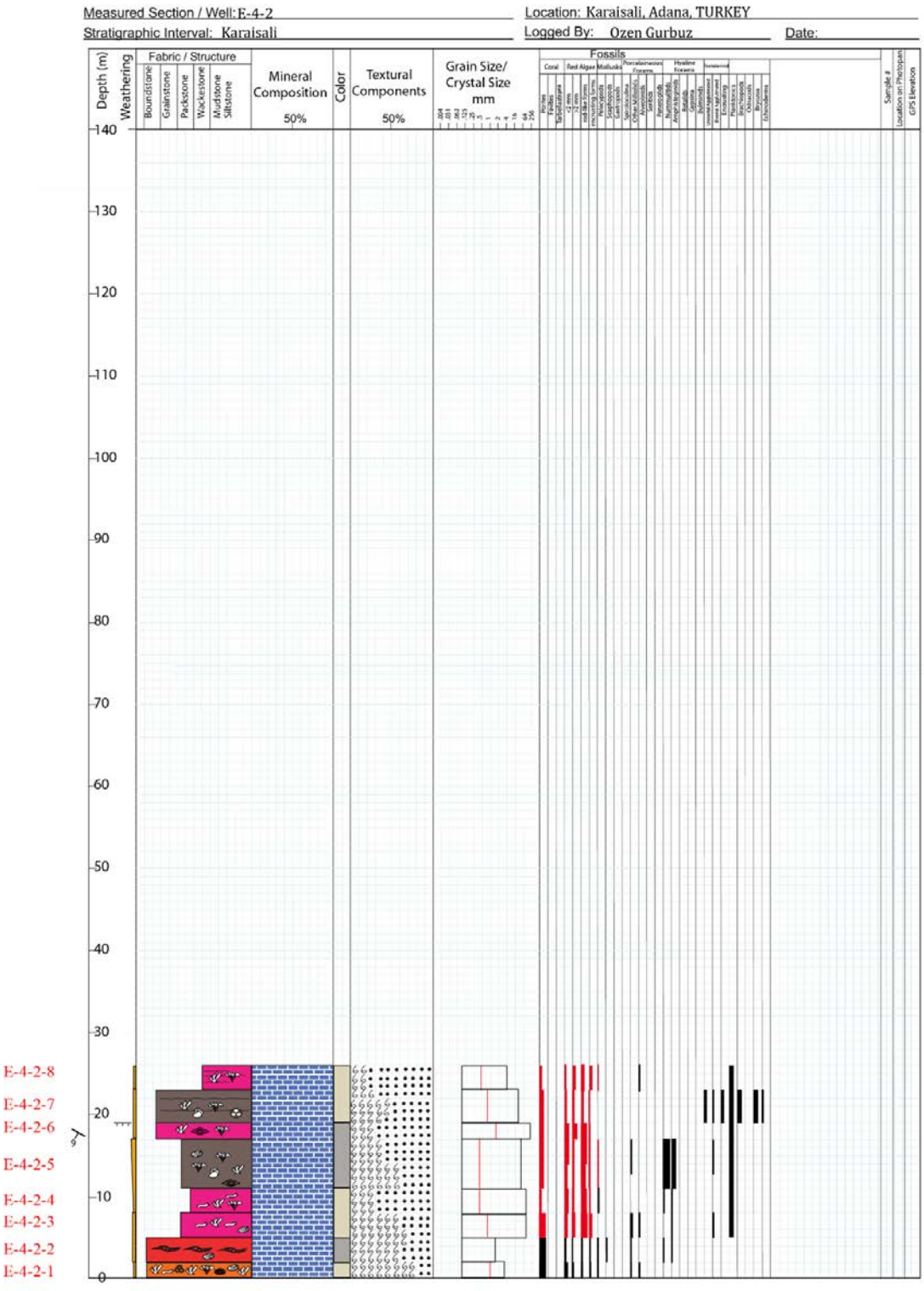


Figure 63: Measured section E-4-2.

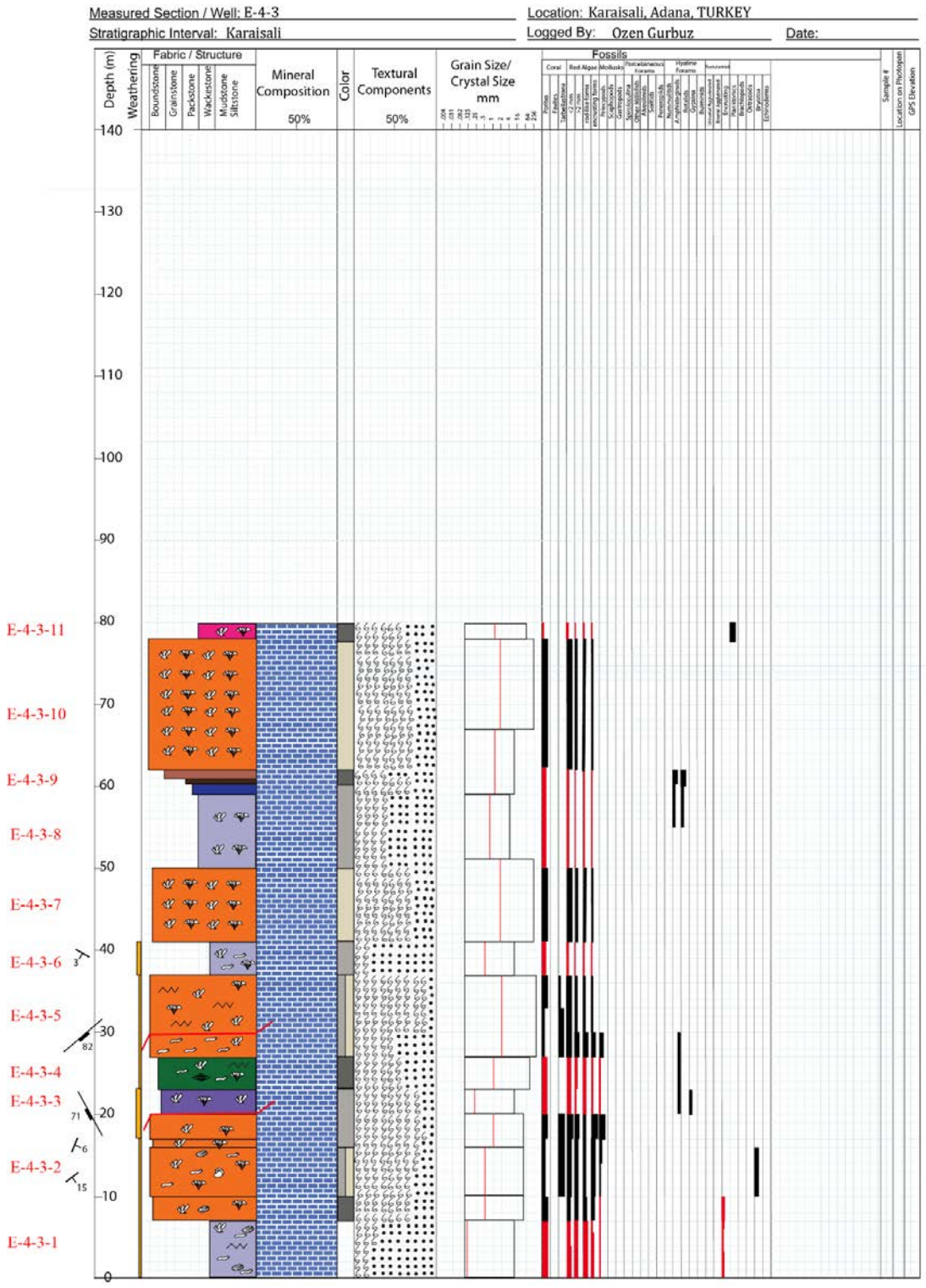


Figure 64: Measured section E-4-3.

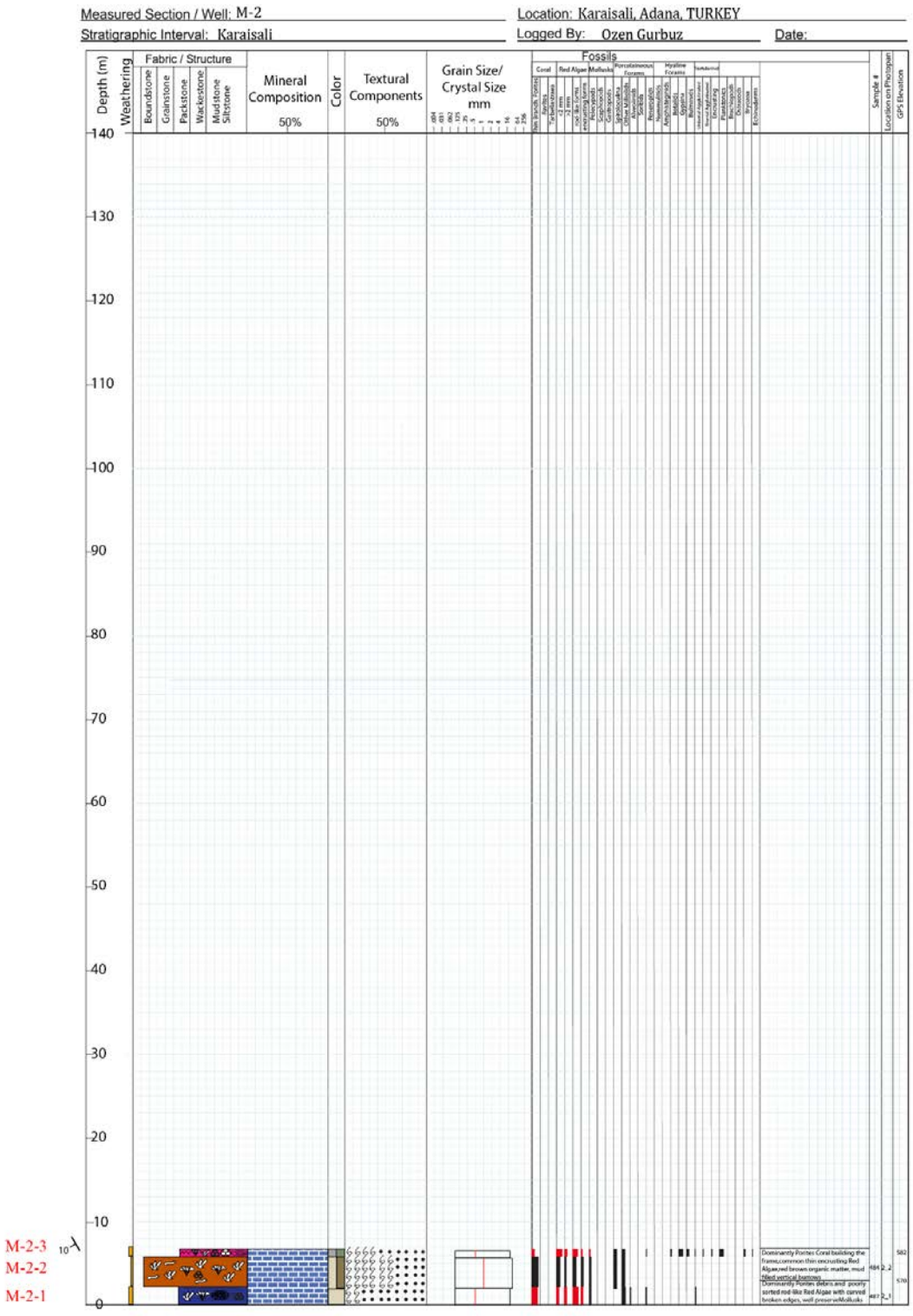


Figure 65: Measured section M-2.

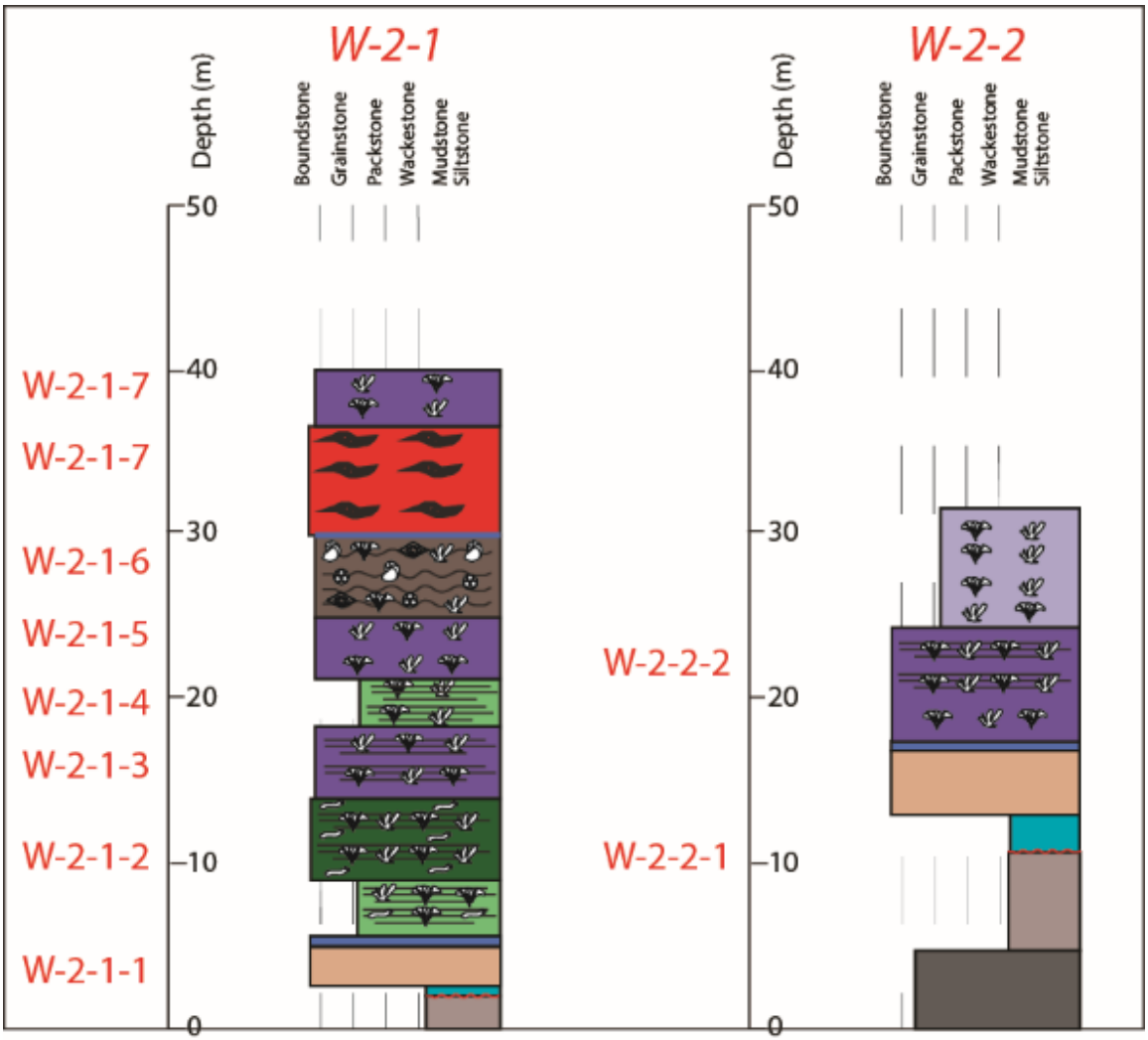


Figure 66: Measured sections W-2-1 and W-2-2.

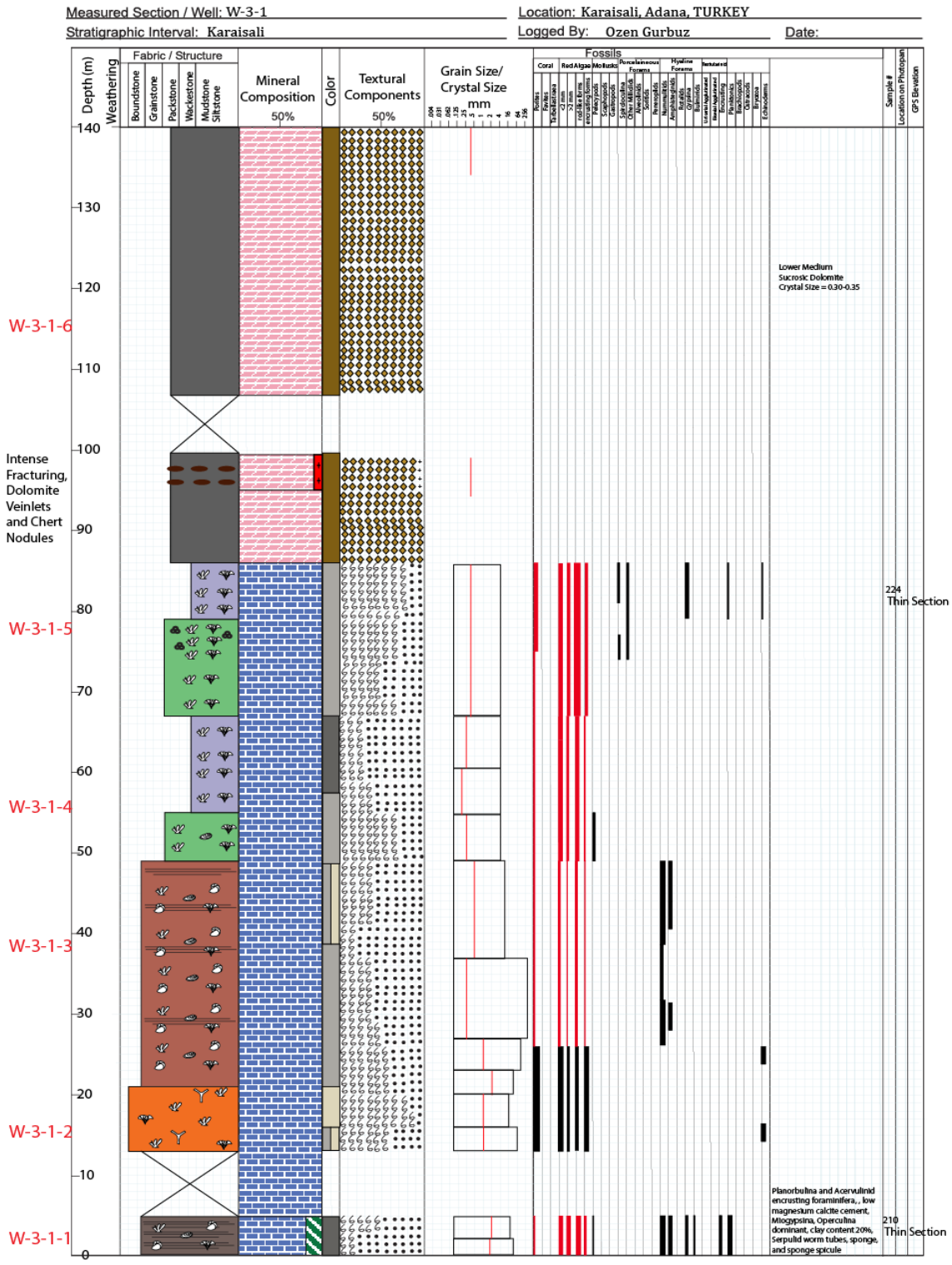


Figure 67: Measured sections W-3-1.

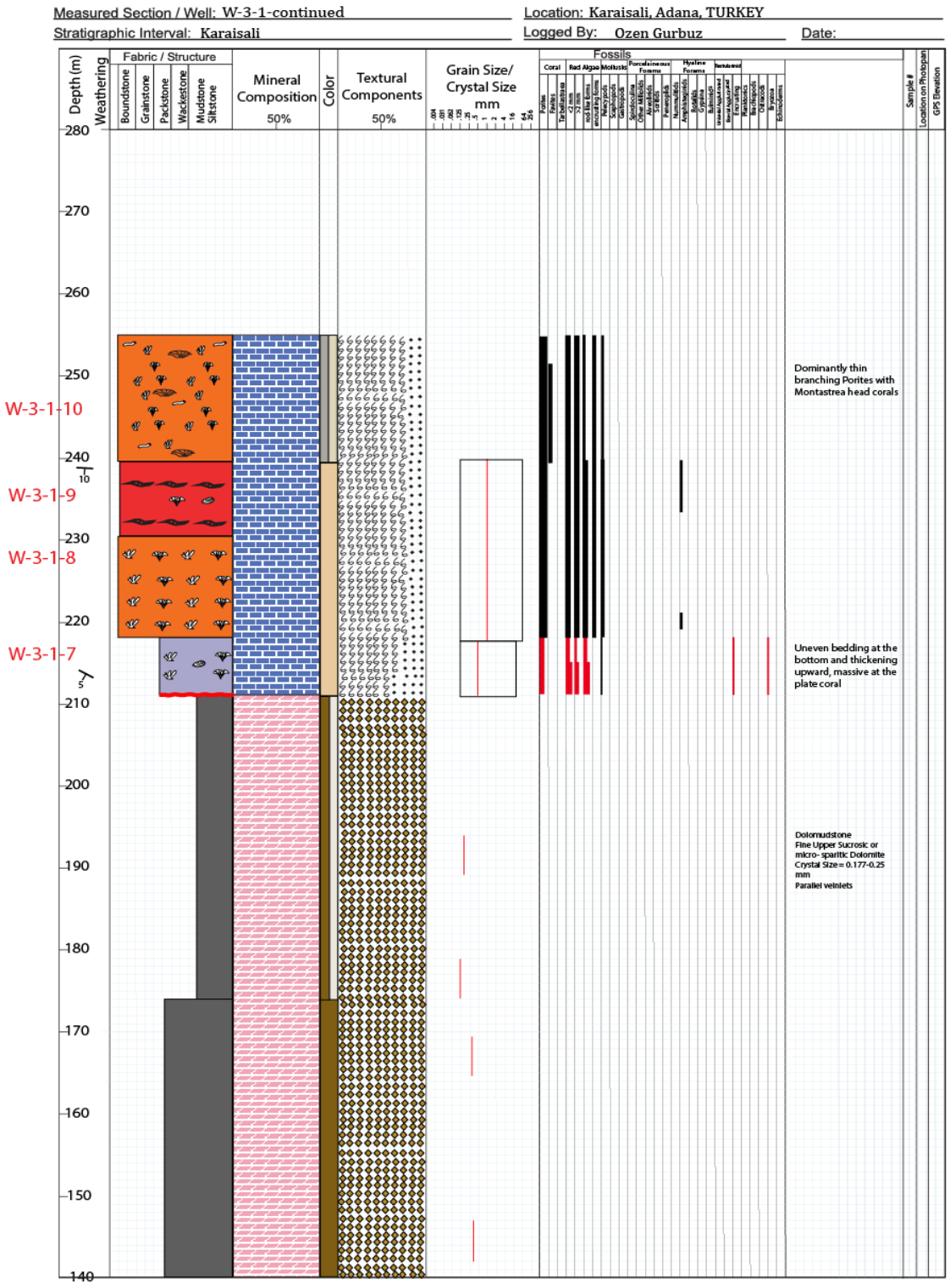


Figure 67: cont.

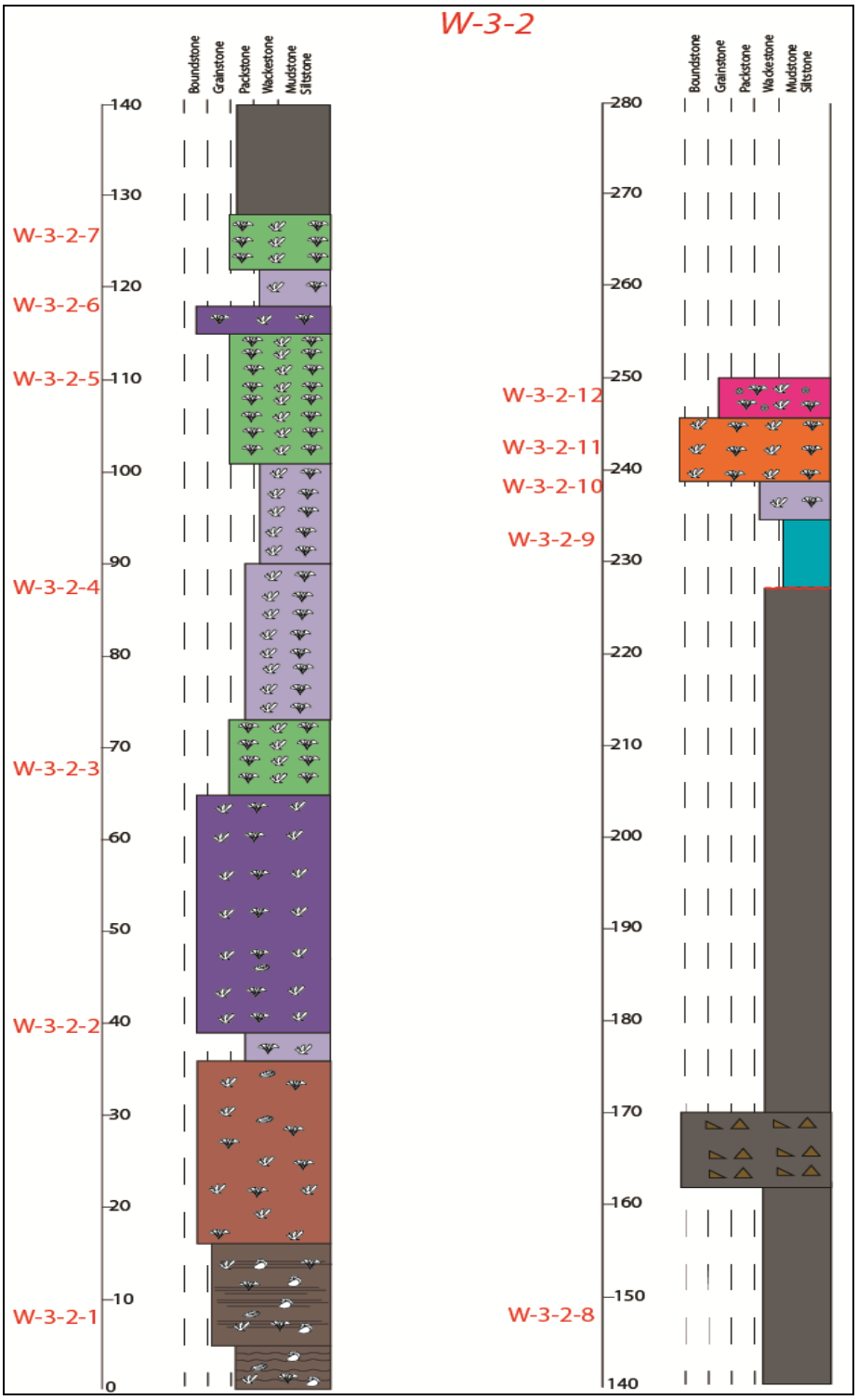


Figure 68: Measured sections W-3-2.

Figure 69: Measured sections T-3.

Figure 70: Measured sections T-4.

# References


*ABREU, V. S., and HADDAD, G. A. 1998, Glacioeustatic Fluctuations: the Mechanism Linking Stable Isotope Events and Sequence Stratigraphy from the Early Oligocene to Middle Miocene. In: GRACIANSKY, P. C., DE HARDENBOL, J., JACQUIN, T. & VAIL, P. R. (eds) Mesozoic and Cenozoic Sequence Stratigraphy of European Basins, Society for Sedimentary Geology (SEPM), Tulsa, OK, 60, p. 245 – 269.*

*AKGUN, F., KAYSERI, M.S., and AKKIRAZ, M.S., 2007, Paleoclimatic Evolution and Vegetational Changes during the Late Oligocene – Miocene Period in Western and Central Anatolia (Turkey), Paleogeography, Paleoclimatology, Paleoecology, 253, p. 56 – 90.*

*AKSU, A.E., ULUG, A., PIPER, D.J.W., KONUK, T., and TURGUT, S., 1992, Quaternary Sediments History of Adana, Cilicia, and Iskenderun Basins, Northeast Mediterranean Sea, Marine Geology, 104, p. 55 – 71.*

*AKSU, A.E., CALON, T.J., HALL, J., MANSFIELD, S., and YASAR, D., 2005, The Cilicia – Adana Basin Complex, Eastern Mediterranean: Neogene evolution of an active fore-arc basin in an obliquely convergent margin, Marine Geology, 221(1), p. 121 – 159.*

*AKSU, A.E., WALSH-KENNEDY S., HALL J., HISCOTT R.N., YALTIRAK C., AKHUN S.D., and CIFTCI G., 2014, The Pliocene – Quaternary Tectonic Evolution of the Cilicia and Adana Basins, Eastern Mediterranean: Special Reference to the Development of the Kozan Fault, Tectonophysics, 2014, p. 22 – 43.*

*ALLEN, J.R.L., 1965. A Review of the Origin and Characteristics of Recent Alluvial Sediments, Sedimentology 5, p. 89 – 191.*

*ALLEN, J.R.L., 1974. Studies in Fluviatile Sedimentation: Implications of Pedogenic Carbonate Units, Lower Old Red Sandstone, Anglo Welsh Outcrop, Geological Journal 9, p. 18 –208.*

*BASSANT, P., 1999, The High – Resolution Stratigraphic Architecture and Evolution of the Burdigalian Carbonate – Siliciclastic Sedimentary Systems of the Mut Basin, Turkey, PhD dissertation, Institute of Geology and Paleontology of University of Fribourg, p. 277.*

*BASSANT, P., VAN BUCHEM, F.S.P., STRASSER, A., GORUR, N., 2005, The Stratigraphic Architecture and Evolution of the Burdigalian Carbonate – Siliciclastic Sedimentary Systems of the Mut Basin, Turkey, Sediment. Geol., 173, p. 187 – 232.*

*BEAVINGTON – PENNEY, S.J. and RACEY A., 2004, Ecology of Extant Nummulitids and Other Larger Benthic Foraminifera: Applications in Palaeoenvironmental Analysis, Earth Science Reviews, 47 p.*

*BIJU–DUVAL, B., and MONTADERT, L., 1977, Introduction to the structural History of Mediterranean Basins; International Symposium on the Structural History of the Mediterranean Basins, Split (Yugoslovia) Editors Technip, Paris, p. 1 – 12.*

*BLANCO, D.F., 2014, Evolution of Orogenic Plateaus at subduction Margins, Sinking and Raising the Southern Margin of the Central Anatolian Plateau, PhD Dissertation, VU University Amsterdam, Faculty of Earth and Life Sciences, Department of Tectonics and Structural Geology, Amsterdam, Holland, 206 p..*

*BLUMENTHAL, M.M., 1947, Belemedik Mesozoyik ve Bunun Paleozoyik Kalker Çerçevesi, M.T.A. Yayını, Ankara, D/3, 93 p. (in Turkish).*

*BLUMENTHAL, M.M., 1952, Toroslar'da Yüksek Aladağ Silsilesinin Coğrafyası, Stratigrafisi ve Tektoniği Hakkında Yeni Etüdler. M.T.A. Yayını, Ankara, D/6, 163 p. (in Turkish).*

*BOSENCE, D.W.J., ALLISON, P.A., 1995, A Review of Marine Palaeoenvironmental Analysis from Fossils. In: Bosence, D.W.J., Allison, P.A. (Eds.), Marine Palaeoenvironmental Analysis from Fossils. Geological Society of London Special Publication, 83, p. 1 – 5.*

*BOZKURT, E., 2001, Neotectonics of Turkey – a Synthesis, Geodinamica Acta, 14, p. 3 – 30.*

*BRADSHAW, J.S., 1957, Laboratory Studies of the Rate of Growth of the Foraminifera Steblus Beccarii (Linne), var. tepida Cushman, Journal of Paleontology, 31, p. 1138 – 1147.*

*BRAGA, J.C., BASSI, D., and PILLER, W.E., 2010, Palaeoenvironmental significance of Oligocene-Miocene Coralline Red Algae – a Review, Int. Assoc. Sedimentol. Spec. Publ., 42, p. 165 – 182.*

*BRIDGE, C., CALON, T.J., HALL., J., and AKSU, A.E., 2005, Salt Tectonics in two Convergent – Margin Basins of the Cyprus Arc, Northeastern Mediterranean, Marine Geology, 2005, 26 p.*

*BROWN, A.A., and LOUCKS, R.G., 1993, Influence of Sediment Type and Depositional Processes on Stratal Patterns in the Permian Basin – Margin Lamar Limestone, McKittrick Canyon, Texas, In: Carbonate Sequence Stratigraphy: Recent Developments and Applications edited by Loucks, R.G., and Sarg, J.F., the American Assocciation of Petroleum Geologists, 57. P. 133 - 156.*

*BURTON, R., 2002, Miocene to Recent Stratigraphy, Structural Architecture and Tectonic Evolution of the Adana Basin, Southern Turkey, MSc Thesis, Department of Earth Sciences, Memorial University of Newfoundland, 168 p.*

*BURTON-FERGUSON, R., AKSU, A.E., Calon, T.J., Hall, J., 2005, Seismic Stratigraphy and Structural Evolution of the Adana Basin, Eastern Mediterranean, Marine Geology, 221, p. 189 – 222.*

*CIPOLLARI, P., COSENTINO, D., RADEFF, G., SCHILDGEN, T.F., FARANDA, C., GROSSI, F., GLIOZZI, E., SMEDILE, A., GENNARI, R., DARBAS, G., DUDAS, F.O., GURBUZ, K., NAZIK, A., ECHTLER, H.P., 2013, Easternmost Mediterranean Evidence of the Zanclean Flooding Event and Subsequent Surface Uplift: Adana Basin, Southern Turkey. In: Robertson, A.H.F., Parlak, O., Ünlügenç, U.C. (Editors), Geological Development of Anatolia and the Easternmost Mediterranean Region. Geological Society of London Special Publications, 372, p. 473 – 494.*

*CLARK, M., and ROBERTSON, A., 2002, The Role of the Early Tertiary Ulukisla Basin, Southern Turkey, in Suturing of the Mesozoic Tethys Ocean. Journal of the Geological Society, London, 159, p. 367 – 378.*

*COSENTINO, D., DARBAS, G., GLIOZZI, E., GROSSI, F., GURBUZ, K., and NAZIK, A., 2010, How did the Messinian Salinity Crisis Impact the Adana Basin? International Symposium on the Eastern Mediterranean Geology, 18-22 October 2010, University of Cukurova, Adana, Turkey, p. 145.*

*COSENTINO, D., SCHILDGEN, T., CIPOLLARI, P., FARANDA, C., GLIOZZI, E., HUDACKOVA, N., LUCIFORA, S., STRECKER, M., 2012, Late Miocene Surface Uplift of the Southern Margin of the Central Anatolian Plateau, Central Taurides, Turkey, Geol. Soc. Am. Bull., 124 (1/2), p. 133 – 145.*

*COSENTINO, D., BUCHWALDT, R., SAMPALMIERI, G., IADANZA, A., CIPOLLARI, P., SCHILDGEN, T., HINNOW, L.A, RAMEZANI, J., and BOWRING, S.A. (2013), Refining the Mediterranean "Messinian Gap" with High –Precision U-Pb Zircon Geochronology, Central and Northern Italy, Geology, 41(3), p. 323 – 326.*

*CRONIN, B.T., GURBUZ, K., HURST, A., and SATUR, N., 2010, Vertical and Lateral Organization of a Carbonate Deep-water Slope Marginal to a Submarine Fan System, Miocene, Southern Turkey, Sedimentology, 47, p. 801 – 824.*

*CROSS, N.E., PURSER, B.H., BOSENCE, and D.W.J., 1998, The Tectono-sedimentary Evolution of a Rift Margin Fault-block Carbonate Platform: Abu Shaar, Gulf of Suez, Egypt. In Purser, B.H., Bosence, D.W.J. (eds.), Sedimentation and tectonics of rift basins: Red Sea-Gulf of Aden, Chapman and Hall, London, p. 271 - 295.*

*DEMIRTASLI, E., TURHAN, N., BILGIN, A.Z., SELIM, M., 1984, Geology of the Bolkar Mountains, International Symposium on the Geology of the Taurus Belt, Ankara, p. 125 – 141.*

*DERMAN, S.A., and GURBUZ, K., 2007, Nature, Provenance and Relationships of Early Miocene Palaeovalley Fills, Northern Adana Basin, Turkey: Their Significance*

*for Sediment-Bypassing on a Carbonate Shelf, Turkish Journal of Earth Sciences, 16, p. 181– 209.*

*DEWEY, J.F., HEMPTON, M.R., KIDD, W.S.F, SAROGLU, F., and SENGOR, A.M.C, 1986, Shortening of Continental Lithosphere: the Neotectonics of Anatolia a Young Collision Zone, Collision Tectonics (eds) Coward M.P. and Ries A.C., Geol. Soc. London Spec. Publ. 22, p. 3 – 36.*

*DILEK, Y., and MOORES, E.M., 1990. Regional Tectonics of the Eastern Mediterranean Ophiolites. MALPAS, J., MOORES, E., PANAYOTOU, A. & XENOPHONTOS, C. (eds), Oceanic Crustal Analogues, Proceeding of the Symposium "Trodos 1987". The Geological Survey Department, Nicosia, Cyprus, p. 295 – 309.*

*DOYURAN, V., GULKAN, P., and KOCYIGIT, A., 1989, Seismotectonic Evaluation of the Akkuyu Nuclear Power Plant Site; Middle East Technical University, Ankara, Unpublished Report Geology and Geophysics Research Center, 69 p.*

*DUMAN, T.Y., and EMRE, O., 2013, The East Anatolian Fault: Geometry, Segmentation and Jog Characteristics, Geol. Soc. Lond. Spec. Publ. 372, p. 475 – 529.*

*DUNHAM, R.J. (1962), Classification of Carbonate Rocks according to Depositional Texture, Classification of Carbonate Rocks (ed. by W.E. Ham), AAPG Mem., 1, p. 108 – 121.*

*EKMEKYAPAR, A., 2006, Asagi Belemedik (Kiralan-Hacikiri) Dolaylarinin Stratigrafik Ozellikleri, Cukurova Universitesi Fen Bilimleri Enstitusu Jeoloji Muhendisligi Bolumu, Yuksek Lisans Tezi, Adana, 89 p. (in Turkish).*

*EMBRY, A.F., and KLOVAN, J.E., 1971, A Late Devonian Reef Tract on Northeastern Banks Island, Northwest Territories, Bull. Can.Petrol. Geol., 19, p. 730 – 781.*

*ESTEBAN, M., 1996, "An Overview of Miocene Reefs from Mediterranean Areas: General Trends and Facies Models" Models for Carbonate Stratigraphy from Miocene Reef Complexes of Mediterranean Regions, SEPM, Concepts in Sedimentology and Paleontology, v 5, p. 3 – 53.*

*FARANDA, C., GLIOZZI, E., CIPOLLARI, P., GROSSI, F., DARBAS, G., GURBUZ, K., NAZIK, A., GENNARI, R., and CASENTINO, D., 2013, Messinian Paleoenvironmental Changes in the Easternmost Mediterranean Basin: Adana Basin, Southern Turkey, Turkish Journal of Earth Sciences, 22, p. 839 – 863.*

*FLUGEL, E., 2009, Microfacies of Carbonate Rocks Analysis, Interpretation, and Application, 2nd Edition, 1006 p.*

*FOLLOWS, E.J., ROBERTSON, A.H.F., and SCOFFIN, T.P., 1996, Tectonic Controls on Miocene Reefs and Related Carbonate Facies in Cyprus, Models for Carbonate Stratigraphy from Miocene Reef Complexes of Mediterranean Regions, SEPM, Concepts in Sedimentology and Paleontology, v 5, p. 295 – 315.*

*FRANSEEN, E.K., and MANKIEWICZ, C., 1991, Depositional Sequences and Correlation of Middle (?) to Late Miocene Carbonate Complexes, Las Negras and Niger Areas, Southeastern Spain. Sedimentology 38, p. 871 – 898.*

*FRANSEEN, E. K., ESTEBAN, M., WARD, W. C., AND ROUCHY, J. M., 1996a, "Models for Carbonate Stratigraphy from Miocene Reef Complexes of Mediterranean Regions: Introduction" Models for Carbonate Stratigraphy from Miocene Reef Complexes of Mediterranean Regions, SEPM, Concepts in Sedimentology and Paleontology, v 5, p. v – ix.*

*FRANSEEN, E. K. and GOLDSTEIN, R.H., 1996b, Upper Miocene Platform Evolution, Las Negras Area, Southeastern Spain, In: Models for Carbonate Stratigraphy from Miocene Reef Complexes of Mediterranean Regions, SEPM Concepts in Sedimentology and Paleontology, 5, p. 159 – 176.*

*GOKCEN, S.L., KELLING, G., GOKCEN, N., and FLOYD, P.A., 1988, Sedimantology of a Late Cenozoic Collisional Sequence: the Misis Complex, Adana, South Turkey; Sedim. Geol. 59, p. 205 – 235.*

*GORUR, N., 1979, Karaisali Kirectasinin (Miyosen) Sedimentolojisi. TJKB 22/2, p. 227 – 234 (in Turkish).*

*GORUR, N., 1985, Depositional History of Miocene Sediments on the NW flank of the Adana Basin, Proc. Sixth Colloquium on Geology of the Aegean Region, Izmir, p. 185 – 208.*

*GORUR, N., 1992, A Tectonically Controlled Alluvial Fan which Developed into a Marine Fan Delta at a Complex Triple Junction: Miocene Gildirli Formation of the Adana Basin, Turkey. Sedimentary Geology, 81, p. 241 – 252.*

*GORUR, N., 1994, Tectonically Control in the Development of a Lower-Middle Miocene Reef at a Complex Triple Junction: Depositional History of the Karaisali Formations of the Adana Basin, Turkey, Geologie Mediterrane'enne, Tome XXI, n 1-2, p. 49 – 67.*

*GUL, M., 2007. Effects of Antecedent Topography on Reefal Carbonate Deposition: Early-*
*Middle Miocene of the Adana Basin, S Turkey. Journal of Asian Earth Sciences, 31, p. 18 – 34.*

*GURBUZ, K., and KELLING, G., 1993. Provenance of Miocene Submarine Fans in the Northern Adana Basin, Southern Turkey: A Test of Discriminant Function Analysis. Geological Journal, 28 (3-4), p. 277 – 293.*

*GURBUZ, K., 1999. Regional Implications of Structural and Eustatic Controls in the Evolution of Submarine Fans: an Example from the Miocene Adana Basin, Southern Turkey. Geological Magazine 136 (3), p. 311 – 319.*

*GURBUZ, K., and UNLUGENC, U. C., 2001, Field Excursion A1 Guide Book - Neogene Adana Basin (26 September 2001), Fourth International Turkish Geology Symposium – Cukurova University, Adana, Turkey, p. 24 – 28.*

*HALLOCK, P., 1979, Trends in Test Shape with Depth in Large, Symbiont – Bearing Foraminifera, Journal of Foraminiferal Research, 9, p. 61 – 69.*

*HALLOCK, P., and GLENN, E.C., 1986, Larger Foraminifera: a Tool for Paleoenvironmental Analysis of Cenozoic Depositional Facies, Palaios, 1, p. 55 – 64.*

*HAQ, B.U., HARDENBOL, J. and VAIL, P.R., 1987, Chronology of fluctuating sea-levels since the Triassic. Science, 235, p. 1167 – 1156.*

*HARDENBOL, J., THIERRY, J., FARLEY, M. B., DE GRACIANSKY, P.-C., and VAIL, P. R., 1998, Mesozoic and Cenozoic Sequence Chronostratigraphic Framework of European Basins. In: GRACIANSKY, P. C., DE HARDENBOL, J., JACQUIN, T. & VAIL, P. R. (eds) Mesozoic and Cenozoic Sequence Stratigraphy of European Basins. Society for Sedimentary Geology (SEPM), Tulsa, OK, 60, p. 3 – 13.*

*HARRISON, R.W., NEWELL, W.L., BATIHANLI, H., PANAYIDES, I., MCGEEHIN, J.P., MAHAN, S.A., OZHUR, A., TSIOLAKIS, E., and NECDET, M., 2004, Tectonic Framework and Late Cenozoic Tectonic History of the Northern Part of Cyprus: Implications for Earthquake Hazards and Regional Tectonics, Journal of Asian Earth Sciences, 23, p. 191 – 210.*

*HOUSE, M.R., MENNER, V.V., BECKER R.T., KLAPPER G., OVNATANOVA, N.S., and KUZ'MIN, V., 2000, Reef Episodes, Anoxia and Sea-level Changes in the Frasnian of the Southern Timan (NE Russain Platform), Geological Society, London, Special Publications, 178, p. 147 – 176.*

*ILGAR, A., NEMEC, W., HAKYEMEZ, A., and KARAKUS, E., 2013, Messinian Forced Regressions in the Adana Basin: a Near-Coincidence of Tectonic and Eustatic Forcing, Turkish Journal of Earth Sciences, 22, p. 864 – 889.*

*İLKER, S., 1975, Adana Baseni Kuzeybatısının Jeoloji ve Petrol Olanakları, T.P.A.O. Arama Arşiv, Ankara, No: 973, 63 p. (not published).*

*INTERGOVERNMENTAL OCEANIC COMMISSION (IOC), 1981, International Bathymetric Chart of the Mediterranean. Published by the Head Department of Navigation and Oceanography, Russia, 10 sheets.*

*JACKSON, J., and MCKENZIE, D. P., 1984, Active Tectonics of the Alpine-Himalayan Belt between Western Turkey and Pakistan; Geophys. J. Roy. Astron. Soc. 77, p. 155 – 264.*

*JAFFEY, N., and ROBERTSON, H.F., 2001, New Sedimentological and Structural Data from the Ecemis Fault Zone, Southern Turkey: Implications For It is Timing and*

*Offset and the Cenozoic Tectonic Escape of Anatolia, Journal of the Geologic Society, 158, p. 367 – 378.*

*JANSON, X., VAN BUCHEM, F.S.P., DROMART, G., EICHENSEER, H.T., DELLAMONICA, X., BOICHARD, R., BONNAFFE, F., and EBERLI, G., 2010, Architecture and Facies Differentiation within a Middle Miocene Carbonate Platform, Ermenek, Mut Basin, Southern Turkey, In: VAN BUCHEM, F.S.P., GERDES, K.D., and ESTEBAN, M. (eds) Mesozoic and Cenozoic Carbonate Systems of the Mediterranean and the Middle East: Stratigraphic and Diagenetic Reference Models, Geological Society, London, Special Publications, 329, 265 – 290.*

*KARIG, D.E., and KOZLU, H., 1990, Late Paleogene–Neogene Evolution of the Triple Junction Region near Maras, South-Central Turkey. J. Geol. Soc. (Lond.) 147, p. 1023 – 1034.*

*KELLING, G., GOKCEN, S.L., Floyd P.A., and GOKCEN, N.S., 1987, New Data from South Turkey Bearing on Neogene Tectonics and Plate Motions in the Eastern Mediterranean Region; Geology 15, p. 425 – 429.*

*KEMPLER, D., and GARFUNKEL, Z., 1994, Structure and Kinematics in the Northeastern Mediterranean: a Study of Irregular Plate Boundary, Tectonophysics 234, p. 19 – 32.*

*KEMPLER, D., 1998, Eratosthenes Seamount: the Possible Sperhead of Incipient Continental Collision in the eastern Mediterranean. Proceedings of the Ocean Drilling Program, Scientific Results, 160, p. 709 - 721.*

*KIM, W., FOUKE, B.W., PETTER, A.L., QUINN, T.M., KERANS, C., and TAYLOR F., 2012, Sea-level Rise, Depth-dependent Carbonate Sedimentation and the Paradox of Drowned Platforms: Sedimentology, v. 59, p. 1677–1694, doi:10.1111/j.1365 - 3091.2012.01321.x*

*KOCYIGIT, A., and BEYHAN, A., 1998, A New Intracontinental Transcurrent Structure: the Central Anatolian Fault Zone, Turkey. Tectonophysics, 284(3), p. 317 - 336.*

*KOMINZ, M.A., BROWNING, J.V., MILLER, K.G., SUGARMAN, P.J., MIZINTSEVAW, S. and SCOTESE, C.R. 2008, Late Cretaceous to Miocene Sea-level Estimates from the New Jersey and Delaware Coastal Plain Coreholes: an Error Analysis, Basin Research, 20, p. 211 – 226.*

*LAGAP, H., 1985, Kiralan-Karakilic-Karaisali (NW Adana) Lithostratigrafik-Kronostratigrapfik Incelemesi, Cukurova Universitesi Fen Bilimleri Enstitusu Jeoloji Muhendisligi Bolumu, Yuksek Lisans Tezi, Adana, 77 p. (in Turkish).*

*LOURENS, L., HILGEN, F. J., SHACKLETON, N. J., LASKAR, J., and WILSON, D., 2004, The Neogene Period. Cambridge University Press, Cambridge.*

*McARTHUR, J. M., HOWARTH, R.J., and BAILEY, T.R., Strontium Isotope Stratigraphy: LOWESS Version 3: Best fit to the Marine Sr- Isotope Cure for 0-509 Ma and Accompanying Look - up Table for Deriving Numerical Age, 109, p. 155 – 170.*

*MILLER, K. G., MOUNTAIN, G. S. ET AL. 1998, Cenozoic Global sea-level, Sequences, and the New Jersey Transect; Results from Coastal Plain and Continental Slope Drilling. Reviews of Geophysics, 36, p. 569 – 601.*

*MILLER, K. G., KOMINZ, M.A. ET AL. 2005, The Phanerozoic Record of Global Sea-level Change, Science, 310, p. 1293 – 1298.*

*MOSBRUGGER, V., UTESCHER, T. & DILCHER, D. L. 2005. Cenozoic continental climatic evolution of Central Europe. Proceedings of the National Academy of Sciences of the United States of America, 102, 14964–14969.*

*NAZIK A. and TOKER V., 1986, Karaisali Yoresi Orta Miyosen istifinin Foraminifer Biyostatigrafisi. Miner Res Explor Inst Bull, 103/104, p. 139 – 150 (in Turkish).*

*NAZIK, A., and GURBUZ, K., 1992, Planktonic Foraminiferal Biostratigraphy of the Lower – Middle Miocene Sequence of Karaisali – Catalan- Egner Region (NW – Adana), Bulletin of the Geological Society of Turkey, 35/1, p. 67 – 80 (in Turkish).*

*NAZIK, A., 2004, Planktonic Foraminiferal Biostratigraphy of the Neocene Sequence in the Adana Basin, Turkey, and its correlation with standard biozones, Geological Magazine, 141(3), p. 379 – 387.*

*OSLICK, J.S., MILLER, K.G., and FEIGENSON, M.D., 1994, Oligocene – Miocene Strontium Isotopes: Stratigraphic Revisions and Correlations to an Inferred Glacioeustatic Record, Paleoceanography, Vol. 9, No. 3, p. 427 – 443.*

*OZCELIK, N. and YETIS, C., 1994, Adana Baseni Guvenc Formasyonunun (Tersiyer) Fasiyes ve Ortamsal Nitelikleri, Turkiye Jeoloji Bulteni, 37, p. 73 – 85 (in Turkish).*

*OZEL, E., ULUG., A, and PEKCETINOZ, O., 2007, Neotectonic Aspects of the Northern Margin of the Adana – Cilicia Submarine Basin, NE Mediterranean, J. Earth Sys. Sci., 116 (2), p. 113 – 124.*

*OZER, B., BIJU-DUVAL. P., COURRIER, P. ve LETZOUEY, J.,1974, Antalya - Mut ve Adana Havzalarının Jeolojisi, Türkiye İkinci Petrol Kongresi Bildiriler Kitabı , p. 57 – 84. (in Turkish).*

*OZTUMER, E., BIZON, G., BIZON, J.J., FEINBERG, H., 1974, Antalya - Mut ve Adana Havzaları Tersiyeri Biyostratigrafi ve Mikopaleontoloji Yenilikleri, Türkiye İkinci Petrol Kongresi Bildiriler Kitabı, p.217-228 (in Turkish).*

*PERRY, C.T., 1999, Biofilm – related Calcification, Sediment Trapping and Constructive Micrite Envelopes: a Criterion for the Recognition of Ancient Grass – Bed Environments, Sedimentology, 46, p. 33 – 45.*

*PILLER, W.E., and RASSER M., 1996, Rhodolith Formation Induced by Reef Erosion in the Red Sea, Egypt, In: Coral Reefs, International Society for Reef Studies, 15, p. 191 – 198.*

*PILLER, W. E., HARZHAUSER, M. and MANDIC, O. 2007, Miocene Central Paratethys Stratigraphy; Current Status and Future Directions. Stratigraphy, 4, p. 151–168.*

*PIPER, J.D.A., GURSOY, H., TATAR, O., BECK, M.E., RAO, A., KOCBULUT, F., and MESCI, B.L., 2010, Distributed Neotectonic Deformation in the Anatolides of Turkey: A palaeomagnetic analysis. Tectonophysics, 488(1), p. 31 - 50.*

*POMAR, L., 1991, Reef geometries, Erosion Surfaces and High Frequency Sea-level Changes, Upper Miocene Reef Complex, Mallorca, Spain. Sedimentology 38, p. 243 – 269.*

*POMAR, L., WARD, C.W., GREEN D.G., 1996, Upper Miocene Reef Complex of the Llucmajor Area, Mallorca, Spain, In: Models for Carbonate Stratigraphy from Miocene Reef Complexes of Mediterranean Regions, SEPM Concepts in Sedimentology and Paleontology, 5, p. 191 – 225.*

*POMAR, L., BRANDANO, M., WESTPHAL, H., 2004, Environmental Factors Influencing Skeletal Grain Sediment Associations: a Critical Review of Miocene Examples from the Western Mediterranean. Sedimentology 51, p. 627 – 651.*

*POOLE, A.J., and ROBERTSON, A.H.F.,1992, Quaternary Uplift and Sea Level Change at an Active Plate Boundary, Cyprus, Journal of Geological Society, London, 148, p. 909 - 921.*

*PRALLE, N., 1994. Structural Evolution of the Noecene Adana and Iskenderun Basins, South Turkey, Msc Thesis, Rice University.*

*RADEFF, G., 2014, Geohistory of the Central Anatolian Plateau Southern Margin (Southern Turkey). PhD Dissertation, Roma Tre University and Potsdam University.*

*ROBERTSON, A.H.F., 1998, Mesozoic- Tertiary Tectonic Evolution of the Easternmost Mediterranean Area: Integration of Marine and Land Evidence. Proceedings of the Ocean Drilling Program, Scientific Results, 160, p. 723 – 782.*

*ROBERTSON, A., UNLUGENC, U.C., INAN, N., and TASLI, K., 2004, The Misis - Andirin Complex: a Mid-Tertiary mélange related to late-stage subduction of the Southern Neotethys in S Turkey, Journal of Asian Earth Sciences, 22, p. 413 – 453.*

*SAFAK, U., KELLING, G., GOKCEN, N.S., and GURBUZ, K., 2005, The mid-Cenozoic Succession and Evolution of the Mut Basin, Southern Turkey, and its Regional Significance. Sedimentary Geology 173 (1-4), p. 121 – 150.*

*SALLER, A., ARMIN, R., ICHRAM, L.O., GLENN-SULLIVAN, C., 1992, Sequence Stratigraphy of Upper Eocene and Oligocene Limestones, Teweh Area, Central*

*Kalimantan. Indonesian Petroleum Association, Proceedings 21ST Annual Convention, p. 69 – 92.*

*SALLER, A., ARMIN, R., ICHRAM, L.O., GLENN-SULLIVAN, C., 1993, Sequence Stratigraphy of Aggrading and Backstepping Carbonate Shelves, Central Kalimantan, Indonesia. In: Loucks, R.G., Sarg, J.F. (Eds.), Carbonate Sequence Stratigraphy, Recent Developments and Applications. American Association of Petroleum Geologists, Memoir, 57, p. 267 – 290.*

*SALLER, A., and VIJAYA, S., 2002, Depositional and Diagenetic History of the Kerendan Carbonate Platform, Oligocene, Central Kalimantan, Indonesia. Journal of Petroleum Geology 25, p. 123 – 150.*

*SATTLER, U., IMMENHAUSER, A., SCHLAGER, W., and ZAMPETTI, V., 2009, Drowning History of a Miocene carbonate platform (Zhujiang Formation, South China Sea), Sedimentary Geology, 219, p. 318 – 331.*

*SATUR, N., 1999, Internal Architecture, Facies Distribution, and Reservoir Modeling of the Cingöz Deepwater Clastic System in Southern Turkey. PhD Thesis, University of Aberdeen (unpublished).*

*SATUR, N., HURST, A., CRONIN, B.T., KELLING, G., AND GURBUZ, K., 2000, Sand Body Geometry in a Sand Rich, Deep Water Clastic System, Miocene Cingöz formation of Southern Turkey. Marine and Petroleum Geology 17, p. 239 – 252.*

*SATUR, N., KELLING, G., CRONIN, B.T., HURST, A. and GURBUZ, K., 2004. Sedimentary Architecture of a Canyon Style Fairway Feeding a Deepwater Clastic System, the Cingöz Formation, Southern Turkey: Significance for Reservoir Characterisation and Modeling, Sedimentary Geology 173, p. 91 – 119.*

*SCHILDGEN, T.F., COSENTINO, D., CARUSO, A., BUCHWALDT, R., YILDIRIM, C., BOWRING, S.A., ROJAY, B., ECHTLER, H., and STRECKER, M.R., 2012, Surface Expression of Eastern Mediterranean Slab Dynamics: Neogene Topographic and Structural Evolution of the Southwest Margin of the Central Anatolian Plateau, Turkey, Tectonics, 21 p..*

*SCHMIDT, G.C., 1961, Stratigraphic Nomenclature for the Adana Region Petroleum District VII. Petroleum Administration Bulletin, 6, p. 47 – 63.*

*SCHLAGER, W., 1989, Drowning Unconformities on Carbonate Platforms. In: Controls on Carbonate Platforms and Basin Development (ed. by P.D. Crevello, J.L. Wilson, J. F. Sarg and J.F. Read). SEPM Special Publications, 44, 15 – 25.*

*SCHLAGER, W., 1992, Sedimentology and Sequence Stratigraphy of Reefs and Carbonate Platforms, the American Association of Petroleum Geologists, Tulsa, Oklahoma, USA, Continuing Education Course Note Series #34, p. 1 - 67.*

*SCHOLLE, P.A., and ULMER-SCHOLLE D.S.A, 2003, A Color Guide to the Petrography of Carbonate Rocks: Grains, Textures, Porosity, and Diagenesis AAPG Memoir, 77, 470 p.*

*SENGOR, A.M.C., and YILMAZ, Y., 1981, Tethyan Evolution of Turkey: A Plate Tectonic Approach. Tectonophysics, 75, p. 181 – 241.*

*SENGOR, A.M.C., GORUR N., and SAROGLU, F., 1985. Strike-slip Faulting and Related Basin Formation in zones of tectonic escape: Turkey as a case study. Strike Slip Deformation, Basin Formation, and Sedimentation (eds) Briddle R T and Christie-Blick N, The Society of Economic Paleontologists and Mineralogists, Special Publication, 37, p. 227 – 264.*

*TERNEK, Z., 1957, Adana Havzasının Alt Miyosen (Burdigaliyen) Formasyonları; Bunların Diğer Formasyonlarla Olan Münasebetleri ve Petrol İmkanları, M.T.A. Der., Ankara, 49, p. 48 – 66 (in Turkish).*

*TOKER, M., EDIGER V., EVANS, G., 2007, Physiographic, Morpho-tectonic Provinces and Sedimentary Patterns of the Cilicia-Adana Basin, the NE-Mediterranean, Geophysical Research Abstracts, Vol. 9, 00287, 2 p..*

*UNLUGENC, U.C., 1986, Kizildag Yayla (Adana) Dolayinin Jeolojik Incelemesi, Cukurova Universitesi Fen Bilimleri Enstitusu Jeoloji Muhendisligi Bolumu, Yuksek Lisans Tezi, Adana, 77 s. (in Turkish).*

*UNLUGENC, U.C., and DEMIRKOL, C., 1988, Stratigraphy of Kizildag Yayla (Adana Region). Geological Engineering, 32-33, p. 17 – 25 (in Turkish).*

*UNLUGENC, U.C., KELLING, G., and DEMIRKOL, C., 1990, Aspects of the Adana Evolution in the Neocene Adana Basin, SE Turkey, Savascin, M.Y., Eronat, A.H., (Eds.), Proc. Int. Earth Science Cong. On Aegean Region, Izmir, Turkey, 1, p. 353 – 370.*

*UNLUGENC, U.C., DEMIRKOL, C., and SAFAK, U., 1991, Stratigraphical and Sedimentological Characteristics of the Karsanti Basin Fill to the NE of the Adana Basin. Proc. A. Suat Erk Geology Symposium, Ankara, p. 215 – 227.*

*UNLUGENC, U., 1993, Controls on Cenozoic Sedimentation in the Adana Basin, Southern Turkey, University of Kent at Canterbury.*

*VAN DE WEERD, A.A., ARMIN, R.A., MAHADI, S., WARE, P.L.B., 1987, Geologic Setting of the Kerendan Gas and Condensate Discovery, Tertiary Sedimentation and Paleogeography of the Northwestern Part of the Kutei Basin, Kalimantan, Indonesia. Indonesian Petroleum Association, Proceedings 16th Annual Convention, p. 317 – 338.*

*VECSEI, A., and SANDERS, D.G.K., 1999, Facies Analysis and Sequence Stratigraphy of a Miocene Warm-Temperate Carbonate Ramp, Montagna della Maiella, Italy. Sedimentary Geology 123, p. 103 – 127.*

*VIDAL N., KLAESCHEN, D., KOPF, A., DOCHERTY, C., VON HUENE, R., and KRASHENINNIKOV, V. A., 2000, Seismic Images at the Convergence Zone from South of Cyprus to the Syrian Coast, Eastern Mediterranean; Tectonophys., 329, p. 157 – 170.*

*WALSH-KENNEDY, S., AKSU, A.E., HALL, J., HISCOTT, R.N., YALTIRAK, C., and CIFTCI, G., 2014, Source to Sink, The Development of the Latest Messinian to Pliocene – Quaternary Cilicia and Adana Basins and Their Linkages with the Onland Mut Basin, Eastern Mediterranean, 2014, Tectonophysics, 622, p. 1 – 21.*

*WILLIAMS, G.D., UNLUGENC U.C., KELLING G., and DEMIRKOL C., 1995, Tectonic Controls on Stratigraphic Evolution of the Adana Basin, Turkey, Journal of Geological Society, London, 152, p. 873 – 882.*

*WILSON, M.E.J., 1999, Prerift and Synrift Sedimentation during Early Fault Segmentation of a Tertiary Carbonate Platform, Indonesia, Marine and Petroleum Geology, v.16, p. 825 - 848.*

*WILSON, M.E.J., and VECSEI, A., 2005, The Apparent Paradox of Abundant Foramol Facies in Low Latitudes: Their Environmental Significance and Effect on Platform Development, Earth-Science Reviews, 69, p. 133-168.*

*YALCIN, N.M., and GORUR, N., 1984, Sedimentological Evolution of the Adana Basin, Tekeli, O. and Goncuoglu, M.C. (Eds.), Proceedings of the International Symposium on the Geology of the Tauride Belt, Ankara, p. 165 – 172.*

*YETIS, C., and DEMIRKOL, C., 1986. Detailed Geologic Investigation of the Western Side of the Adana Basin, MTA Rep. No: 8037 – 8037a, 70 p. (unpublished, in Turkish).*

*YETIS, C., 1988. Reorganization of the Tertiary Stratigraphy in the Adana Basin, Southern Turkey. Newsletter Stratigraphy 20, p.43 – 58.*

*YETIS, C., KELLING, G., GOKCEN, S.L., and BAROZ F., 1995. A Revised Stratigraphic Framework for Later Cenozoic Sequences in the Northeastern Mediterranean Region. Geologische Rundschau, 84(4), p. 794 – 812.*

*ZACHOS, J., PAGANI, M., SLOAN, L., THOMAS, E. and BILLUPS, K. 2001. Trends, rhythms, and aberrations in global climate 65 Ma to present. Science, 292(5517), 686–693.*

*ZEMPOLICH, W.G., 1993, The Drowning Succession in Jurassic Carbonates of the Venetian Alps, Italy: A Record of subcontinent Breakup, Gradual Eustatic Rise, and eutrophication of Shallow-Water Environments, In: Loucks, R.G., Sarg, J.F. (Eds.), Carbonate Sequence Stratigraphy, Recent Developments and Applications. American Association of Petroleum Geologists, Memoir, 57, p. 63 – 105.*

# VITA

Mehmet Ozen Gurbuz was born in Ankara, TURKEY. After completing her work at Gazi Anatolian High School, Ankara, TURKEY, he entered Middle East Technical University in Ankara, TURKEY. During the summers of 2008 and 2009 he worked as an intern in two successive petroleum companies; Turkish Petroleum Corporation and Merty Energy Petroleum Exploration and Education Inc. He received the degree of Bachelor of Science from Middle East Technical University in 2010. He employed as an exploration geologist and junior project manager at Teck Resources Ltd for one and half year. During the following years, he has performed his military task as a paid geological engineer (reserve officer – remote sensing) and then, employed as petroleum geologist (wellsite geologist) at Perenco Oil and Gas Company. In September, 2013, he entered the Graduate School at the University of Texas at Austin.

Address: 8. Cad. 2494.sok. Çamlıca Bulvar sit. F-Blok No:10
P.K. 06810 Umit Mah. Çayyolu
Ankara/TURKEY
mozengurbuz@gmail.com

This manuscript was typed by Mehmet Ozen Gurbuz.